Title
Neural and Behavioral Analysis of Object Detection in Drosophila

Author
Keles, Mehmet

Publication Date
2017

Peer reviewed|Thesis/dissertation

UNIVERSITY OF CALIFORNIA

Los Angeles

Neural and Behavioral Analysis of Object Detection in *Drosophila*

A dissertation submitted in partial satisfaction of the requirements

for the degree of Doctor of Philosophy

in Molecular, Cellular and Integrative Physiology

by

Mehmet Fatih Keleş

2017

ABSTRACT OF THE DISSERTATION

Neural and Behavioral Analysis of Object Detection in *Drosophila*

By

Mehmet Fatih Keleş

Doctor of Philosophy in Molecular, Cellular and Integrative Physiology

University of California, Los Angeles, 2017

Professor Mark A. Frye, Chair

As we move through the world, our visual system constantly detects and tracks objects around us, using cues such as movement, texture, brightness, color and shape. A solid mechanistic understanding of how an object is distinguished from its background has eluded researches examining this question across many model organisms. In this thesis, we describe a novel object-detecting neuron class in the fly optic lobe by characterizing its anatomy and physiology. We then show direct evidence that inhibitory currents play a major role in mediating object-selectivity. To find origins of inhibition, we screen publicly available libraries and identify candidate presynaptic input neurons. In addition, we examine the receptor expression profile of object-detecting neurons and identify receptor types that are likely to mediate inhibition and excitation. Our results provide insights into the only known object-detector neuron in *Drosophila.*

To elucidate the possible behavioral contributions of object-detecting neurons, we investigate the object tracking behavior in flies. We show that luminance and motion cues contribute to object tracking behavior in distinct ways. Specifically, flies exhibit quantitatively and qualitatively distinct behavioral responses to luminance-defined and motion-defined objects. Our results complement previously published research and demonstrate the existence of parallel visual streams carrying different information (motion or luminance) that are relevant for object tracking behaviors.

The dissertation of Mehmet Fatih Keleş is approved

David William Walker

Alapakkam P. Sampath

Stephen Lawrence Zipursky

Mark Arthur Frye, Committee Chair

University of California, Los Angeles

2017

Anneme, babama ve kardeşlerime.

TABLE OF CONTENTS

ACKNOWLEDGEMENTS

It is a great pleasure to express gratitude to those who made this dissertation possible. I will be forever indebted to my advisor, Mark Frye, for his continuous support, guidance and patience he generously offered over the past five years. His mentorship style allowed me to be independent and develop my own scientific ideas, but also to be self-aware. Thank you for providing an incredible environment to do research (including the delicious cocktails). Thank you for always finding time to listen and bringing positivity to my never-ending pessimism.

I was a junior exchange student at UCSC when Larry Zipursky welcomed me to his lab at UCLA, even though I had no real understanding of neuroscience. I might have lacked knowledge; however, I had sheer will to learn. Without your support, I would not have been fortunate enough to be here.

Thank you Jacob Aptekar for sharing and passing down your expertise on fly neurobiology and programming. Thank you to Matt Bramble, Katie Ingraham, Karen Cheng, Jaison Omoto, Sara Wasserman, Ben Hardcastle, Patrick Lu, Jean Mongeau, Brian Duistermars, Shivan Bonanno, Carola Städele and Sufia Sadaf for support, friendship, advice and making the past five years a fun experience. Thank you to other members of my thesis committee – David Walker and Alapakkam Sampath for your invaluable guidance and mentorship. Thank you Peter Narins for teaching me so much on neuroethology and showing me what great teaching looks like. Thank you Orkun Akın, for kindly sharing so many reagents with me and providing me with an immense amount of scientific knowledge on fly genetics.

I cannot express how lucky and grateful I am for having the most supporting parents and siblings. To my mother and father, Gülşan and Murat, I owe more than I could ever express. My dad, the most hardworking and tenacious person I've ever known, was the first one to go to college from his family and made sure that I had the best education possible. My mom's endless love and support, as well as the incredible food and snacks she sent all the way from Turkey, kept me going through hard times. My sister, Betül, visited me every year throughout the graduate school, cooked me delicious meals and made me feel home. My brother, Emin, the ironman of the family, despite living on the other side of the ocean, used every opportunity to motivate me to become a healthier person. My older sister, Sündüz, has been my north star, guiding me and mentoring me ever since I was a kid. I owe a huge part of my accomplishments to her. Without the path she paved, I would not have been here. My brother-in-law, Derviş, contributed so much to my intellectual growth and showed me what the strongest moral compass looks like. I feel so grateful to have Sündüz and Derviş in my life. During holidays when going back to Turkey was not an option, I took refuge in their home and was always welcomed. My beautiful nieces Arya, Eliz, Bukle, Alis and my handsome nephew Ege brought so much fun, joy and happiness to my life.

Finally, thank you Emily Bates for bringing happiness to my life and always encouraging me to look on the bright side.

Chapter 2 is adapted from Keleş, M.F., Frye, M.A., 2017. Object-Detecting Neurons in Drosophila. Curr. Biol. 27, 680–687. doi:10.1016/j.cub.2017.01.012. M.F.K. and M.A.F. designed the research. M.F.K. performed and analyzed experiments. M.F.K. and M.A.F.

wrote the manuscript. This work was supported by the National Institutes of Health RO1 EY026031 to M.A.F. and UCLA Edith Hyde Fellowship to M.F.K.

Chapter 5 is adapted from Omoto, J.J., Keleş, M.F., Nguyen, B.C.M., Bolanos, C., Lovick, J.K., Frye, M.A., Hartenstein, V., 2017. Visual Input to the Drosophila Central Complex by Developmentally and Functionally Distinct Neuronal Populations. Curr. Biol. 27, 1098–1110. doi:10.1016/j.cub.2017.02.063. J.J.O., M.F.K., V.H. and M.A.F. designed the research. J.J.O., M.F.K., B.C.M.N., C.B. and J.F.K. performed experiments. J.J.O. and M.F.K. analyzed the data. J.J.O., M.F.K., M.A.F. and V.H. wrote the manuscript.

VITA

Education

2012 - Present UCLA, Los Angeles, CA
Ph.D. Candidate, Molecular, Cellular and Integrative Physiology

2008 - 2012 Bilkent University, Ankara, TURKEY
B.Sc. in Molecular Biology and Genetics with High Honors

2010 - 2011 UCSC, Santa Cruz, CA
Exchange Student in Molecular, Cellular and Developmental Biology

Research Experience

2012 – Present Graduate Student, UCLA, Los Angeles, CA
Laboratory of Mark Frye, Ph.D.
Thesis topic: Neural mechanisms of visual feature detection

2011 Summer Undergraduate Researcher, UCLA, Los Angeles, CA
Laboratory of Larry Zipursky, Ph.D.
Conducted an RNAi based screen to identify novel cell signaling molecules.

2010 Summer Undergraduate Resarcher, Albert Einstein College of Medicine, New York
Laboratory of Ertugrul Ozbudak, Ph.D.
Worked on a project to identify novel genes involved in left-right asymmetry in zebrafish.

Publications

2017 Omoto, J.J.*, **Keleş, M.F.***, Nguyen, B.-C.M., Bolanos, C., Lovick, J.K., Frye, M.A., and Hartenstein, V. (2017). Visual input to the Drosophila central complex by developmentally and functionally distinct neuronal populations. *Current Biology. 27*, 1098–1110. http://doi.org/10.1016/j.cub.2017.02.063
**Co-first author*

Keleş, M.F., and Frye, M.A. (2017). The eyes have it. *eLife*. e24896. http://dx.doi.org/10.7554/eLife.24896
Insight article

Keleş, M.F., and Frye, M.A. (2017). Object-detecting neurons in Drosophila. *Current Biology.* 27, 680–687. http://doi.org/10.1016/j.cub.2017.01.012

2015 Aptekar, J.W., **Keleş, M.F**., Lu, P.M., Zolotova, N.M., and Frye, M.A. (2015). Neurons forming optic glomeruli compute figure-ground discriminations in Drosophila. *Journal of Neuroscience*. 35, 7587–7599. https://doi.org/10.1523/JNEUROSCI.0652-15.2015

Wasserman, S.M., Aptekar, J.W., Lu, P., Nguyen, J., Wang, A.L., **Keles, M.F.**, Grygoruk A., Krantz D.E., Larsen C., and Frye, M. A. (2015). Olfactory neuromodulation of motion vision circuitry in Drosophila. *Current Biology*. 25, 467–72. doi:10.1016/j.cub.2014.12.012

2014 Aptekar, J. W., **Keles, M.F.**, Mongeau, J.-M., Lu, P. M., Frye, M.A., and Shoemaker, P.A. (2014). Method and software for using m-sequences to characterize parallel components of higher-order visual tracking behavior in Drosophila. *Frontiers in Neural Circuits*, 8, 130. doi:10.3389/fncir.2014.00130

Ho, V.M., Dallalzadeh, L.O., Karathanasis, N., **Keles, M.F**., Vangala, S., Grogan, T., Poirazi P., and Martin, K.C. (2014). GluA2 mRNA distribution and regulation by miR-124 in hippocampal neurons. *Molecular and Cellular Neuroscience*, 61, 1–12. doi:10.1016/j.mcn.2014.04.006

Presentations

2017 Keles, M.F. and Frye M.A. "Object-detecting neurons in *Drosophila*". MCIP Graduate Program Retreat, UCLA, Los Angeles, CA.

2016 Keles, M.F. and Frye M.A. "Object-detecting neurons in *Drosophila*". Synapse to Circuits Seminar Series, UCLA, Los Angeles CA.

2015 Keles, M.F. and Frye M.A. "Neural Correlates of Small Target Detection in *Drosophila*". Visual Neuroscience Affinity Group, UCLA, Los Angeles, CA.

Keles, M.F. and Frye M.A. "Neural Correlates of Small Target Detection in *Drosophila*". MCIP Student Seminar, UCLA, Los Angeles, CA.

Keles, M.F. "Neural basis of parallel object detection streams in *Drosophila*". Insect Vision: Cells, Circuits and Computations, Janelia Research Campus, Ashburn, VA.

Posters

2015 Keles, M.F. and Frye M.A. "Neural Correlates of Small Target Detection in *Drosophila*". Brain Resarch Institute, UCLA, Los Angeles, CA.

Keles, M.F. and Frye M.A. "Neural correlates of parallel object detection streams in *Drosophila*". Neurobiology of *Drosophila*, Cold Spring Harbor Laboratory, New York City, NY.

Awards and Fellowships

2015 Edith Hyde Fellowship, UCLA – 31,000$

2016 Dissertation Year Fellowship, UCLA – 20,000$ Stipend and Tuition

Teaching

2014-2015 Teaching Assistant for PS173 – Anatomy and Physiology of Sense Organs (2 quarters)
Prepared weekly presentations and quizzes on seminal research articles covering sensory physiology.

Outreach/Service

2016 SWIRLSS/Campbell Hall High School Outreach
Visited a local high school to guide in setting up *Drosophila* flight simulators for a mini-lab.

2015-2017 UCLA Brain Awareness Week (Annual event)
Gave lab tours to high school students and discussed science careers.

Mentored Students

2015- Rachel Mernoff, undergraduate
2015-2016 Nina Fukuma, undergraduate
2014-2015 Ryan Tsiao, undergraduate, now a technician at UCSF
2014-2015 Nelson Nunez, high school student, now undergraduate
2013-2014 Delaine Quaresma, undergraduate, now student of veterinary medicine at UC Davis

Chapter 1

What the Fly's Eyes Tells Fly's Brain

Introduction

From the moment we wake up until the moment we sleep, our sensory systems work at an incredible pace to decode and interpret the environment. Our visual system detects and classifies thousands of objects around us, from the cup of coffee sitting on our desk to the tennis ball flying towards us at 150 miles per hour. It has been six decades since the discovery of the first object-detecting neuron in the frog by Lettvin and colleagues (Lettvin et al., 1959), yet the exact cell and circuit mechanisms of how visual systems extract object information remains enigmatic. Here, I review some of the widely-studied object detectors across taxa, discuss *Drosophila's* extensive behavioral repertoire that rely on object vision and argue that the tiny fruit fly is emerging as a model organism to dissect mechanisms of object detection.

Brief History of Object-detecting Neurons

Object detecting neurons have been found in animals across taxa. Although Lettvin and colleagues had stated in their seminal paper that their work on object vision "has been done on the frog, and [their] interpretation applies only to the frog", shortly after their discovery similar neurons were found in the rabbit retina by Levick (Levick, 1967). Both papers described a retinal ganglion cell (RGC) type that responds strongly to small objects filling the full or partial extent of their receptive field; the response is abolished when objects fill the receptive field surround. Since then, similar RGCs have been found in mice (Zhang et al., 2012) and zebrafish (Semmelhack et al., 2014). Furthermore, cells with additional selectivity not for just size but contrast and movement have been found in the feline cortex (Hubel and Wiesel, 1965, 1962), mouse superior colliculus

(Gale and Murphy, 2016, 2014), zebrafish tectum (Preuss et al., 2014), dragonfly and hoverfly optic lobe (for review see: Nordström, 2012), fruit fly protocerebrum (Kim et al., 2015) and most recently, fruit fly optic lobe (Keleş and Frye, 2017).

The existence of object detecting neurons in a wide variety of animals across taxa suggests the importance of this computation for survival. Visual object-detection is required to track conspecifics, navigate complex environments and detect potential prey and predators. August Krogh masterfully proposed in his seminal 1929 paper titled “The Progress of Physiology” that to understand a physiological phenomenon, one must study organisms that exhibit extremes of adaptation. Following Krogh’s principle, researchers have developed a rich and fruitful research program focusing on understanding object-vision and, in a broader context, feature detection in dragonflies. Dragonflies are excellent aerial predators. Equipped with one of the largest insect eyes and almost 360° of visual field (Sherk, 1978), dragonflies make predictive maneuvers during prey pursuit and actively react to changes in prey trajectory, leading to a successful capture rate of 95% in recorded attempts (Mischiati et al., 2014; Olberg et al., 2007; Olberg et. al., 2012). Investigation of the underlying circuitry revealed extraordinary neurons that are capable of tracking one object in the visual field while ignoring another (Wiederman and O’Carroll, 2013) and effectively predicting the future location of a moving object (Wiederman et al., 2017).

Fruit flies, on the other hand, are likely to have inferior object-vision in terms of speed and resolution compared to dragonflies. Fruit flies have almost ~40 times less number of ommatidia (30,000 vs 700), do not capture prey out in the wild and, unlike dragonflies

perform courtship on land. Interestingly, however, the behavioral repertoire that depends on fruit fly object-vision is extensive and matches the specific ecological demand (see below).

Object-driven Behaviors in *Drosophila*

Flies rely on object vision to perform behaviors such as aggression (B. Duistermars, personal comms.) and courtship (Markow, 1975). The role of vision in aggression has not been investigated thoroughly, but it is proposed that visual cues play a significant role (Asahina et al., 2014), possibly through object-detecting neurons. In courtship, vision is not required for successful copulation: flies are able to mate in the dark (Spieth and Hsu, 1950). However, vision is essential for different steps that increase the chances of successful copulation, such as orientation and chasing (Cook, 1979). Vision is also essential to amplitude modulation with distance (AMD), a behavior that is part of courtship. Male flies modulate the intensity of their courtship song based on their distance to female flies (Coen et al., 2016). When placed in the dark, male flies failed to modulate this intensity, revealing that vision is required. Furthermore, motion detecting neurons that are not part of the object-vision circuitry are dispensable for this behavior (see below).

Flies are not only able to detect conspecifics for courtship but will also modify their behavior upon detecting predators and parasites. A recent paper demonstrated that flies use their vision to detect parasitic wasps to change their oviposition preference (Kacsoh et al., 2013). Flies were given the option to lay eggs in two food dishes: one containing 6% ethanol and one with no ethanol. A high proportion of flies laid eggs into the dish

containing no ethanol. When parasitic female wasps were introduced, flies switched their oviposition preference, and laid the majority of their eggs into the dish with 6% ethanol. Although this reduces the survivability of the eggs, due to alcohol exposure, the protection afforded by the alcohol against the wasp appears to lead to a better overall outcome (Kacsoh et al., 2013). Remarkably, flies can distinguish between female and male wasps, showing preference to alcohol only in the presence of female wasps that can potentially infest. Surprisingly, vision and not olfaction is the sensory modality that mediates this behavior. It is not clear how flies achieve this with relatively poor spatial vision and which visual cues (size, color, contrast etc.) are essential. Regardless, this is a prime example that high performance object vision exists in fruit flies.

Detection of predators using visual cues is an essential first step to anti-predatory strategies. Fruit flies are prey for many other animals, yet little is known about the anti-predatory behavioral repertoire and the underlying sensory systems. How flies evade predators in their natural habitat has been the subject of recent investigation (De La Flor et al., 2017; Parigi et al., 2014). When placed in a circular arena with predatory species such as jumping spiders, flies exhibited distinct behaviors, such as freezing to avoid detection (Parigi et al., 2014). In addition, flies exhibited predator-specific responses. When a mantis was introduced to the arena, flies responded by walking in reverse and retreating, which was not seen when flies were exposed to spiders. Additionally, flies increase locomotion speed in the presence of predators (De La Flor et al., 2017). Visually impaired flies do not exhibit the same increase in locomotion speed when in proximity to the predators. These studies revealed complex anti-predatory behaviors

that had not previously been reported in a lab environment. Thus, visually mediated behaviors that require object detection might be extremely diverse and hard to dissect without considering the natural habitat of fruit flies.

Several observations have been made in studies done in the lab using stationary or moving objects. When placed in an arena with objects of different heights and widths, flies showed a preference for tall and steep objects (Robie et al., 2010). In a different study, a fly-sized controllable magnet used to test flies' interaction with a moving object. When an object is moved regressively, from the rear visual field to the frontal, flies responded by stopping locomotion. Interestingly, progressive movement of an object, from the frontal visual field to the rear, does not elicit such a response, suggesting a saliency of regressive motion (Zabala et al., 2012). Furthermore, an object as small as 1.5° (one third of the acceptance angle of an individual ommatidium) can elicit a response, suggesting a highly sensitive high performance object vision in fruit flies (Zabala et al., 2012).

Fruit flies spend much of their lifetime walking near food sources and laying their eggs to rotting fruits. Adult flies fly to disperse and find new food sources for the next generation. It is not known, to my knowledge, what percentage of their adult life they spend flying compared to walking. It is possible that a wide variety of object-oriented behaviors are not present in flying flies. When tested in a virtual reality flight simulator and a free-flight environment, flying flies showed attraction to long vertical bars and aversion to small objects (Maimon et al., 2008). However, attraction to small stimuli is required in walking flies to initiate courtship (Agrawal et al., 2014). It is not clear if the

object vision circuitry operates in a state dependent manner or there are dedicated circuits that get recruited in different states.

How does the fly visual system process the complex visual environment? What are the cells and circuits that extract object information? Although, I just discussed a wide variety of behaviors that are likely to be dependent on object-detecting neurons, little is known about the underlying circuitry. A huge swath of knowledge on visual circuits came from the study of motion vision (Mauss et al., 2017). Unlike feature detection, which encapsulates object-detection, studies of motion vision mainly focused on cells that process optic flow that is generated by the self-movement of the animal. Among these, Horizontal System (HS) cells that are highly sensitive to the movement of large-field motion in the yaw axis have been studied in detail. Unlike the object-detecting neurons, motion sensitive cells in the fly show directional selectivity and generally prefer large stimuli (Schnell et al., 2010). The cells that supply directionally selective motion information to the HS cells and many others are two sets of columnar neurons called T4 and T5 (Maisak et al., 2013). Flies are able to perform object-directed behaviors when T4/T5 cells are silenced (Bahl et al., 2015, 2013). This suggests that directional motion information itself might be dispensable for object-oriented behaviors. Furthermore, visual information that is detected by the retina and processed by the two most peripheral neuropiles, the lamina and the medulla, feed into two parallel neuropiles; the lobula and lobula plate. T4 and T5 cells have pre-synaptic terminals in the lobula-plate which has 4 layers, each receiving directional motion information from a subtype of T4 and T5 (Maisak et al., 2013). Thus, each layer in the lobula plate corresponds to one of the four cardinal directions. The role of T4/T5 cells and the downstream motion pathway

in the lobula plate are becoming ever clearer (Bahl et al., 2015, 2013; Maisak et al., 2013). Current efforts are concentrated on assigning functional roles to cells supplying T4/T5 (Strother et al., 2017). Yet, the circuitry and function of its neighboring neuropile, the lobula, have remained mysterious in comparison, due in part to its complex structure and the lack of anatomical characterization of its cells.

Lobula Neurons as Candidate Feature Detectors

The fruit fly lobula consists of 6 layers and was first described after analyzing innervation patterns of Golgi-impregnated neurons (Fischbach and Dittrich, 1989). It is not yet clear whether the identified layers have functional meanings in the lobula, as in the lobula plate. The initial and recent anatomical characterization of lobula cells has mostly focused on the lobula columnar cells (LC) that have dendritic innervations in the lobula and project to the ventrolateral protocerebrum, forming synapse-rich output domains called optic glomeruli (Otsuna and Ito, 2006; Wu et al., 2016). Each cell class consists of multiple cells, varying between 20 to 200 in number. Individual members of each cell class sample a unique visual field and innervate the lobula retinotopically. Yet, the terminals of sibling cells occupy their respective target glomerulus uniformly, suggesting that retinotopy is discarded. Only a few classes show somewhat conserved retinotopy: cells with neighboring dendritic fields occupying neighboring regions in their respective glomerulus (Wu et al., 2016).

In the lobula, the dendritic fields of sibling cells overlap with one another, raising the possibility of dendro-dendritic interactions. In most cases, the high cell count and extensive dendrites for each individual cell allows coverage of the receptive field by the

cell class up to 5 times over. Furthermore, almost all described LCs (17/22) have putative pre-synaptic sites in the lobula, suggesting the existence of feedback circuits. Such circuits could operate by integrating input from a given LC and modulating other LCs or even the same LC class. The anatomical organization of the lobula and the morphology of individual LCs suggest complex processing of visual information.

Due to their convergent structure into unique glomerular regions, lobula neurons have been compared to olfactory sensory neurons (OSNs) (Mu et al., 2012). Each OSN expresses a specific olfactory receptor and innervates unique glomerular regions, thus assigning each glomerulus a unique molecular identity (Vosshall et al., 2000). Although this anatomical similarity is striking and highly indicative that each LC responds to a specific visual feature, it is not yet known whether each LC carries a unique molecular code that can be linked to its physiology. Future experiments combining cell-type specific RNA sequencing with physiological investigations have the potential to unravel the molecular mechanisms of feature selection.

A behavioral screen classifying the effect of optogenetic activation of LCs revealed that LCs can drive robust behaviors (Wu et al., 2016). Activation of several classes of LCs lead to escape responses, backward walking or jumping, whereas almost half of them did not lead to any behaviors. Although, this data is informative, it is likely that optogenetic activation of the entire cell class in this manner does not capture how these cells respond to natural visual stimuli. Thus, refined genetic manipulations and targeted activations of individual or multiple sibling cells within a cell class is required to investigate how LCs can drive ecologically relevant behaviors. In addition, the

optogenetic activation is performed in walking flies, raising the possibility that the lack of a behavioral phenotype in some classes of LCs might be due to behavioral-state dependent modulation; some cells may only trigger behavior during flight, for instance. Nevertheless, the fact that many of the responses seen in LCs are related to avoidance and escape behaviors raises the possibility that lobula neurons are feature-selective and separate from the canonical motion pathway discussed above.

Feature-selective circuits might be tuned to function in walking or stationary flies. For example, an interesting behavior that was observed with LC10 activation was “reaching” behavior in which a fly raises its front legs. Similar behaviors have been observed as part of gap-climbing (Pick and Strauss et al., 2005), fly aggression (Chen et al., 2002) and courtship (Sokolowski et al., 2001), behaviors that flies perform only when on land. Thus, many LCs that innervate similar layers to LC10 in the lobula likely receive similar input that matches the spatiotemporal dynamics of the visual environment. The fly visual system experiences drastically different visual environments when flying. Here I propose that the majority of LCs mediate behaviors that are tuned to the ecological demand of land-related behaviors. At least 3 cell types in the lobula, LC4 (von Reyn et al., 2017), LC6 (Wu et al., 2016) and LC16 (Sen et al., 2017; Wu et al., 2016), play an active role in escape behaviors that are elicited when the animal is stationary or walking. Specifically, LC4 encodes angular velocity of a looming object (von Reyn et al., 2017), LC16 indirectly connects and transmits visual information to the moonwalker descending neurons (MDNs) that mediate backward walking behavior (Bidaye et al., 2014; Sen et al., 2017) and both LC6 and LC16 respond to a looming object (Wu et al., 2016). Although a similar behavior to looming objects is also observed in flying flies

(Muijres et al., 2014), it requires an additional step: the comparison of self-generated optic flow signals against a looming object. Such a cell would necessarily innervate the lobula plate where signals conveying this information are present and should work on a faster timescale. The abovementioned study (Wu et al., 2016) described at least 2 cell types (LPLC1 and LPLC2) that is suited for such a computation. Both cells innervate the lobula and the lobula plate and likely receive directional motion input.

An object can also be distinguished from the background by its color, brightness, texture and shape. Flies have the ability to distinguish different colors and it has been proposed that color discrimination is mediated by lobula neurons (Behnia and Desplan et al., 2015). Functional evidence for this comes from studies of cells and circuits carrying spectral information that are independent of achromatic circuits. For example, two cell types (Tm5 and Tm20) that project from medulla to lobula both receive input from the chromatic R7 and R8 photoreceptors (Gao et al., 2008). These cells form presynaptic terminals in the lobula, connecting to multiple cell types including some LCs (Lin et al., 2016), suggesting that the lobula might mediate spectral sensitive behaviors.

We have recently shown that one of the LCs, LC11, is highly selective for small objects and exhibits diminished responses to rotating panoramas and elongated large objects (Keleş and Frye et al., 2017). Although insect neurons that are tuned to small moving objects were first described in hawkmoths (Collett et al., 1971), later in dragonflies (O'Carroll et al., 1993) and then hoverflies (Barnett et al., 2007), sophisticated tools to study how these cells achieve object selectivity were lacking. Our results revealed that, LC11 is selective for the omni-directional movement of dark objects and can be

sensitive to objects almost 1/4th the acceptance angle of a single ommatidium (Gonzalez-Bellido et al., 2011). LC11, like many other LCs discussed above, discards retinotopic information in the glomerulus. Each individual LC11 cell covers roughly 70 columns but has a receptive field size of only 10-15 columns. 60-70 sibling cells cover the entire eye, providing 5 times coverage of the visual field (Keleş and Frye, 2017; Wu et al., 2016). Currently, it is the only known object detecting cell in *Drosophila* but there are likely other LCs with similar physiological properties.

Circuit Computations that Shape Object Selectivity

How does LC11 achieve object-selectivity? What are the inputs to LC11? A detailed anatomical characterization of the cells that feed into the lobula and LC11 is yet to be carried out. Based on the previous characterization of lobula-innervating cells and the dendritic layer identification of LC11, there are 6 types of cells (Tlp, Tm, TmY, T2-3, Y and Loi) that are likely to be presynaptic partners of LC11 (Fischbach and Dittrich, 1989). Although it is hard to speculate on the exact cell classes that provide synaptic input to LC11, the likely physiology can be deduced from what we know about LC11.

To better understand what the candidate cell types are that provide selective input to LC11, the known object-coding circuits in mice can provide clues. Recent work in the mouse retina suggests that object sensitive W3-RGCs (Zhang et al., 2012) receive glutamergic excitatory input from a VGluT3+ amacrine cells (VG3-ACs) (Kim et al., 2015b). An additional cell type that is sensitive to panoramic motion provides inhibitory input to W3 cells, suppressing the responses to large-field stimuli (Kim and Kerschensteiner, 2017), forming a three cell circuit composed of 1) excitatory inputs

(VGluT3+) responsive to object motion and 2) inhibitory inputs that are sensitive to panoramic motion. Both of these cells types then converge onto 3) object sensitive W3-RGCs. Such a circuit architecture is also seen in the mouse visual cortex (Adesnik et al., 2012); stimulation of the receptive field surround leads to suppressed responses in pyramidial cells, where as it leads to activation in somatostatin-expressing inhibitory cells. Interestingly, such surround suppression is diminished when the inhibitory cells are silenced. Thus, it is possible that a similar mechanism is utilized in the fly visual system.

A major difference between previously reported cells in the mouse retina and LC11 is the response to static light increments/decrements. Unlike W3-RGCs, which are sensitive to static changes in local luminance, LC11 does not respond to similar stimuli, indicating that it requires a moving object. Furthermore, light increments and increments do not necessarily signal an object in motion. A recent report showed that a wide-field cell (WF) located one synapse downstream of RGCs is tuned specifically to object motion and, like LC11, does not respond to static changes in luminance (Gale and Murphy, 2016, 2014). WF cells are found in superficial superior colliculus (sSC) and receive inhibitory input from a second class of cells called Horizontal cells (HC), which respond to the sudden appearance/disappearance of large field stimuli. The size tuning and selectivity of WF cells are reduced when HCs are silenced. Based on such physiology I propose that LC11 is likely to be the invertebrate analogue of WF cells and receive input from cells similar to W3-RGCs.

Object sensitivity is not a well-studied property in cells that are likely to be pre-synaptic to LC11. However, size tuning, a requirement for object selectivity, is shown in the medulla cells (Strother et al., 2017). As proposed before, (Sanes and Zipursky, 2010), RGCs (like W3) in the retina are likely to be the homologues of Tm neurons in the medulla. This is in agreement with the fact that SC neurons, e.g. WF cells, show similar tuning properties to LC11. It is expected that like RGCs (Baden et al., 2016), that form more than 30 functional output channels, Tm neurons exhibit diverse functions. Thus, the study of lobula cells should help our understanding of how neurons in SC, which get input from 90% of all RGCs in rodents (Ellis et al., 2016) integrate diverse input.

Conclusion

Our ability to manipulate and probe neural circuits in flies has expanded vastly in recent years. Complementing the methods that have allowed optical recording (through GCaMP (Akerboom et al., 2012)) and manipulation of neural activity (with Channelrhodopsin (Klapoetke et al., 2014)) to become commonplace for nearly all model systems, fly specific tools that allow genetic access to almost every neuron type create a unique opportunity for understanding some of the fundamental circuits that are essential for visual behavior.

Here I discussed anatomical, physiological and behavioral evidence for object detection circuitry in *Drosophila* and proposed that:

1. A wide range of behaviors relying on object vision in *Drosophila* suggest complicated, high-performance object-vision circuitry. The natural habitat of flies might hold clues to

undiscovered behaviors that can explain observations in ongoing neurophysiological studies.

2. Anatomical and physiological evidence on LCs suggest a role in behaviors that are performed on land. Unlike the lobula plate which is proposed to play a significant role in flight control and self-motion estimation, lobula neurons likely mediate object-oriented behaviors and are tuned to specific visual features such as brightness, size, color, shape, contrast and velocity of objects.
3. Object detecting circuitry in mouse suggests that LC11 likely receives inhibitory input to restrict its response to larger stimuli. The inhibitory cell type possibly responds to larger stimuli and acts via GABA-A receptors.

References:

Adesnik, H., Bruns, W., Taniguchi, H., Huang, Z.J., Scanziani, M., 2012. A neural circuit for spatial summation in visual cortex. Nature 490, 226–231. doi:10.1038/nature11526

Agrawal, S., Safarik, S., Dickinson, M., 2014. The relative roles of vision and chemosensation in mate recognition of Drosophila melanogaster. J. Exp. Biol. 217, 2796–805. doi:10.1242/jeb.105817

Akerboom, J., Chen, T.-W., Wardill, T.J., Tian, L., Marvin, J.S., Mutlu, S., Calderon, N.C., Esposti, F., Borghuis, B.G., Sun, X.R., Gordus, A., Orger, M.B., Portugues, R., Engert, F., Macklin, J.J., Filosa, A., Aggarwal, A., Kerr, R.A., Takagi, R., Kracun, S., Shigetomi, E., Khakh, B.S., Baier, H., Lagnado, L., Wang, S.S.-H., Bargmann, C.I., Kimmel, B.E., Jayaraman, V., Svoboda, K., Kim, D.S., Schreiter, E.R., Looger, L.L., 2012. Optimization of a GCaMP Calcium Indicator for Neural Activity Imaging. J. Neurosci. doi:10.1523/JNEUROSCI.2601-12.2012

Asahina, K., Watanabe, K., Duistermars, B.J., Hoopfer, E., González, C.R., Eyjólfsdóttir, E.A., Perona, P., Anderson, D.J., 2014. Tachykinin-expressing neurons control male-specific aggressive arousal in drosophila. Cell 156, 221–235. doi:10.1016/j.cell.2013.11.045

Baden, T., Berens, P., Franke, K., Román Rosón, M., Bethge, M., Euler, T., 2016. The functional diversity of retinal ganglion cells in the mouse. Nature 529, 345–350. doi:10.1038/nature16468

Bahl, A., Ammer, G., Schilling, T., Borst, A., 2013. Object tracking in motion-blind flies.

Nat Neurosci 16, 730–8. doi:10.1038/nn.3386

Bahl, A., Serbe, E., Meier, M., Ammer, G., Borst, A., 2015. Neural Mechanisms for Drosophila Contrast Vision. Neuron 88, 1240–1252. doi:10.1016/j.neuron.2015.11.004

Barnett, P.D., Nordström, K., O'Carroll, D.C., 2007. Retinotopic Organization of Small-Field-Target-Detecting Neurons in the Insect Visual System. Curr. Biol. 17, 569–578. doi:10.1016/j.cub.2007.02.039

Behnia, R., Desplan, C., 2015. Visual circuits in flies: Beginning to see the whole picture. Curr. Opin. Neurobiol. doi:10.1016/j.conb.2015.03.010

Bidaye, S.S., Machacek, C., Wu, Y., Dickson, B.J., 2014. Neuronal Control of Drosophila Walking Direction. Science (80-.). 344, 97–101. doi:10.1126/science.1249964

Chen, S., Lee, A.Y., Bowens, N.M., Huber, R., Kravitz, E.A., 2002. Fighting fruit flies: a model system for the study of aggression. Proc. Natl. Acad. Sci. U. S. A. 99, 5664–8. doi:10.1073/pnas.082102599

Coen, P., Xie, M., Clemens, J., Murthy, M., 2016. Sensorimotor Transformations Underlying Variability in Song Intensity during Drosophila Courtship. Neuron 89, 629–644. doi:10.1016/j.neuron.2015.12.035

Collett, T., Collett, 1971. visual neurones for tracking moving targets. Nature 232, 127–130. doi:10.1038/232127a0

Cook, R., 1979. The courtship tracking of Drosophila melanogaster. Biol. Cybern. 34, 91–106. doi:10.1007/BF00365473

De La Flor, M., Chen, L., Manson-Bishop, C., Chu, T.C., Zamora, K., Robbins, D., Gunaratne, G., Roman, G., 2017. Drosophila increase exploration after visually detecting predators. PLoS One 12, 1–17. doi:10.1371/journal.pone.0180749

Ellis, E.M., Gauvain, G., Sivyer, B., Murphy, G.J., 2016. Shared and distinct retinal input to the mouse superior colliculus and dorsal lateral geniculate nucleus. J. Neurophysiol. 116, 602–10. doi:10.1152/jn.00227.2016

Fischbach, K.-F., Dittrich, a P., 1989. The optic lobe of Drosophila melanogaster. I: A. Golgi analysis of wild-type structure. Cell Tissue Res 258, 441–475. doi:doi: 10.1007/BF00218858

Gale, S.D., Murphy, G.J., 2016. Active Dendritic Properties and Local Inhibitory Input Enable Selectivity for Object Motion in Mouse Superior Colliculus Neurons. J. Neurosci. 36, 9111–23. doi:10.1523/JNEUROSCI.0645-16.2016

Gale, S.D., Murphy, G.J., 2014. Distinct representation and distribution of visual information by specific cell types in mouse superficial superior colliculus. J. Neurosci. 34, 13458–71. doi:10.1523/JNEUROSCI.2768-14.2014

Gao, S., Takemura, S. ya, Ting, C.Y., Huang, S., Lu, Z., Luan, H., Rister, J., Thum, A.S., Yang, M., Hong, S.T., Wang, J.W., Odenwald, W.F., White, B.H., Meinertzhagen, I.A., Lee, C.H., 2008. The Neural Substrate of Spectral Preference in Drosophila. Neuron 60, 328–342. doi:10.1016/j.neuron.2008.08.010

Gonzalez-Bellido, P.T., Wardill, T.J., Juusola, M., 2011. Compound eyes and retinal information processing in miniature dipteran species match their specific ecological demands. Proc. Natl. Acad. Sci. U. S. A. 108, 4224–9.

doi:10.1073/pnas.1014438108

Hubel, D.H., Wiesel, T.N., 1965. Receptive Fields and Functional Architecture in Two Nonstriate Visual Areas (18 and 19) of the Cat. J. Neurophysiol. 28, 229–289.

Hubel, D.H., Wiesel, T.N., 1962. Receptive fields, binocular interaction and functional architecture in the cat's visual cortex. J. Physiol. 160, 106–154.2. doi:10.1523/JNEUROSCI.1991-09.2009

Kacsoh, B.Z., Lynch, Z.R., Mortimer, N.T., Schlenke, T.A., 2013. Fruit Flies Medicate Offspring After Seeing Parasites. Science (80-.). 339, 947–950. doi:10.1126/science.1229625

Keleş, M.F., Frye, M.A., 2017. Object-detecting neurons in Drosophila. Curr. Biol. 27, 680–687.

Kim, A.J., Fitzgerald, J.K., Maimon, G., 2015. Cellular evidence for efference copy in Drosophila visuomotor processing. Nat. Neurosci. 18, 1247–1255. doi:10.1038/nn.4083

Kim, T., Kerschensteiner, D., 2017. Inhibitory Control of Feature Selectivity in an Object Motion Sensitive Circuit of the Retina. Cell Rep. 19, 1343–1350. doi:10.1016/j.celrep.2017.04.060

Kim, T., Soto, F., Kerschensteiner, D., Meister, M., Pastan, I., Nakanishi, S., Feldheim, D., Kandler, K., Noebels, J., Glowatzki, E., Lustig, L., Edwards, R., 2015. An excitatory amacrine cell detects object motion and provides feature-selective input to ganglion cells in the mouse retina. Elife 4, E2391–E2398. doi:10.7554/eLife.08025

Klapoetke, N.C., Murata, Y., Kim, S.S., Pulver, S.R., Birdsey-Benson, A., Cho, Y.K., Morimoto, T.K., Chuong, A.S., Carpenter, E.J., Tian, Z., Wang, J., Xie, Y., Yan, Z., Zhang, Y., Chow, B.Y., Surek, B., Melkonian, M., Jayaraman, V., Constantine-Paton, M., Wong, G.K.-S., Boyden, E.S., 2014. Independent optical excitation of distinct neural populations. Nat. Methods 11, 338–46. doi:10.1038/nmeth.2836

Lettvin, J., Maturana, H., McCulloch, W., Pitts, W., 1959. What the Frog's Eye Tells the Frog's Brain. Proc. IRE 47, 1940–1951. doi:10.1109/JRPROC.1959.287207

Levick, W.R., 1967. Receptive fields and trigger features of ganglion cells in the visual streak of the rabbit's retina. J. Physiol. 188, 285–307. doi:10.1113/jphysiol.1967.sp008140

Lin, T., Luo, J., Shinomiya, K., Ting, C., Lu, Z., Meinertzhagen, I.A., Lee, C., 2016. Mapping Chromatic Pathways in the Drosophila Visual System 227, 213–227. doi:10.1002/cne.23857

Maimon, G., Straw, A.D., Dickinson, M.H., 2008. A Simple Vision-Based Algorithm for Decision Making in Flying Drosophila. Curr. Biol. 18, 464–470. doi:10.1016/j.cub.2008.02.054

Maisak, M.S., Haag, J., Ammer, G., Serbe, E., Meier, M., Leonhardt, A., Schilling, T., Bahl, A., Rubin, G.M., Nern, A., Dickson, B.J., Reiff, D.F., Hopp, E., Borst, A., 2013. A directional tuning map of Drosophila elementary motion detectors. Nature 500, 212–6. doi:10.1038/nature12320

Markow, T.A., 1975. Effect of light on egg-laying rate and mating speed in phototactic strains of Drosophila. Nature 258, 712–714. doi:10.1038/258712a0

Mauss, A.S., Vlasits, A., Borst, A., Feller, M., 2017. Visual Circuits for Direction Selectivity. Annu. Rev. Neurosci. 40, 211–230. doi:10.1146/annurev-neuro-072116-031335

Mischiati, M., Lin, H.-T., Herold, P., Imler, E., Olberg, R., Leonardo, A., 2014. Internal models direct dragonfly interception steering. Nature 517, 333–338. doi:10.1038/nature14045

Mu, L., Ito, K., Bacon, J.P., Strausfeld, N.J., 2012. Optic Glomeruli and Their Inputs in Drosophila Share an Organizational Ground Pattern with the Antennal Lobes. J. Neurosci. 32, 6061–6071. doi:10.1523/JNEUROSCI.0221-12.2012

Muijres, F.T., Elzinga, M.J., Melis, J.M., Dickinson, M.H., 2014. Flies Evade Looming Targets by Executing Rapid Visually Directed Banked Turns. Science (80-.). 344, 172–177. doi:10.1126/science.1248955

Nordström, K., 2012. Neural specializations for small target detection in insects. Curr. Opin. Neurobiol. 22, 272–278. doi:10.1016/j.conb.2011.12.013

O'Carroll, D., 1993. Feature-detecting neurons in dragonflies. Nature 362, 541–543. doi:10.1038/362541a0

Olberg, R.M., 2012. Visual control of prey-capture flight in dragonflies, Current Opinion in Neurobiology. Elsevier Current Trends. doi:10.1016/j.conb.2011.11.015

Olberg, R.M., Seaman, R.C., Coats, M.I., Henry, A.F., 2007. Eye movements and target fixation during dragonfly prey-interception flights. J. Comp. Physiol. A 193, 685–693. doi:10.1007/s00359-007-0223-0

Otsuna, H., Ito, K., 2006. Systematic analysis of the visual projection neurons of

Drosophila melanograster. I. Lobula-specific pathways. J. Comp. Neurol. 497, 928–958. doi:10.1002/cne.21015

Parigi, A., Porter, C., Cermak, M., Pitchers, W.R., Dworkin, I., 2014. How predator hunting-modes affect prey behaviour: Capture deterrence in Drosophila melanogaster. bioRxiv 10330. doi:10.1101/010330

Pick, S., Strauss, R., 2005. Goal-driven behavioral adaptations in gap-climbing Drosophila. Curr. Biol. 15, 1473–1478. doi:10.1016/j.cub.2005.07.022

Preuss, S.J., Trivedi, C.A., vom Berg-Maurer, C.M., Ryu, S., Bollmann, J.H., 2014. Classification of Object Size in Retinotectal Microcircuits. Curr. Biol. 24, 2376–2385. doi:10.1016/j.cub.2014.09.012

Robie, A.A., Straw, A.D., Dickinson, M.H., 2010. Object preference by walking fruit flies, *Drosophila melanogaster*, is mediated by vision and graviperception. J. Exp. Biol. 213, 2494–2506. doi:10.1242/jeb.041749

Sanes, J.R., Zipursky, S.L., 2010. Design Principles of Insect and Vertebrate Visual Systems, Neuron. doi:10.1016/j.neuron.2010.01.018

Schnell, B., Joesch, M., Forstner, F., Raghu, S. V, Otsuna, H., Ito, K., Borst, A., Reiff, D.F., 2010. Processing of horizontal optic flow in three visual interneurons of the Drosophila brain. J. Neurophysiol. 103, 1646–1657. doi:10.1152/jn.00950.2009

Semmelhack, J.L., Donovan, J.C., Thiele, T.R., Kuehn, E., Laurell, E., Baier, H., Blondel, M., Prettenhofer, P., Weiss, R., Dubourg, V., 2014. A dedicated visual pathway for prey detection in larval zebrafish. Elife 3, E2391–E2398. doi:10.7554/eLife.04878

Sen, R., Wu, M., Branson, K., Robie, A., Rubin, G.M., Dickson, B.J., 2017. Moonwalker Descending Neurons Mediate Visually Evoked Retreat in Drosophila. Curr. Biol. 27, 766–771. doi:10.1016/j.cub.2017.02.008

Sherk, T.E., 1978. Development of the compound eyes of dragonflies (odonata). III. Adult compound eyes. J. Exp. Zool. 203, 61–79. doi:10.1002/jez.1402030107

Sokolowski, M.B., 2001. Drosophila: Genetics meets behaviour. Nat. Rev. Genet. 2, 879–890. doi:10.1038/35098592

Spieth, H.T., Hsu, T.C., 1950. The Influence of Light on the Mating Behavior of Seven Species of the Drosophila melanogaster Species Group. Evolution (N. Y). 4, 316. doi:10.2307/2405598

Strother, J.A., Wu, S.T., Wong, A.M., Nern, A., Rogers, E.M., Le, J.Q., Rubin, G.M., Reiser, M.B., 2017. The Emergence of Directional Selectivity in the Visual Motion Pathway of Drosophila. Neuron 94, 168–182.e10. doi:10.1016/j.neuron.2017.03.010

von Reyn, C.R., Nern, A., Williamson, W.R., Breads, P., Wu, M., Namiki, S., Card, G.M., 2017. Feature Integration Drives Probabilistic Behavior in the Drosophila Escape Response. Neuron 94, 1190–1204. doi:10.1016/j.neuron.2017.05.036

Vosshall, L.B., Wong, A.M., Axel, R., 2000. An Olfactory Sensory Map in the Fly Brain. Cell 102, 147–159. doi:10.1016/S0092-8674(00)00021-0

Wiederman, S.D., Fabian, J.M., Dunbier, J.R., O'Carroll, D.C., 2017. A predictive focus of gain modulation encodes target trajectories in insect vision. Elife 6, e26478. doi:10.7554/eLife.26478

Wiederman, S.D., O'Carroll, D.C., 2013. Selective attention in an insect visual neuron. Curr. Biol. 23, 156–161. doi:10.1016/j.cub.2012.11.048

Wu, M., Nern, A., Williamson, W.R., Morimoto, M.M., Reiser, M.B., Card, G.M., Rubin, G.M., 2016. Visual projection neurons in the Drosophila lobula link feature detection to distinct behavioral programs. Elife 5. doi:10.7554/eLife.21022

Zabala, F., Polidoro, P., Robie, A., Branson, K., Perona, P., Dickinson, M.H., 2012. A simple strategy for detecting moving objects during locomotion revealed by animal-robot interactions. Curr. Biol. 22, 1344–1350. doi:10.1016/j.cub.2012.05.024

Zhang, Y., Kim, I.-J., Sanes, J.R., Meister, M., 2012. The most numerous ganglion cell type of the mouse retina is a selective feature detector. Proc. Natl. Acad. Sci. doi:10.1073/pnas.1211547109

Chapter 2

Object-detecting neurons in *Drosophila*

Summary

Many animals rely on vision to detect objects such as conspecifics, predators, and prey. Hypercomplex cells found in feline cortex and small target motion detectors found in dragonfly and hoverfly optic lobes demonstrate robust tuning for small objects with weak or no response to larger objects or movement of the visual panorama (Hubel and Wiesel, 1962; Nordström and O'Carroll, 2006; O'Carroll, 1993). However, the relationship between anatomical, molecular, and functional properties of object detection circuitry is not understood. Here, we characterize a specialized object detector in Drosophila, the lobula columnar neuron LC11 (Otsuna and Ito, 2006). By imaging calcium dynamics with two-photon excitation microscopy we show that LC11 responds to the omni-directional movement of a small object darker than the background, with little or no responses to static flicker, vertically elongated bars, or panoramic gratings. LC11 dendrites innervate multiple layers of the lobula, and each dendrite spans enough columns to sample 75-degrees of visual space, yet the area that evokes calcium responses is only 20-degrees wide, and shows robust responses to a 2.2-degree object spanning less than half of one facet of the compound eye. The dendrites of neighboring LC11s encode object motion retinotopically, but the axon terminals fuse into a glomerular structure in the central brain where retinotopy is lost. Blocking inhibitory ionic currents abolishes small object sensitivity and facilitates responses to elongated bars and gratings. Our results reveal high acuity object motion detection in the *Drosophila* optic lobe.

Results and Discussion

Whether flying or walking, flies readily orient toward large moving objects such as elongated vertical bars or edges representing landscape features, and this behavior is mediated by interactions between motion vision and motion-independent feature detection (Aptekar et al., 2012; Bahl et al., 2015, 2013; Poggio and Reichardt, 1976). Flies are able to perform some object-directed behaviors when directionally selective columnar motion detectors (T4 and T5) supplying the third optic ganglion (lobula plate) are silenced (Bahl et al., 2015, 2013; Coen et al., 2016). This finding supports the existence of object detection circuitry that acts independently from the canonical motion vision pathway (Bahl et al., 2013). Whereas many of the cells, circuits and computations for motion processing by T4 and T5 and the downstream lobula plate are becoming ever clearer (Ammer et al., 2015; Joesch et al., 2010; Maisak et al., 2013; Meier et al., 2014), the circuitry and functional role of the neighboring neuropile, the lobula, which houses 80% of all neurons in the lobula complex (Strausfeld, 1976), is poorly understood in *Drosophila*.

The lobula contains more than 22 types of visual projection neurons (VPNs) including lobula columnar (LC) neurons that project to the ventrolateral protocerebrum (VLPR) and form synapse-rich output domains called optic glomeruli for their structural similarity to olfactory glomeruli (Otsuna and Ito, 2006; Panser et al., 2016; Wu et al., 2016). Neurons downstream of LCs that interconnect multiple optic glomeruli in the central brain respond to small objects (Kim et al., 2015), raising the possibility that select LCs may themselves be tuned to small objects. Optophysiological and electrophysiological methods have demonstrated that several LCs are broadly sensitive to visual features

such as edges or bars (Aptekar et al., 2015; Mu et al., 2012), yet no study to date has thoroughly explored LCs with small two-dimensional objects.

We visually screened the publicly-available Janelia Gal4 lines (Jenett et al., 2012) and identified the R22H02-Gal4 driver which labels ~51 LC11s (±4, n=5) and each LC11 neuron has dendritic arborizations in layers 2,3,4 and 5 of the lobula (Figure 1A-C Figure S1A and C, (Wu et al., 2016)). The dendrites of a single LC11 span 14-15 lobula columns in the dorso-ventral axis and 6-8 columns in the antero-posterior axis (Figure 1 C and D). Taking into account that LC11 dendrites form an ellipse in the lobula (Figure 1E), we estimated the total span of a single LC11 to be 65 to 85 neighboring columns thereby comprising a 'multi-pixel' neuron. Considering the dendritic span (~15x8 columns), the number of LC11 cells (~50), and the full array of retinal ommatidia and neuropile columns (~28x28), it would seem that LC11 dendrites must overlap with one another rather extensively. Multicolor stochastic labeling of individual cells confirmed that LC11s overlap rather than tile the lobula (Figure 1F-I). Sampling the inputs of many columns could underlie spatial pooling important for increased photon capture in dim light (Warrant et al., 2004).

Previous work suggested that all LC11 output synapses are confined to the cognate glomerulus within the posterior VLP (PVLP) (Otsuna and Ito, 2006; Panser et al., 2016). We observe presynaptic sites not only in the PVLP glomerulus but also within layer 5 innervations of LC11 (Figure S1A and S1B), consistent with other recent findings by a recent article (Wu et al., 2016). A second distinct cell labeled by our Gal4 line is intrinsic to the lobula near the base of LC11 dendrites (Figure S1C, and Supplemental Experimental Procedures). Calcium imaging from dendrites could have been

contaminated by the intrinsic cell, but this seems unlikely since dendritic responses were consistently identical to cell body and axon terminal responses in LC11 (see below).

By contrast to the retinotopic organization of the columnar dendrites in the lobula, labeling a single LC11 neuron reveals spatially-distributed presynaptic terminals ramifying throughout the output glomerulus formed by LC11 terminals (Figure 1Bi-ii). Furthermore, multicolor labeling of two individual LC11 cells (Figure S1D) shows fully interspersed axon terminals (Figures S1E, F). This convergent organization indicates the loss of retinotopic structure by LC11 within the glomerulus, consistent with findings in other LCs (Panser et al., 2016; Wu et al., 2016).

To physiologically characterize LC11, we utilized GCaMP6m under two-photon imaging (Figure 1J, K) to record LC11 dendrites, axon terminals, and cell bodies (see Figure S1G-I for ROI images) in response to an object that may represent another fly nearby or a larger animal moving at a distance, a vertical bar that may represent a landscape feature such as a plant stalk, and a rotating wide-field grating representing optic flow generated during self-motion. We recorded from the axon terminals of LC11 (Figure S1I) and observed large responses to a 30 by 8-degree object (Figure 1L). The response diminished markedly for the vertical bar, and there was no response to the wide-field grating (Figure 1L). We tested whether LC11 is necessary for avoidance of similarly sized objects in flight (Maimon et al., 2008), but did not observe a clear phenotype (Figure S1J-L). LC11 could instead contribute to social behaviors such as courtship (Agrawal et al., 2014; Coen et al., 2016). Alternatively, given the complex spatial interactions of LC11 and its normal mode of action by individual members of the

columnar array, activating or inactivating the entire population may produce spurious effects within the visual system.

Drosophila can detect and respond to objects that appear smaller than 5° (Zabala et al., 2012). We found that a moving 2.2° object drove LC11 responses well above noise and greater than half-amplitude response to a 4.4° object (Figure 1M). Both objects span less than one inter-ommatidial separation angle of 5° (Heisenberg and Wolf, 1984). To confirm that flies are capable of perceiving such small objects on our LED display, we used a systems identification method during tethered flight (Theobald et al., 2010) to show robust steering responses to either a single pixel object or two-pixel object displaced in single-pixel increments (Figure 1M inset). In principle, any photoreceptor could respond to the luminance decrement generated by an object spanning less than its total acceptance angle, yet it is remarkable that simple hyperacuity has been documented within lobula neurons of hoverflies (Nordström and O'Carroll, 2006) and more recently within *Drosophila* photoreceptors (Juusola et al., 2016).

We next compared the calcium response dynamics within dendrites, cell bodies, and axon terminals in the same preparation. Normalized response trajectories demonstrated that dendrite and terminal responses were temporally synchronized (Figure 1N), but by comparison cell bodies exhibited a significantly delayed response onset (Figure 1O) followed by a slow decay to baseline. These differences may be attributed to the unipolar morphology of some invertebrate neurons such as LC11, in which the cell body is situated at the end of a long neurite and does not participate in synaptic integration.

Despite the slow response kinetics, imaging from the cell bodies is required to access individual neurons within the palisade of labeled LC11 cells due to the spatial intermingling of their dendrites and axon terminals (Figure S1D-F). To map the receptive field of individual LC11s we swept an 8.8° square object in horizontal and vertical directions at each elevation and azimuthal angle, respectively (Figure 2A). For each LC11 recording, peak ΔF/F values were fit to Gaussian functions of azimuth and elevation and used to estimate the two-dimensional spatial receptive field (Figure 2B and S2). We enclosed the spatial receptive field with a contour representing the full-width at 25% max of the Gaussian fits (Figure 2B, see Supplemental Experimental Procedures). We were generally able to record several distinct LC11 cell bodies from each preparation (Figure 2C). Some receptive fields we sampled overlapped, providing functional evidence that individual LC11s have overlapping dendrites (Figure 2C). Although we did not record from all LC11s, the receptive fields of those we sampled were distributed throughout the fronto-lateral visual field (Figure 2D and D'). The average receptive field size was 24.1° by 18.8° with standard deviation of 5.7° and 5.7°, respectively, measured from 27 individual cell recordings. The functional receptive field size is well below the anatomical dendritic field size (70°-75° by 30°-40°, Figure 1), a property unique to LC11 by comparison to neurons of the lamina, medulla or lobula plate identified to date (Behnia et al., 2014; Schnell et al., 2010; Tuthill et al., 2014).

To confirm whether or not the population of LC11 dendrites samples the full visual field in a retinotopic manner, we imaged from dendritic arborizations of many LC11s simultaneously and scanned an object horizontally at varying elevation angles (Figure 2E). Objects that are presented at higher elevations elicited responses from anteriorly

located dendrites (Figure 2E'). Shifting the object from higher to lower elevations on the display corresponded to shifts in calcium responses from anterior to posterior dendrites (Figure 2E') confirming the retinotopic organization of LC11 dendritic inputs and suggesting that the visual field is sampled uniformly.

Given the sluggish on and off response kinetics observed in the cell bodies (Figure 1N), the tight temporal coupling between GCaMP responses in the dendrites and axon terminals (Figure 1N), and the innervation by individual LC11 cells throughout the output glomerulus (Figure 1Bi-ii, Figure S1E and F), we characterized the object response properties of LC11 with recordings from the axon terminals in the VLPR. Small target motion detectors (STMDs) examined to date in the dragonfly (Wiederman et al., 2013) and hoverfly (Nordström and O'Carroll, 2006) show preference for objects darker than the background. We therefore presented a light object moving across a dark background (ON) and dark object moving on a light background (OFF) (Figure 3A). Our results indicate that LC11 responds to both OFF and ON stimuli to varying extent, showing significant preference for OFF (Figure 3A', paired t-test $p<0.001$). Another characteristic feature of STMDs is flicker insensitivity (Barnett et al., 2007). Stimulating luminance increments (ON) or decrements (OFF) by a stationary object localized within the receptive failed to elicit responses in LC11 terminals (Figure 3A'').

We next systematically varied the brightness of an object moving across a fixed intensity background (Figure 3B). Interestingly, reduction of the OFF-object contrast from 100% to 30% nearly doubled the amplitude of the calcium response (Figure 3B'). The object size in these experiments (30°) was chosen based on prior behavioral findings (Maimon et al., 2008), yet is larger than the estimated receptive field size (24°).

It is likely that a 30° object traverses both the excitatory receptive field and the inhibitory end zones. Reducing the contrast of a sufficiently large object may in turn reduce the inhibition generated by the object edges, resulting in increased response amplitude observed in LC11 for reduced contrast (Figure 3B'). LC11 responds only weakly to moving ON objects and does not show a significant change in amplitude across contrast (Figure 3B'), providing more evidence that LC11 is OFF object-specific. In flies, ON and OFF signals are separated within the lamina and relayed to deeper neuropils via parallel pathways (Ammer et al., 2015; Joesch et al., 2010; Meier et al., 2014; Serbe et al., 2016; Strother et al., 2014). Layers 2-4 of lobula are innervated by ON-selective Tm3 and OFF-selective Tm4 neurons (Fischbach and Dittrich, 1989; Wu et al., 2016). LC11 could potentially receive direct input from parallel ON and OFF channels *via* Tm3 and Tm4. Correlating a delayed OFF signal with an un-delayed ON signal arising from a single photoreceptor, i.e. within the same column, fully captured the contrast selectivity of the dragonfly STMD (Wiederman et al., 2013) and suggests a potential mechanism for small object sensitivity by LC11.

We next tested for directional selectivity by moving an 8.8° by 8.8° object in eight different directions. The recordings show that LC11 is not significantly selective for motion direction (Figure 3C and C', one-way ANOVA n.s.), although shows a slight trend for vertical directions, which is consistent with previous membrane patch clamp recordings from the soma (Mu et al., 2012). The glomerular output from the population of LC11s therefore serves to detect an object moving in any direction through the receptive field, a finding which we corroborated at the level of individual LC11s (Figure S3B and S3B').

The selectivity for small moving objects over elongated bars suggests that LC11 is size-tuned. The classical mechanism for size tuning is end-stopped inhibition, a hypercomplex property in which an elongated contour stimulates the inhibitory end zones of a receptive field with an excitatory center (Hubel and Wiesel, 1962). We parameterized the vertical dimension of a horizontally moving object of fixed width. Note that most of our experiments move an object in the horizontal (azimuthal) direction, and thus the characteristic object size is defined as the angle subtended by the vertical edge, perpendicular to the axis of movement. The optimum LC11 response occurs for a vertical extent of 8.8°, which is $1/4^{th}$ the vertical projection of the anatomical receptive field or ½ the functional receptive field (Figure 3D). The response magnitude asymptotes as the vertical size spans one functional receptive field (Figure 3D').

To test whether LC11 is size-tuned in the dimension parallel with the axis of motion, we presented objects of fixed vertical height and varying horizontal widths moving horizontally. For objects of increasing width, the response amplitude peaked near 4.4° (Figure 3E). The peak amplitude decreased until the width of the object was approximately one LC11 receptive (24°) (Figure 3E'). Note that the vertically oriented object moving horizontally generates more inhibition (Figure 3D, responses are clipped for the largest vertical bar) than an object oriented horizontally moving parallel to its orientation (Figure 3E, half-maximum response remain for largest horizontal bar). This would be expected because the former object stimulates more ommatidia, thus activates more LC receptive fields and their presynaptic inputs, and thereby generates more spatial inhibition. Furthermore, parameterizing the vertical size of the horizontally moving object (Figure 3D), we would expect each object to sweep through different

numbers of LC11 receptive fields in time, resulting in varying onset timing of the GCaMP signals in the glomerulus for each size (Figure 3D). By contrast, for the horizontally moving object, the spatial extent of the stimulus orthogonal to the motion vector is invariant and therefore the leading edge stimulates the same ensemble of LC11 receptive fields for each stimulus size. Hence, the onset delay is invariant for this experiment (Figure 3E).

Owing to the close match between the spatial extent of the receptive field and optimum object size, we reasoned that the end-stopped property of LC11 could be shaped by lateral inhibition generated by nearest neighbor LC11s. If so, then the end-stopped inhibition generated by two nearby objects should be fully relieved once the objects are separated by one receptive field increment. By presenting two 8.8° square objects moving horizontally, we confirmed that as spatial inhibition was released by increased object separation, response amplitude increased (Figure 3F). The separation distance had no effect on response amplitude once the two objects were separated by 18°, roughly the size of a single LC11's functional receptive field (Figure 3F'). Furthermore, separation distances flanking the preferred object size (8.8°) led to the biggest change in response amplitude. These results support the hypothesis that end-stopped inhibition occurs on the spatial scale of nearest neighbor LC11 functional receptive fields.

One consistent characteristic of the response to two objects is a 'double peak' for object separation less than 18° (Figure 3E). We did not observe this bi-phasic response when presenting the same stimuli in the reverse back-to-front direction (Figure S3A and A'). Thus, we attribute the 'double peak' phenomenon either to subtle differences in the spatial distribution of LC11 receptive fields converging in the axon terminals, or to

differences in the spatial properties of inhibition between the lateral-ventral field of view by comparison to the frontal-dorsal field.

Taken together, the results presented thus far implicate end-stop lateral inhibition in sculpting object response properties, suggesting that LC11 may receive GABAergic input. Previous immunohistochemical studies of the lobula indicate that antibodies targeting GABAergic signaling pathways such as glutamic acid decarboxylase (GAD), the $GABA_A$ receptor subunit RDL, and GABA itself, are present in a layer-specific manner (Buchner et al., 1988; Harrison et al., 1996). In particular, an enrichment of GABAergic neurotransmission, indicated by dense labeling of all three antibodies, is observed in layers 2 and 3 of the lobula. Our own co-labeling experiments indicate a strong overlap between the dendritic arborizations of LC11 and enriched vesicular GABA transporter (VGAT) staining (Figure 4A and C). In contrast, the dendrites of LC11 are spatially-excluded from layer 1, known to be enriched with cholinergic signaling within T5 cells (Figure 4B and D) (Mauss et al., 2014).

To test for functional consequences of GABAergic inhibition on the response properties of LC11, we imaged from the LC11 glomerular outputs before and after blocking $GABA_A$-mediated inhibitory currents with picrotoxin (PTX). Prior to PTX application, LC11 responded robustly to an object, showed a slight excitation in response to a bar, and was not at all excited by a wide-field grating (Figure 4E, F and G). Applying PTX in the perfusion saline within the same recording preparations resulted in strongly reduced object responses, large amplitude bar responses, and large amplitude sustained responses to wide-field motion (Figure 4E, F, and G). Remarkably, PTX not only resulted in a loss of selectivity for an object, but also small sensitivity to the object

(Figure 4E', F' and G'). Thus, inhibitory currents not only 'end-stop' LC11 to tune its size selectivity, similar currents also actively mediate the detection of small objects. By contrast, figure detecting cells (FD) of the lobula plate in larger flies are excited by small-field gratings and receive GABAergic inhibition from wide-field cells, yet under GABA-blockade FD continues to respond to small-field motion (Warzecha et al., 1993). In STMDs, small object tuning has been attributed to lateral inhibition at the level of pre-synaptic neighboring ON-OFF channels that are correlated and summed (Wiederman et al., 2013, 2008). However, in the absence of inhibition the model described in (Wiederman et al., 2013, 2008) predicts that STMDs would be driven by dark edges of any size. Our finding that small object detection itself requires intact inhibition (Figure 4E) may come to promote a revised model.

The finding that LC11 dendrites span 14-15 columns of the optic lobe yet the functional receptive field is the equivalent of 4-6 columns wide, with peak size tuning less than the equivalent of two columns, suggests complex inhibitory spatial interactions. We propose that an excitatory-center inhibitory-surround mechanism, driven by inhibition on the spatial scale of a neighboring LC11, spatially sharpens the receptive field of LC11 making it both sensitive and selective for small contrasting objects. In summary, we show the first comprehensive physiological characterization of object selectivity by a visual projection neuron in *Drosophila,* one that shares functional properties of object detectors in other insects and vertebrates.

Materials and Methods

Fly Stocks and Histology

Flies were raised on a standard cornmeal diet and kept at 25 °C on a 12 hrs light/ 12 hrs dark cycle. 3-7 day old female flies were used in all experiments. The following fly stocks were used: LC11 was labeled by R22H02-Gal4 (Bloomington ID: #49304), 20XUAS-GCaMP6m (#42748), 10XUAS-GFP (#32185), UAS-DenMark, UAS-syt.EGFP (#33065),and pJFRC49-10XUAS-IVS-eGFPKir2.1 (Janelia), pBDPGal4U ("empty-Gal4", Janelia). Single cell experiments were achieved by crossing R22H02 driver line to R57C10-Flp2::PEST driving the expression of a multi-color flip out cassette (#64089) and dissecting 2-3 day old flies. To achieve labeling of multiple LC11s with different epitopes we dissected 6-7 day old flies from the same cross. For inactivation experiments following genotypes were used: w-;;R22H02-Gal4/10XUAS-IVS-eGFPKir2.1 and w-;;R22H02-Gal4/pBDPGal4U. We used the following genotype for Figure S4: w-;20XUAS-GCaMP6m/+;R22H02-Gal4/20XUAS-TTS-Shi^{ts1}.

2-5 day old flies were dissected in PBS and fixed in 4% PFA for 25 minutes followed by 3x15 min washes in PBST (0.3% Triton). Brains were then blocked in 5% goat serum for 30 minutes and incubated in primary antibodies for 2 days at 4 °C. This was followed by 3x15 min washes in 0.3% PBST at RT and incubation in secondary antibodies for 2 days at 4 °C. Brains were mounted on glass slides in Vectashield mounting medium and imaged with a Zeiss LSM700 confocal microscope. Images were analyzed using ImageJ and single cells were traced using the simple neurite tracer. Stochastic labeling was done as described in (Nern et al., 2015). We used the following primary and secondary antibodies: mouse nc82 (1:10, Development Studies Hybridoma bank),

mouse anti-ChAT (1:25, DSHB), rabbit anti-VGAT (1:100, gift of D. Krantz), rabbit anti-dsRed (1:1000, Clontech #632496), rabbit anti-GFP (1:1000, Invitrogen), rabbit anti-HA (1:300, Cell Signaling Technologies), rat anti-FLAG (1:200, Novus Biologicals), goat anti-mouse AlexaFluor-488 (1:200, Invitrogen), goat anti-rabbit AlexaFluor-488 (1:200,Invitrogen), goat anti-mouse AlexaFluor-568 (1:200, Invitrogen), donkey anti-rabbit AlexaFluor-594 (1:500, Jackson Immuno Research).

Acquired Z-stacks of cell bodies labeled above the dorsal optic peduncle were used to manually count cell bodies. We have identified total of 4-5 cells that have cell bodies in the vicinity of LC11 somata. 2 of these cell bodies belong to a lobula intrinsic neurons (Loi, Figure S1C). This cell type innervate the boundary between layers 3 and 4 in the lobula and overlap with LC11. The overlap region is not extensive and it doesn't cover LC11 innervations in layer 2 and 5. To achieve LC11 specific calcium imaging we mainly targeted LC11 glomerulus in the Ventrolateral Protocerebrum (VLPR). Loi cells also have cell bodies located ventral to LC11 cell bodies which allowed us to target LC11 cell bodies specifically. Lastly, the responses from lobula where LC11 dendrites located and from the optic peduncle where LC11 cell bodies located matched the responses from LC11 glomerulus confirming that our imaging plane was specific to LC11.

Behavior

3- to 6- day old wild type flies were cold anesthetized and glued to a tungsten pin and placed in a 360° by 120° LED arena with each pixel subtending 3.75° at the eye. A white noise method was adapted from prior work (Theobald et al., 2010) to measure

fly's behavioral impulse response to a single display pixel or 2x2 pixel square centered near zero-degree azimuth and zero-degree elevation.

3-4 day old flies carrying either R22H02-Gal4 or empty-Gal4 with UAS-Kir2.1 cold anesthetized and glued to a tungsten pin as described before (Aptekar et al., 2015). Flies are incubated at room temperature 1-2 hours prior to the experiment. Experiment consisted of 3 stimuli (a 30° by 15° object, 30° by 120° bar and a wide field grating with a spatial frequency of 30°). Each stimulus presented in two directions (clockwise and counter clockwise) and each direction is repeated 8 times. Presentation order was randomized and each presentation consisted of 4 seconds stimulus presentation at 90°/sec. Between each presentation a 30° by 120° bar was presented under closed loop feedback control to ensure that the fly is actively engaging in the visual task and is oriented towards the visual midline. In Note that the bar sweeping across the visual midline is preceded by DWBA and the mean trace continues to rise as the bar moves from front to back (Figure S1J – bar tracking). By contrast, the steering effort in response to the small object crossing midline decreases (Figure S1K – object avoidance). Aside from an overall reduction in response amplitude generated by the empty Gal-4 genetic background, we observed no discernable effect of LC11 block on the qualitative responses to bar, object, or wide-field grating.

Wing beat data collected using Digidata 1440a digitizer and Axoscope 10 (Molecular Devices). Data are imported to MATLAB for offline analysis. Trials from individual flies were averaged and the first data point is subtracted from the averaged responses resulting in a single trace for each experimental condition for each fly. The data is filtered with a 200 Hz low-pass digital Butterworth filter to remove high frequency noise.

Calcium Imaging

Imaging was done as previously described [S3]. Briefly, flies were anesthetized on a cold block and placed in a hole cut from stainless steel shim centered in a custom made acetal holder. The head capsule and thorax were secured to the shim using UV-activated glue. The proboscis, antennae and legs were immobilized with low melt point beeswax. A small hole was cut with sharpened forceps (Dumont, #5SF) from the head cuticle above the posterior dorsal rim. M1 and M16 muscles were excised and an air sac was removed to enable optical access to the brain. The head was bathed in saline (103mM NaCl, 3mM KCl, 1.5mM CaCl2, 4mM $MgCl_2$, 26mM $NaHCO_3$, 1mM NaH_2PO_4, 10mM trehalose, 10mM glucose, 5mM TES, 2mM sucrose (Wilson et al., 2004)). Saline was perfused at 1.5 ml/min via a gravity drip system and the bath temperature was kept at 22 °C. LC11 neurons expressing GCaMP6m was imaged using a two-photon excitation scanning microscope (Intelligent Imaging Innovations). Images were acquired at 10 frames/sec, approximately 150X256 pixels with pixel spacing varying between 0.2 to 0.3 microns.

Picrotoxin (PTX) experiments were performed by diluting 1 mM PTX (P1675, Sigma) 100 mM NaCl stock solution in saline with a final concentration of 10 uM PTX. The PTX saline was perfused for 30-40 minutes prior to the imaging experiment. We observed transient responses in the LC11 glomerulus to light increments and decrements generated by turning the LED screen on and off after long periods of PTX perfusion (data not shown). However, these responses were very short by comparison to motion driven responses and could possibly be attributed to the release of inhibition within peripheral visual pathways (Freifeld et al., 2013)

Visual Stimulus

The 96x32 pixel LED display is cylindrical. The fly is placed 78mm from the display. The vertical elevation of the cylinder subtends 63.22 degrees at the eye. Each individual pixel subtends 2.2 degrees in the coronal plane, but the pixels at the top and bottom of the display are further away and thus subtend 1.63 degrees. The maximum apparent size distortion amounts to ¼ of one pixel. Given that our receptive field estimates are greater than the equivalent of 10 pixels on average, an error of ¼ pixel small would not change our results. Indeed, scrutinizing our data we found no relationship between the size of the vertical axis of individual LC11 receptive fields and their vertical elevation in the visual field, as would be expected from systematic over-estimate from uncorrected elevation perspective. For this reason, to our knowledge none of the many labs using this LED display correct for the varying distance to the pixels along the uncurved vertical dimension of the arena.

Object speed was 22 deg/sec for most of the experiments, which at 10Hz frame acquisition allowed the calcium response to be imaged at each display pixel displacement of the stimulus. In order to reduce the duration of one experiment, receptive fields were mapped using an object speed of 33 deg/sec. For each experiment described in the Results, presentation order was randomized and each stimulus condition was presented three times except for the experiments presented in Figure S4 and Figure S3B' which we presented the stimulus once. The LED arena was turned off for 4 seconds between each stimulus condition. In most experiments, the visual stimuli were presented in multiple directions but for clarity we present only front-

to-back since we show that LC11 is not directionally selective. Experimental details (size, contrast etc.) are written in the figure captions.

In Figure 3B and B' Weber Contrast is calculated by subtracting the light intensity of the object from the background and dividing by the background intensity.

Image Analysis

Acquired images were aligned to the first image using a novel motion correction algorithm (Dubbs et al., 2016) in ImageJ. When, by visual inspection, this method did not sufficiently stabilize in-plane motion we used a slice alignment algorithm that allowed us to choose a specific landmark on the image (ImageJ – Template Matching Plugin). Images that could not be aligned or contained persistent motion artifacts generated by the live fly were discarded. Aligned images were then exported to MATLAB and ROI selection was in accord with the anatomical region that was recorded. For images of the glomerular region, a single ROI was defined by setting a threshold for pixels equal or greater to two-times the mean of the entire image. The fluorescent value at all resultant pixels were summed at each time point and represented as a single time series trace. Cell body and dendritic ROIs were handpicked by either drawing a quadrilateral around dendritic regions, or a polygon around cell bodies. Each trace was then filtered using a Savitzky-Golay filter with a timespan of 150 ms. For each stimulus condition, repeated three trials were averaged and $\Delta F/F$ was calculated by dividing the signal by the mean intensity over the 2 seconds preceding stimulus motion and subtracting 1.

For receptive field mapping experiments, two matrices were generated with each vector representing the time series response of a single cell body to horizontal motion of an 8.8-by-8.8-degree object at each elevation angle, and vertical motion at each azimuthal angle, respectively. These two matrices were then downsampled to the step size of the stimulus and multiplied together to map the 2-D spatial receptive field. The mean vertical projection and mean horizontal projection were calculated from the multiplied matrices, and 1-D Gaussians were then fit to each of the two projections. Receptive field calculation was stopped and the recording was rejected if any of the fits had R^2 value lower than 0.90. Rejected receptive fields were due to overlap in the imaging frame. These recordings invariably resulted in non-Gaussian multi polar GCaMP responses. Receptive fields that passed these criteria were then reconstructed from the Gaussian fits and enclosed by the full-width at 25% maximum.

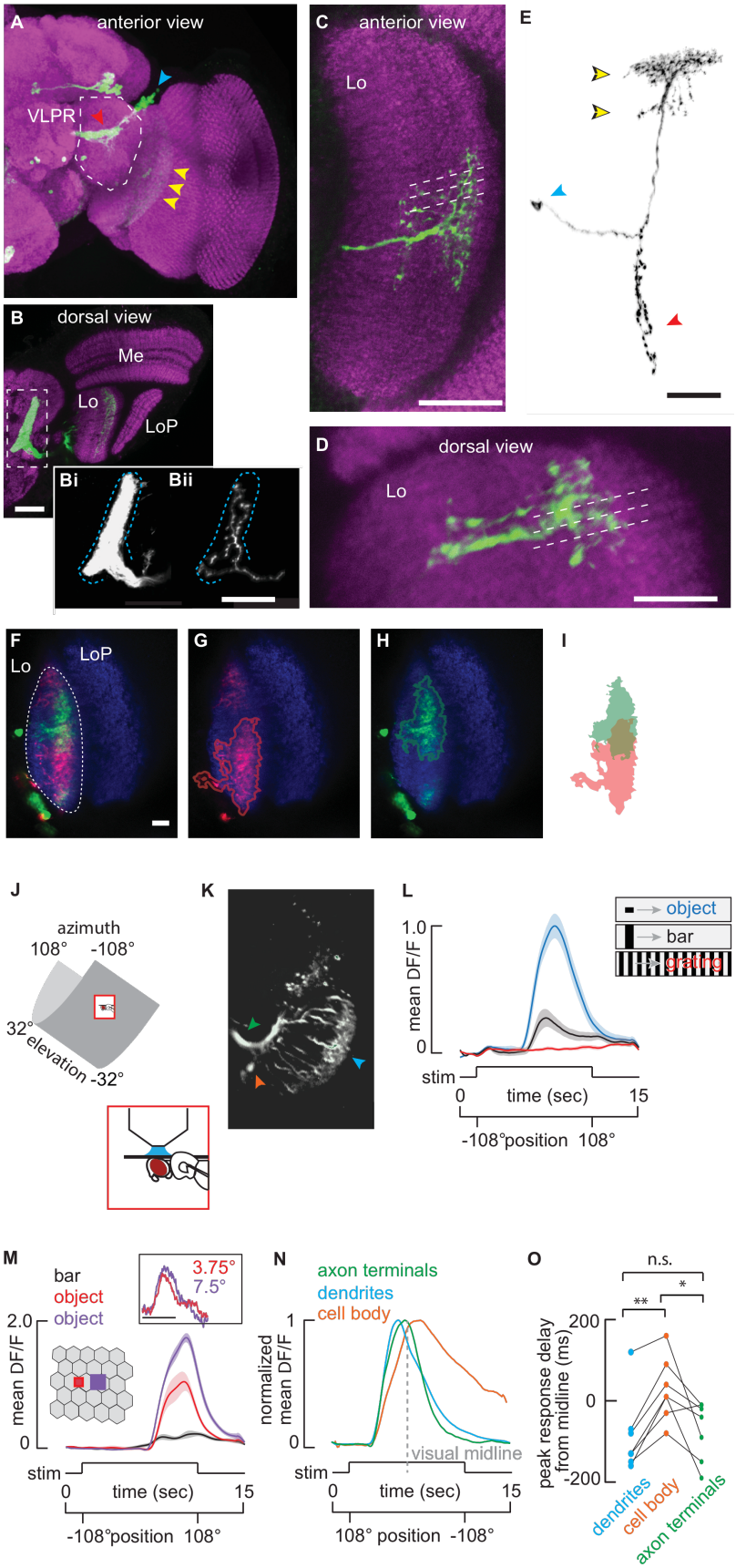
A
anterior view
VLPR
B
dorsal view
Me
Lo
LoP
Bi
Bii
C
anterior view
Lo
D
dorsal view
Lo
E
F
Lo
LoP
G
H
I
J
azimuth
108°
-108°
32°
elevation
-32°
K
L
object
bar
grating
1.0
mean DF/F
0
stim
0
time (sec)
15
-108°position
108°
M
bar
object
object
3.75°
7.5°
2.0
mean DF/F
0
stim
0
time (sec)
15
-108°position
108°
N
axon terminals
dendrites
cell body
1
normalized
mean DF/F
0
visual midline
stim
0
time (sec)
15
108° position
-108°
O
n.s.
*
**
200
peak response delay
from midline (ms)
0
-200
dendrites
cell body
axon terminals

Figure 2.1. **Anatomy and object selectivity of Lobula Columnar 11.** A) Maximum intensity projection of the anterior view of a brain from a fly expressing membrane tethered GFP under the control of R22H02-Gal4 and labeled with anti-GFP (green) and nc82 (magenta). Dashed lines indicate the boundary of the ventrolateral protocerebrum. Arrowheads indicate cellular compartments; blue-cell bodies, red-terminals, yellow-dendrites. B) Dorsally mounted view of R22H02-Gal4>UAS-mCD8::GFP flies. Dashed rectangle indicates the unique foot shaped LC11 glomerulus. Me: Medulla, Lo: Lobula, LoP: Lobula Plate. Comparison of the labeling of ~50 LC11s innervating the glomerulus (Bi) vs. stochastic labeling of a single LC11 (Bii). Single LC11 shows the full glomerular innervation with no evidence of retinotopic organization. Blue dashed line indicates the glomerular boundary. C) Anterior view of a stochastic labeling of a single LC11. Dashed lines indicate individual columns within the lobula. The dendritic arbor of a single LC11 covers about 14-15 lobula retinotopic columns in this plane. D) Dorsal view of a single LC11. Dendritic arbors span 6-7 columns in this plane. E) Morphology of a single LC11. Yellow arrows indicate the bistratified dendritic morphology of LC11 within lobula. Blue and red arrowheads indicate cell body and terminals respectively. All scale bars are 25 um. F-H) Single confocal plane images of multicolor stochastic labeling of LC11s. Multiple cells were labeled and tagged with myristoylated smGFP attached to either HA (green) or FLAG (red) epitopes. Neuropile is labeled with nc82 (blue). The lobula is traced with a dashed line. Scale bar is 10 um. G,H) Red and green channels are displayed separately, and labeling is traced to highlight dendritic overlap (I). See also Figure S1. J-O) 2-photon imaging. J) The fly's head is fixed and the surrounding LED arena covers 216° in azimuth and 63.2° in elevation. K) Image of LC11s

expressing GCaMP6m under two-photon microscopy. Arrowheads indicate dendrites (cyan), axon terminals forming optic glomerulus (green) and cell bodies (orange). L) Mean GCaMP6m (±S.E.M. shading) signal from LC11 glomerulus in response to the movement of a 30°by 8.8° object (blue), a 30° by 70° bar (black) and a wide-field grating (red, n = 7 flies). M) Mean GCaMP6m (±S.E.M. shading) signal from LC11 glomerulus in response to the movement of a 30° by 70° bar (black), a 2.2° square object (red) and a 4.4° square object (purple) (n = 6 flies). Inset: From tethered flies, normalized mean steering responses to single pixel impulsive displacement of objects, sizes indicated (scale bar: t=0-100 ms, n = 10 flies). N) Normalized mean ΔF/F of cell body (orange), dendrites (cyan) and axon terminals (green) responses to the movement of a 30° by 8.8° object as in C. Visual midline indicated with a dashed grey line. n = 7 flies. O) Comparison of the peak onset delay between the dendrites (blue), terminal (red), and cell body (black) (*$p<0.05$, **$p<0.01$, paired t-test, n = 7 flies). All visual stimuli moved at 22 °/sec.

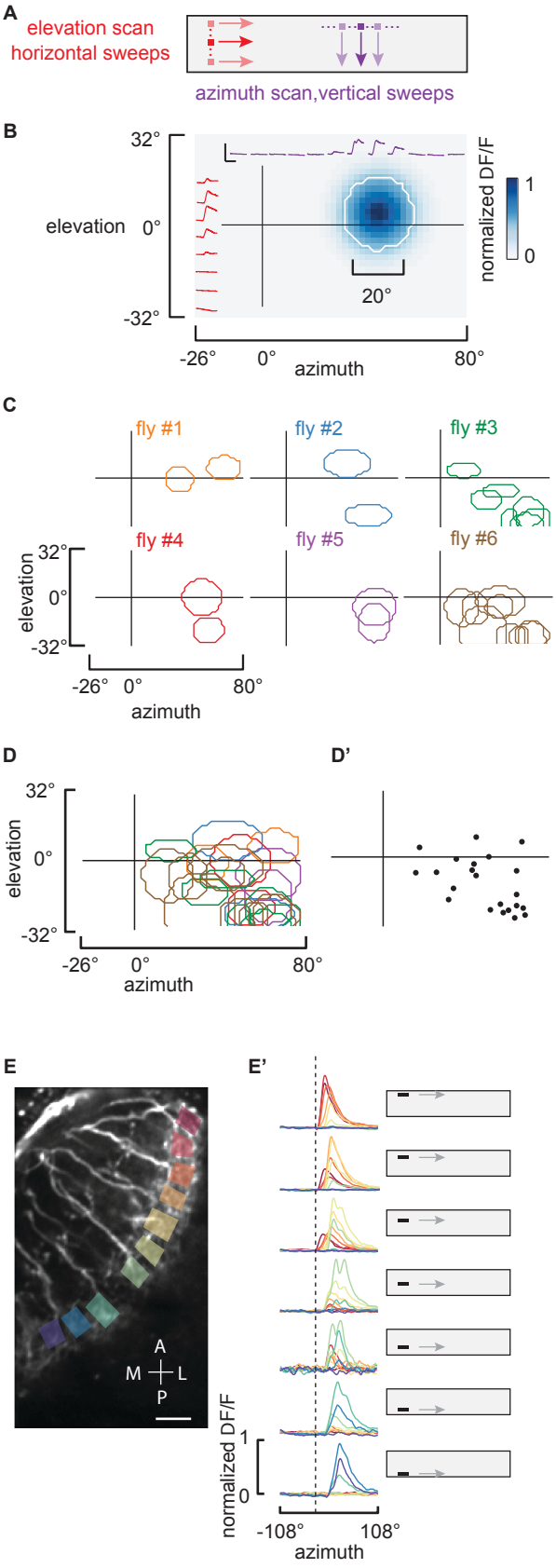
A
elevation scan
horizontal sweeps
azimuth scan,vertical sweeps
B
32°
elevation 0°
-32°
-26°
0°
azimuth
80°
20°
normalized DF/F
1
0
C
fly #1
fly #2
fly #3
fly #4
fly #5
fly #6
elevation
32°
0°
-32°
-26°
0°
80°
azimuth
D
D'
elevation
32°
0°
-32°
-26°
0°
80°
azimuth
E
A
M
L
P
E'
normalized DF/F
1
0
-108°
108°
azimuth

Figure 2.2. **Individual LC11 receptive fields.** A) Schematic of the experimental stimuli used to map individual LC11 receptive fields from individual cell body recordings. An 8.8° square dark object was scanned along non-overlapping trajectories along both horizontal and vertical paths at 33 °/sec. B) Reconstructed receptive field of a single LC11. Individual imaging responses from a single LC11 to the horizontal and vertical sweeps indicated in red and purple, respectively (scale bar inset represents 200% ΔF/F, 5 seconds). Reconstructed estimate of a single LC11 receptive field shown in blue (see Supplemental Experimental Procedures), the full-width at 25% max contour was drawn in white. C) Representative receptive field contours (25% max) from six preparations are mapped onto the projection of the visual display. D) 11 receptive fields from 6 flies are overlaid and color coded as in C. D') a dot is plotted at the centroid of each receptive field to indicate the spatial distribution of sampled LC11 recordings. E) To analyze the retinotopy in the dendrites of neighboring LC11 columnar cells, ROIs from separate dendritic compartments are indicated by colored box. An object swept was horizontally at elevations indicated by the cartoon display. ΔF/F responses from all 10 ROIs are overlaid for each elevation. E') To facilitate spatial comparisons, the responses are normalized to the maximum ΔF/F calcium signal at each ROI. Note that anterior (red) ROIs are activated by object motion across the top of the display, whereas posterior (blue) ROIs are activated by object motion across the bottom of the display. Dashed line indicates the earliest responses of anterior ROIs. Scale bar for the two-photon image represents 10 um. Abbreviations for anatomical directions; A: Anterior, P: Posterior, M: Medial and L: Lateral. See also Figure S2.

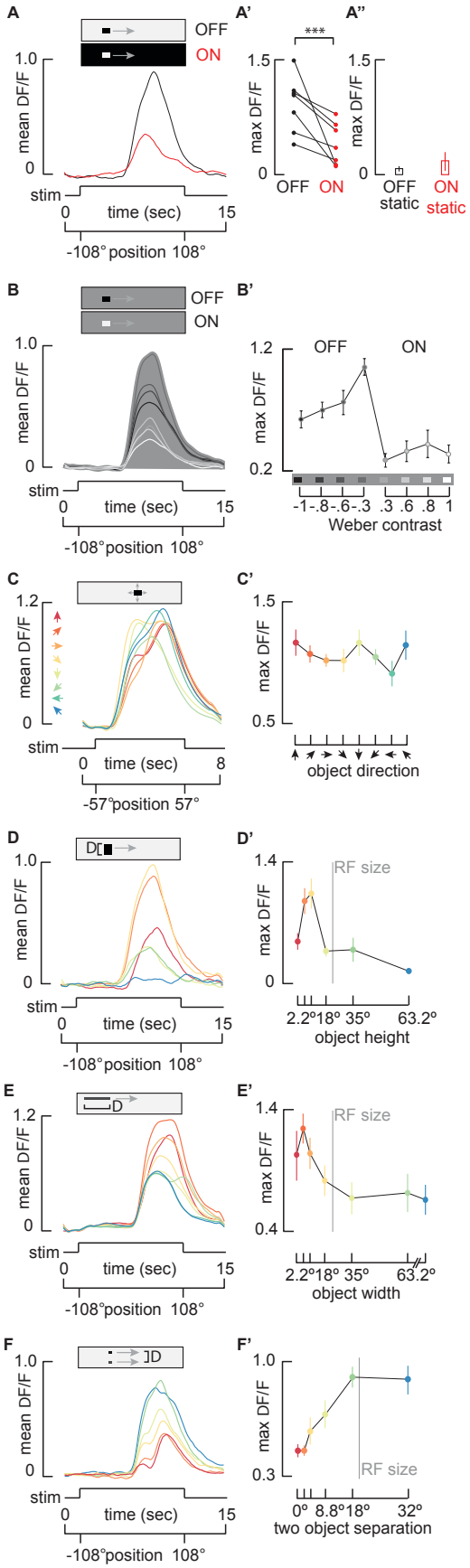
A
OFF
ON
1.0
mean DF/F
0
stim
0
time (sec)
15
-108° position 108°
A'
***
1.5
max DF/F
0
OFF ON
A''
1.5
max DF/F
0
OFF
static
ON
static
B
OFF
ON
1.0
mean DF/F
0
stim
0
time (sec)
15
-108° position 108°
B'
1.2
max DF/F
0.2
OFF
ON
-1 -.8 -.6 -.3 .3 .6 .8 1
Weber contrast
C
1.2
mean DF/F
0
stim
0
time (sec)
8
-57° position 57°
C'
1.5
max DF/F
0.5
object direction
D
1.0
mean DF/F
0
stim
0
time (sec)
15
-108° position 108°
D'
1.4
max DF/F
0
RF size
2.2° 18° 35° 63.2°
object height
E
1.2
mean DF/F
0
stim
0
time (sec)
15
-108° position 108°
E'
1.4
max DF/F
0.4
RF size
2.2° 18° 35° 63.2°
object width
F
1.0
mean DF/F
0
stim
0
time (sec)
15
-108° position 108°
F'
1.0
max DF/F
0.3
RF size
0° 8.8° 18° 32°
two object separation

Figure 2.3. **LC11 is contrast selective, omni-directional, and end-stopped on the spatial scale of one receptive field.** A) Mean GCaMP6m signal from the LC11 terminal output glomerulus in response to a 30°by 8.8° moving ON object (red) and moving OFF object (black, n = 7 flies). A'). Pairwise comparison of maximum ΔF/F of responses from each preparation (***p<0.001, paired t-test, n = 7 flies). A'') Average maximum responses (±S.E.M.) of LC11 glomerulus to a stationary 30°by 8.8°OFF and ON object placed within the hotspot of the receptive field (n = 6 flies). B) Mean GCaMP6m signal from the LC11 glomerulus in response to varying contrast objects. Grayscale of the filled area is used to indicate the intensity of the visual background, whereas grayscale of the response line indicates intensity of the stimulus object (n = 9 flies). The most contrasting objects do not elicit the maximum responses from LC11. B') Average of maximum responses (±S.E.M.) of the LC11 glomerulus to objects of varying contrast. Schematic on the x-axis shows the intensity of the background compared to each object. Weber contrast values are indicated numerically (see Supplemental Experimental Procedures, one-way ANOVA, n = 9 flies). C-F) LC11 glomerulus responses to parameterized direction (C, C'), vertical height (D, D') horizontal width (E, E'), and two-object separation distance (F, F'). Time series responses shown in A-F, and color-coded parameter values and maximum responses (±S.E.M) shown in C'-F'. C and C') LC11 is omni-directional. An 8.8° square object was moved in 8 different directions in 45° steps as indicated by color-coded arrowheads (n = 7 flies, see single cell responses in Figure S3). D and D') LC11 is vertically size tuned. A 30° wide object was moved on the same horizontal trajectory, with varied vertical heights: 2.2°, 4.4°, 8.8°, 18°, 35°, 73.2°, colors mapped to object size in B' (n = 7 flies). Vertical gray line

indicates average receptive field (RF) size (Figure 2). E and E') LC11 is horizontally size tuned. An object of fixed height (8.8°) and varied width: 2.2°, 4.4°, 8.8°, 18°, 35°, 70°, 210°, was moved horizontally (n = 15 flies). The leading edge of each object appeared on the LED display at the same time. Vertical gray line indicates average estimated functional RF size (Figure 2). F and F') LC11 is inhibited by a second object. Two 8.8° square objects moved on parallel trajectories. The distance between them was 0°, 2.2°, 4.4°, 8.8°, 18° and 32°, colors mapped to separation distance in C' (n = 6 flies). Vertical gray line indicates average RF size (Figure 2). See also Figure S3.

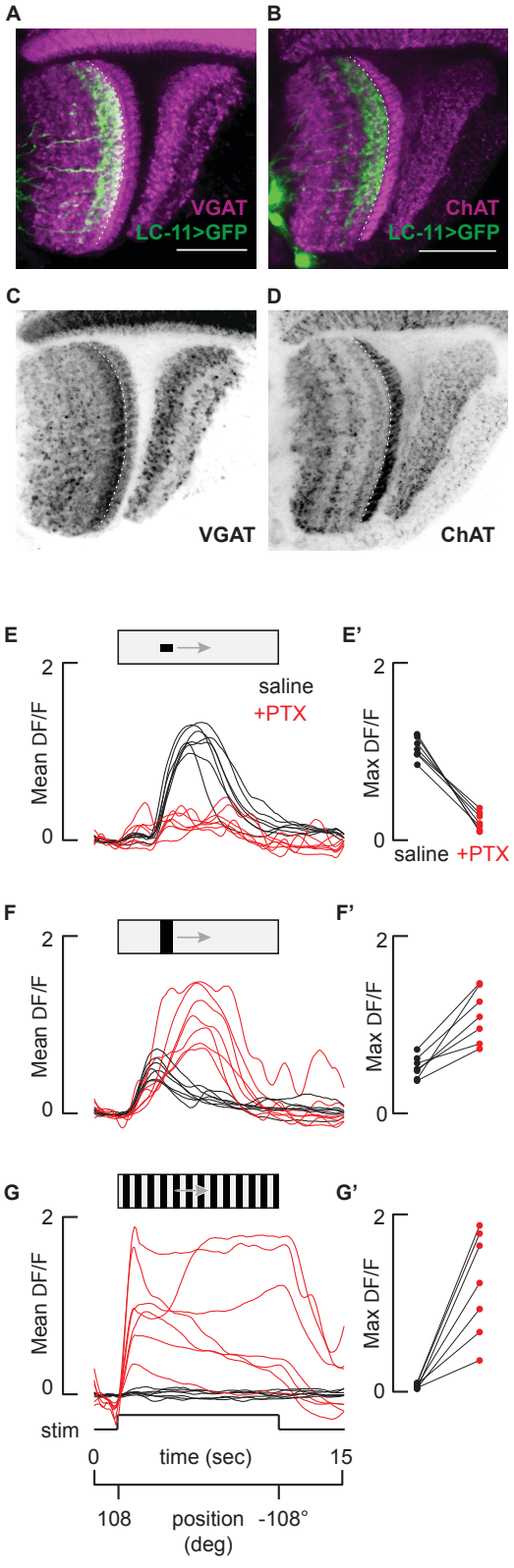
A
B
VGAT
LC-11>GFP
ChAT
LC-11>GFP
C
D
VGAT
ChAT
E
E'
saline
+PTX
Mean DF/F
Max DF/F
2
0
saline +PTX
F
F'
G
G'
stim
0
time (sec)
15
108
position
(deg)
-108°

Figure 2.4. **Both sensitivity and selectivity for objects by LC11 requires inhibition.** A and B) LC11 dendritic layer is enriched with the vesicular GABA transporter (VGAT), and the adjacent presumably presynaptic layer is enriched with choline acetyltransferase (ChAT). Dorsal view of GFP labeled LC11 neurons (green) co-labeled with either anti-ChAT (A, magenta) or VGAT (B, magenta). Dashed line indicates the border between the first and second lobula strata. Scale bars 25 um. C and D) Layering of VGAT and ChAT are highlighted with the same labeling as in A and B, but without LC11 overlaid. Scale bars are 25 um. E – G) Inhibition sculpts object responses and inhibits bar and grating responses. Time series glomerular LC11 responses from n = 7 flies in response to a 30°by 8.8° object (E), a 30° by 70° bar (F) and a wide-field grating (G) with (red) or without (black) 10 um picrotoxin. E' – G') Average maximum responses from each fly (E - G) with (red) or without (black) picrotoxin.

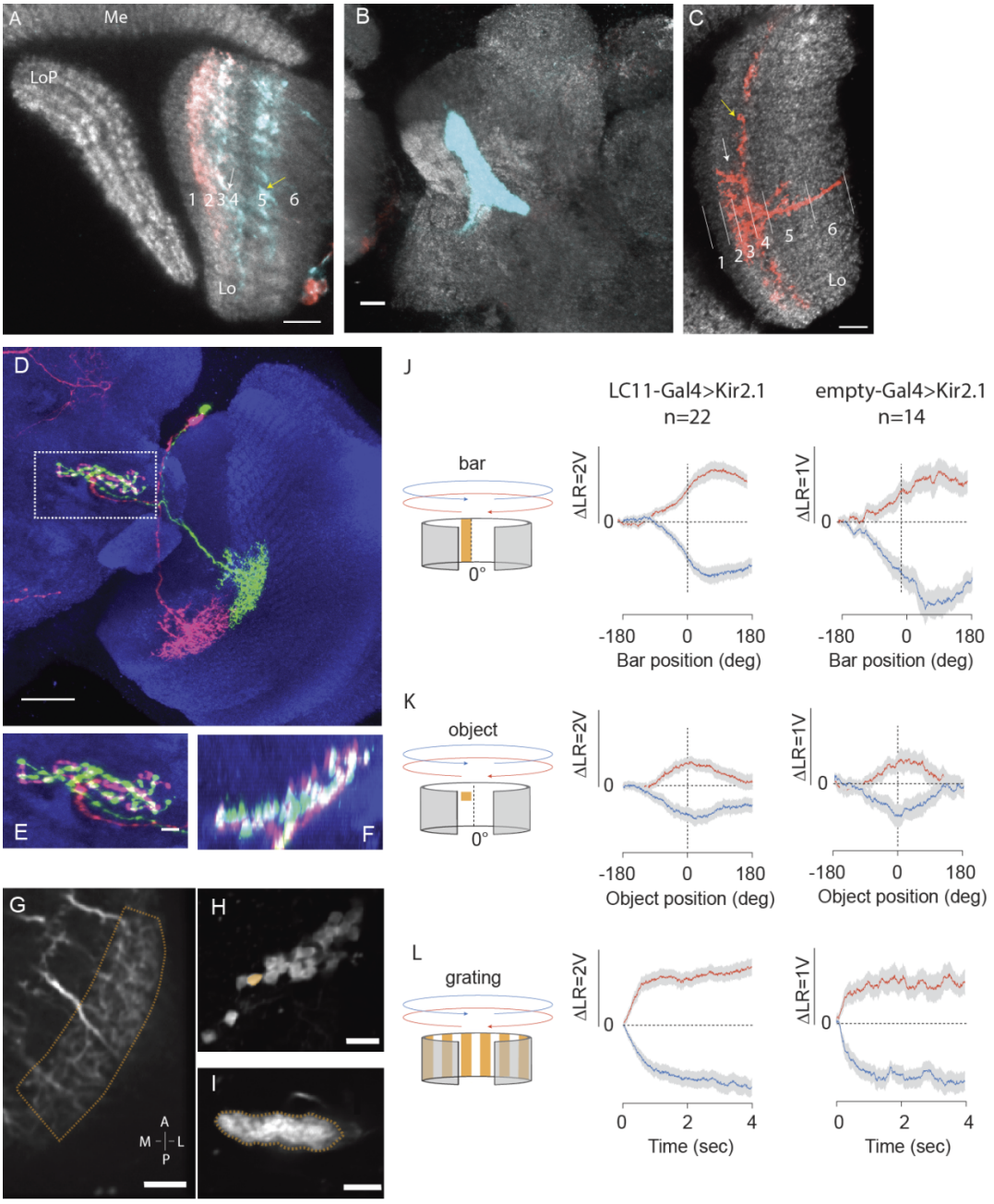

Figure 2.S1 related to Figure 2.1: A-C) Pre and post synaptic organization of LC11 in the Lobula. A) R22H02-Gal4 shows pre-synaptic labeling in the lobula. Dorsal view of R22H02-Gal4 driving the expression of dendritic marker UAS-DenMark (red) and pre-synaptic marker UAS-Syt-EGFP (cyan) in lobula (gray). Yellow arrowhead indicates the layer (5) only innervated by LC11 and white arrowhead indicates the layers innervated

by both LC11 and Loi. Both layers show pre-synaptic labeling (cyan). B) Dorsal view of VLPR and LC11 glomerulus labeled with pre (cyan) and post (red) synaptic markers. C) R22H02-Gal4 labels LC11 and Lobula intrinsic neurons (Loi). Stochastic labeling R22H02-Gal4 driver revealed two cell types in lobula. LC11 (red, white arrowhead) innervates layers 2,3,4, and 5 (neuropile in gray), whereas Lois (red, yellow arrowhead) innervates the border of 3rd and 4th strata in lobula (compare with Figure 1C). Scale bars are 10 um and layer identification is based on [S7]. D-F) Multicolor stochastic labeling of LC11. D) Anterior view of two LC11s tagged with HA (green) and FLAG (red). Dashed rectangle indicates the glomerulus. Scale bar is 25 um E) Anterior view of LC11 glomerulus modified from D. F) Dorsal view of two LC11s innervating VLPR. Image is modified from D. Scale bar is5 um in E and F. G-I) Representative images of 2 photon calcium imaging experiments illustrating extracted region of interests (ROIs) from different cellular compartments. G) Example dendritic ROI is shown. Orange dashed border represents the included pixels for analysis. H) Example cell body ROI is shown. Orange region represents a single cell body and extracted pixels for analysis. I) Example glomerular ROI is shown. Orange dashed line represent included pixels for analysis. Anatomical reference is provided with following letters: A: Anterior, P: Posterior, M: Medial and L: Lateral. Scale bars are 10 um. J-L) Effects of blocking LC11 on steering responses to bar, object, and full-field gratings. Mean response traces are color coded for stimulus direction and shaded region indicates ± S.E.M.

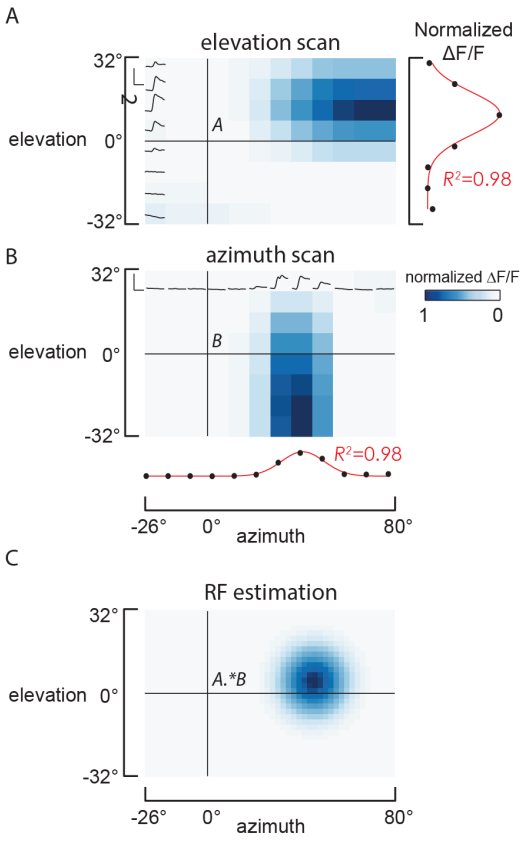

Figure 2.S2 related to Figure 2.2: Receptive field reconstruction. A and B) Responses of a single LC11 to an 8.8° square object swept at 8 different trajectories (right side of the heatmap) on both axis. Data then downsampled and a matrix for each axis was generated and represented as a heatmap. The two matrices were multiplied and a Gaussian curve was fit (red) to both axes in the resulting matrix (data not shown, see Supplemental Experimental Procedures). C) Receptive fields are estimated using the Gaussian fits in (A) and (B) to match a pixel step size in the LED screen (see Supplemental Experimental Procedures).

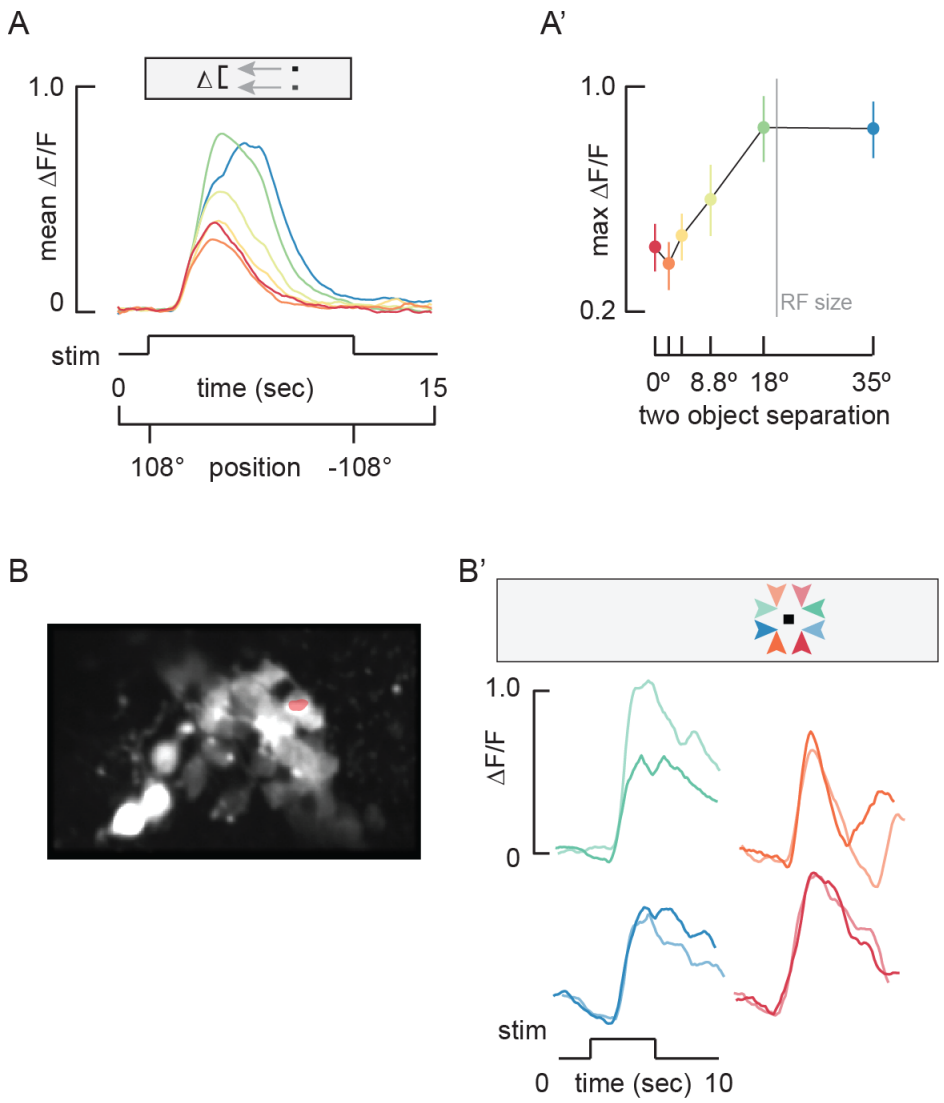

Figure 2.S3 related to Figure 2.3: LC11 is inhibited by a second object. A and A') Two 8.8° square object moved on parallel trajectories in the back-to-front direction (compare with Figure 3E and3E'). The distance between them was 0°, 2.2°, 4.4°, 8.8°, 18° and 35°, colors mapped to separation distance in C' (n = 6 flies). Vertical gray line indicates average receptive field (RF) size (Figure 3). B and B') A single LC11 is not directionally selective. B) Representative image of the 2-photon imaging plane. Orange region represents the imaged ROI for the data presented in B'. B') Calcium traces from

a single cell body presented with an 8.8° by 8.8° object moving 33° deg/sec in 4 cardinal directions. Two trajectories were used for each cardinal direction.

References:

Agrawal, S., Safarik, S., Dickinson, M., 2014. The relative roles of vision and chemosensation in mate recognition of Drosophila melanogaster. J. Exp. Biol. 217, 2796–805. doi:10.1242/jeb.105817

Ammer, G., Leonhardt, A., Bahl, A., Dickson, B.J.J., Borst, A., 2015. Functional Specialization of Neural Input Elements to the Drosophila on Motion Detector. Curr. Biol. 25, 2247–2253. doi:10.1016/j.cub.2015.07.014

Aptekar, J.W., Keleş, M.F., Lu, P.M., Zolotova, N.M., Frye, M.A., 2015. Neurons forming optic glomeruli compute figure-ground discriminations in Drosophila. J. Neurosci. 35, 7587–99. doi:10.1523/JNEUROSCI.0652-15.2015

Aptekar, J.W., Shoemaker, P.A., Frye, M.A., 2012. Figure tracking by flies is supported by parallel visual streams. Curr. Biol. 22, 482–487. doi:10.1016/j.cub.2012.01.044

Bahl, A., Ammer, G., Schilling, T., Borst, A., 2013. Object tracking in motion-blind flies. Nat Neurosci 16, 730–8. doi:10.1038/nn.3386

Bahl, A., Serbe, E., Meier, M., Ammer, G., Borst, A., 2015. Neural Mechanisms for Drosophila Contrast Vision. Neuron 88, 1240–1252. doi:10.1016/j.neuron.2015.11.004

Barnett, P.D., Nordström, K., O'Carroll, D.C., 2007. Retinotopic Organization of Small-Field-Target-Detecting Neurons in the Insect Visual System. Curr. Biol. 17, 569–578. doi:10.1016/j.cub.2007.02.039

Behnia, R., Clark, D. a., Carter, A.G., Clandinin, T.R., Desplan, C., 2014. Processing

properties of ON and OFF pathways for Drosophila motion detection. Nature 512, 427–430. doi:10.1038/nature13427

Buchner, E., Bader, R., Buchner, S., Cox, J., Emson, P.C., Flory, E., Heizmann, C.W., Hemm, S., Hofbauer, A., Oertel, W.H., 1988. Cell-specific immuno-probes for the brain of normal and mutant Drosophila melanogaster - I. Wildtype visual system. Cell Tissue Res. 253, 357–370. doi:10.1007/BF00222292

Coen, P., Xie, M., Clemens, J., Murthy, M., 2016. Sensorimotor Transformations Underlying Variability in Song Intensity during Drosophila Courtship. Neuron 89, 629–644. doi:10.1016/j.neuron.2015.12.035

Dubbs, A., Guevara, J., Yuste, R., 2016. moco: Fast Motion Correction for Calcium Imaging. Front. Neuroinform. 10, 6. doi:10.3389/fninf.2016.00006

Fischbach, K.-F., Dittrich, a P., 1989. The optic lobe of Drosophila melanogaster. I: A. Golgi analysis of wild-type structure. Cell Tissue Res 258, 441–475. doi:doi: 10.1007/BF00218858

Freifeld, L., Clark, D. a, Schnitzer, M.J., Horowitz, M. a, Clandinin, T.R., 2013. GABAergic Lateral Interactions Tune the Early Stages of Visual Processing in Drosophila. Neuron 78, 1075–1089. doi:10.1016/j.neuron.2013.04.024

Harrison, J.B., Chen, H.H., Sattelle, E., Barker, P.J., Huskisson, N.S., Rauh, J.J., Bai, D., Sattelle, D.B., 1996. Immunocytochemical mapping of a C-terminus anti-peptide antibody to the GABA receptor subunit, RDL in the nervous system of Drosophila melanogaster. Cell Tissue Res. 284, 269–278. doi:10.1007/s004410050587

Heisenberg, M., Wolf, R., 1984. Vision in Drosophila, genetics of microbehavior. Springer-Verlag, New York.

Hubel, D.H., Wiesel, T.N., 1962. Receptive fields, binocular interaction and functional architecture in the cat's visual cortex. J. Physiol. 160, 106–154.2. doi:10.1523/JNEUROSCI.1991-09.2009

Jenett, A., Rubin, G.M., Ngo, T.T.B., Shepherd, D., Murphy, C., Dionne, H., Pfeiffer, B.D., Cavallaro, A., Hall, D., Jeter, J., Iyer, N., Fetter, D., Hausenfluck, J.H., Peng, H., Trautman, E.T., Svirskas, R.R., Myers, E.W., Iwinski, Z.R., Aso, Y., DePasquale, G.M., Enos, A., Hulamm, P., Lam, S.C.B., Li, H.H., Laverty, T.R., Long, F., Qu, L., Murphy, S.D., Rokicki, K., Safford, T., Shaw, K., Simpson, J.H., Sowell, A., Tae, S., Yu, Y., Zugates, C.T., 2012. A GAL4-Driver Line Resource for Drosophila Neurobiology. Cell Rep. 2, 991–1001. doi:10.1016/j.celrep.2012.09.011

Joesch, M., Schnell, B., Raghu, S.V., Reiff, D.F., Borst, A., 2010. ON and OFF pathways in *Drosophila* motion vision. Nature 468, 300–4. doi:10.1038/nature09545

Juusola, M., Dau, A., Song, Z., Solanki, N., Rien, D., Jaciuch, D., Dongre, S., Blanchard, F., de Polavieja, G.G., Hardie, R.C., Takalo, J., 2016. Microsaccadic information sampling provides Drosophila hyperacute vision. bioRxiv.

Kim, A.J., Fitzgerald, J.K., Maimon, G., 2015. Cellular evidence for efference copy in Drosophila visuomotor processing. Nat. Neurosci. 18, 1247–1255. doi:10.1038/nn.4083

Maimon, G., Straw, A.D., Dickinson, M.H., 2008. A Simple Vision-Based Algorithm for

Decision Making in Flying Drosophila. Curr. Biol. 18, 464–470. doi:10.1016/j.cub.2008.02.054

Maisak, M.S., Haag, J., Ammer, G., Serbe, E., Meier, M., Leonhardt, A., Schilling, T., Bahl, A., Rubin, G.M., Nern, A., Dickson, B.J., Reiff, D.F., Hopp, E., Borst, A., 2013. A directional tuning map of Drosophila elementary motion detectors. Nature 500, 212–6. doi:10.1038/nature12320

Mauss, A.S., Meier, M., Serbe, E., Borst, A., 2014. Optogenetic and pharmacologic dissection of feedforward inhibition in Drosophila motion vision. J. Neurosci. 34, 2254–63. doi:10.1523/JNEUROSCI.3938-13.2014

Meier, M., Serbe, E., Maisak, M.S., Haag, J., Dickson, B.J., Borst, A., 2014. Neural circuit components of the Drosophila OFF motion vision pathway. Curr. Biol. 24, 385–392. doi:10.1016/j.cub.2014.01.006

Mu, L., Ito, K., Bacon, J.P., Strausfeld, N.J., 2012. Optic Glomeruli and Their Inputs in Drosophila Share an Organizational Ground Pattern with the Antennal Lobes. J. Neurosci. 32, 6061–6071. doi:10.1523/JNEUROSCI.0221-12.2012

Nern, A., Pfeiffer, B.D., Rubin, G.M., 2015. Optimized tools for multicolor stochastic labeling reveal diverse stereotyped cell arrangements in the fly visual system. Proc. Natl. Acad. Sci. 112, 201506763. doi:10.1073/pnas.1506763112

Nordström, K., O'Carroll, D.C., 2006. Small object detection neurons in female hoverflies. Proc. Biol. Sci. 273, 1211–1216. doi:10.1098/rspb.2005.3424

O'Carroll, D., 1993. Feature-detecting neurons in dragonflies. Nature 362, 541–543.

doi:10.1038/362541a0

Otsuna, H., Ito, K., 2006. Systematic analysis of the visual projection neurons of Drosophila melanograster. I. Lobula-specific pathways. J. Comp. Neurol. 497, 928–958. doi:10.1002/cne.21015

Panser, K., Tirian, L., Schulze, F., Villalba, S., Jefferis, G.S.X.E., Bühler, K., Straw, A.D., 2016. Automatic Segmentation of Drosophila Neural Compartments Using GAL4 Expression Data Reveals Novel Visual Pathways. Curr. Biol. 26, 1943–1954. doi:10.1016/j.cub.2016.05.052

Poggio, T., Reichardt, W., 1976. Visual control of orientation behaviour in the fly: Part II. Towards the underlying neural interactions. Q. Rev. Biophys. 9, 377. doi:10.1017/S0033583500002535

Schnell, B., Joesch, M., Forstner, F., Raghu, S. V, Otsuna, H., Ito, K., Borst, A., Reiff, D.F., 2010. Processing of horizontal optic flow in three visual interneurons of the Drosophila brain. J. Neurophysiol. 103, 1646–1657. doi:10.1152/jn.00950.2009

Serbe, E., Meier, M., Leonhardt, A., Borst, A., 2016. Comprehensive Characterization of the Major Presynaptic Elements to the Drosophila OFF Motion Detector. Neuron 89, 829–841. doi:10.1016/j.neuron.2016.01.006

Strausfeld, N.J., 1976. Atlas of an Insect Brain. Springer 52, 1096–1109. doi:10.1111/j.1475-4754.2010.00526.x

Strother, J.A., Nern, A., Reiser, M.B., 2014. Direct observation of on and off pathways in the drosophila visual system. Curr. Biol. 24, 976–983.

doi:10.1016/j.cub.2014.03.017

Theobald, J.C., Ringach, D.L., Frye, M.A., 2010. Dynamics of optomotor responses in Drosophila to perturbations in optic flow. J. Exp. Biol. 213, 1366–75. doi:10.1242/jeb.037945

Tuthill, J.C., Nern, A., Rubin, G.M., Reiser, M.B., 2014. Wide-Field Feedback Neurons Dynamically Tune Early Visual Processing. Neuron 82, 887–895. doi:10.1016/j.neuron.2014.04.023

Warrant, E.J., Kelber, A., Gislén, A., Greiner, B., Ribi, W., Wcislo, W.T., 2004. Nocturnal vision and landmark orientation in a tropical halictid bee. Curr. Biol. 14, 1309–1318. doi:10.1016/j.cub.2004.07.057

Warzecha, A.K., Egelhaaf, M., Borst, A., 1993. Neural circuit tuning fly visual interneurons to motion of small objects. I. Dissection of the circuit by pharmacological and photoinactivation techniques. J. Neurophysiol. 69, 329–339.

Wiederman, S.D., Shoemaker, P.A., O'Carroll, D.C., 2008. A model for the detection of moving targets in visual clutter inspired by insect physiology. PLoS One 3. doi:10.1371/journal.pone.0002784

Wiederman, S.D., Shoemaker, P. a, O'Carroll, D.C., 2013. Correlation between OFF and ON channels underlies dark target selectivity in an insect visual system. J. Neurosci. 33, 13225–32. doi:10.1523/JNEUROSCI.1277-13.2013

Wilson, R.I., Turner, G.C., Laurent, G., 2004. Transformation of olfactory representations in the Drosophila antennal lobe. Science (80-.). 303, 366–70.

doi:10.1126/science.1090782

Wu, M., Nern, A., Williamson, W.R., Morimoto, M.M., Reiser, M.B., Card, G.M., Rubin, G.M., 2016. Visual projection neurons in the Drosophila lobula link feature detection to distinct behavioral programs. Elife 5. doi:10.7554/eLife.21022

Zabala, F., Polidoro, P., Robie, A., Branson, K., Perona, P., Dickinson, M.H., 2012. A simple strategy for detecting moving objects during locomotion revealed by animal-robot interactions. Curr. Biol. 22, 1344–1350. doi:10.1016/j.cub.2012.05.024

Chapter 3

Inhibitory Control of Object Selectivity in *Drosophila*

Abstract

Visual object detection is a fundamental behavior and critical to the survival of organisms in the wild. Many animals depend on object-vision to detect conspecifics, predators and preys. A number of studies investigated the behavioral correlates of object vision in fruit flies, providing an ever-clearer picture. Yet, the circuitry underlying object-dependent behaviors remained largely elusive. Here we build on our previous work and provide first insights on how the only known object detector in fruit flies, LC11, achieves its object selectivity.

Introduction

Flies perform a wide-variety of object-oriented behaviors including courtship and aggression (Agrawal et al., 2014; Asahina et al., 2014). Flies also show preference towards tall steep objects during walking (Robie et al., 2010). Flying flies are attracted to long vertical bars and avoid small objects (Maimon et al., 2008). In addition, male flies can modulate the intensity of their courtship song based on the distance to female flies even if they are motion blind (Coen et al., 2016). Motion blind flies can track objects (Bahl et. al., 2013). Together, these findings suggest the existence of an object-detection circuitry.

We have recently shown that a lobula columnar cell type, LC11, responds to the movement of small objects. Our results revealed that LC11 prefers objects that are 8° in height and 4° in width that are darker than the background (Keleş and Frye, 2017). LC11 is inhibited when large objects or panoramic gratings presented. When the inhibitory currents are abolished by GABAA receptor antagonist picrotoxin, LC11 no

longer responds to objects and loses its size selectivity, responding to large objects. Thus, we established in our previous report that the inhibition is required for both object sensitivity and selectivity. Similar cells that are tuned to small objects have been previously described in the vertebrate retina (Lettvin et al., 1959; Levick, 1967; Semmelhack et al., 2014; Zhang et al., 2012). In mice, a simple circuit mechanism that is composed of object motion sensitive excitatory cells and cells that are sensitive to panoramic motion converge onto a third cell, which itself is sensitive to small object motion. Here, we hypothesize a similar mechanism for how LC11 achieves its feature selectivity. We propose that excitatory inputs provide size-tuned input to LC11 and an inhibitory cell spatially sums incoming visual information and provides inhibitory input. This mechanism allows LC11 to be inhibited by large objects and partially explains the inhibitory requirement for size selectivity.

Results

Here, we investigate the origins of inhibitory currents mediating size selectivity in LC11. We propose three circuit mechanisms that could explain the size selectivity we observed previously (Figure 1). 1) Inhibitory circuits could act on pre-synaptic excitatory inputs to LC11. Such a circuit mechanism would allow inhibitory input to directly tune the presynaptic excitatory input to LC11. In this mechanism, LC11 is not receiving direct inhibition. 2) Inhibitory circuits could act directly on to LC11. In this scenario, object selectivity is achieved by the excitation/inhibition ratio to LC11. 3) In our previous study, we have observed putative pre-synaptic terminals of LC11 near where LC11 post-synaptic dendrites located (Keleş and Frye, 2017). Such anatomy would allow a circuit configuration in which an excited cell inhibits the neighboring cell leading to cell type

autonomous inhibition. We first tested if such circuit architecture mediates inhibitory currents and provides size selectivity. We expressed genetically encoded calcium indicator and temperature sensitive dominant negative allele of dynamin (Shibire^{ts1}) to record the calcium currents and while blocking the cells output (Figure 2). However, we did not observe significant differences between the responses at permissive temperature and restrictive temperature. Although, we cannot directly measure how successfully synaptic vesicle formation is blocked, these results suggest that LC11s output does not influence its input.

To further demonstrate that neighboring LC11s do not inhibit and influence each other's responses, we checked if LC11s produce the inhibitory neurotransmitter GABA (Figure 3). LC11s are not GABAergic and likely do not involve in a mechanism where feedback inhibition mediates the size selectivity. Our results prompted us to test if LC11 is capable of directly receiving inhibition. To test if LC11 expresses any of the known GABA-A receptors we utilized a recently developed technique that allows faithful expression of a desired protein in the same expression pattern of a targeted gene. We used a line that allows co-transcription of Gal4 with GABA-A receptor *Rdl,* thus recapitulating *Rdl* expression. This allowed us to test if LC11 transcribes *Rdl* by expressing GFP in LC11 cells using the LexA system and RFP in *Rdl* positive cells using Rdl-T2G4 (Figure 3B and B'). This provides an indirect evidence for *Rdl* in LC11. However, since the expression of Gal4 is dependent on *Rdl* transcription*,* we claim that LC11 transcribes *Rdl.*

To understand the physiological properties of LC11 and dissect the circuit mechanisms that give rise to such physiology, we decided to test if LC11 expresses other receptors.

We tested two nicotinic acetylcholine receptor subunits (one and five) and found that LC11 might express subunit one but not subunit five. These results suggested that LC11 receives excitatory input via cholinergic receptors.

What are the cells that provide inhibitory and excitatory input to LC11? To answer this question, we first tested if LC11 receives input from previously identified cells. A wide variety of cells in the optic lobe have been identified through Golgi impregnations (Fischbach and Dittrich, 1989). However, necessary genetic tools to target majority of them is not yet developed. Thus, we concentrated on known cell types that are likely candidates to provide input to LC11. Recent efforts to understand visual processing in the fly optic lobe identified and made tools to target motion vision circuitry (Shinomiya et al., 2014; Strother et al., 2017; Takemura et al., 2017, 2013). Out of the available toolbox, we tested four cell types that innervate lobula (Tm2, Tm3, Tm4 and Tm9). As it has been previously described, Tm9 does not innervate lobula layer 2 where LC11 dendrites are (Figure 4A) (Fischbach and Dittrich, 1989; Fisher et al., 2015). Tm2 seems to be largely innervating lobula layer 1 and does not come in contact with LC11 dendrites (Figure 4C). Tm3 and Tm4 seems to be likely candidates since they terminate in medial layers of lobula. However, close examination revealed that Tm3 predominantly innervates the lateral portion of the lobula layer 2, whereas LC11 largely occupies the medial portion (Keleş and Frye, 2017; Wu et al., 2016). Tm3 then sends projections to the medial layers in the lobula terminating in layer 4. Our dual labeling results, revealed that the deeper innervations of Tm3 does not overlap with LC11 dendrites (Figure 4B). Tm4 predominantly innervates lobula layers 2 and 4. Labeling LC11 and Tm4 together, revealed that Tm4 terminals overlap slightly in Layer4 with LC11 dendrites (Figure 4D).

However, none of the cells we tested overlapped with LC11 in lobula layers 2 and 3, where the bulk of LC11 dendrites lie.

To find the presynaptic candidates of LC11 we performed an unbiased computational screen using the publicly available Janelia Gal4 database (Jenett et al., 2012). We first downloaded 3500 registered stacks of Gal4 lines that contain the expression pattern of each line. We then wrote a custom MATLAB script to search specific anatomical locations for GFP expression within each registered stack. This allowed us to specify a unique region where LC11 dendrites are located. We then excluded all the lines that contain expression in the optic glomeruli. This resulted in ~800 candidate lines out of 3500 total. Finally, we manually went through each line to ensure that it had significant expression in the targeted region (LC11 dendrites). Additionally, we excluded lines with broad expression patterns. We decided on ~70 candidate Gal4 lines to further test anatomical overlap by expressing GFP in LC11 and RFP in candidate Gal4. From this screen, we identified three promising pre-synaptic candidates, showing strong overlap with LC11 dendrites (Figure 5). Two of the Gal4 lines label projection neurons that are likely to be T2 or/and T3. Cell bodies are located between the posterior rim of the medulla and lobula plate. Such location is unique, as there are only 4 known cell types to have cell bodies there (C2, C3, T2 and T3, (Fischbach and Dittrich, 1989). Although single cell analysis for each Gal4 line is required to confirm the cell type identity, dendritic overlap is encouraging and indicate likely input to LC11.

Third cell type we have identified is a lobula intrinsic neuron which innervates multiple layers in the lobula. There are 8-10 cells in this cell type covering entire ~700 retinotopic columns in the lobula indicating that each cell must have a large anatomical receptive

field. We are currently performing experiments to determine the functional connectivity of these cells to LC11 and describe their physiological properties.

To further understand how inhibition shapes LC11 we performed a series of experiments looking at the interaction between object and background. In our previous study, we show that large field stimulus does not elicit a response in LC11. However, moving animals perceive optic flow on their retina. Such large stimuli should inhibit responses to moving objects when the animal is moving. To test this, we presented an object on a moving background (Figure 6) and measured calcium currents in LC11. To our surprise, LC11 did not show any responses to objects on moving backgrounds, regardless of which direction the background moved. Even though the object was distinct from the background by not only its motion but by its luminance, LC11 was not able to respond. This led us to speculate that in a natural environment with optic flow, LC11 fails to detect objects. Thus, such a cell would be only useful if the animal is stationary.

Next, we tested if coherent motion is required to inhibit LC11. A stimulus with random dot texture composed of bright and dark pixels used. The brightness of the individual dark and bright pixels flickered at 10 Hz, while passing an object. Elementary motion detectors are not sensitive to such stimuli since they require correlation of neighboring signals in space and time. LC11 responses were suppressed when the object was moved with the flickering background suggesting that the inhibitory circuit can detect flicker and does not require coherent motion (Figure 7).

To test if the order of excitation/inhibition differentially shapes the responses, we designed an experiment where inhibition from the background movement trailed the excitation from the object moving on a stationary background. Moving an object through LC11s receptive field in the absence of the background motion elicited strong responses (Figure 8, black trace). Excitation was suppressed when the background moved after the object entered the receptive field (Figure 8, red and blue traces). Direction of either background or object motion had no effect on this (Figure 8, red and blue traces). Thus, inhibition acts on LC11 independent of strong excitatory currents.

Does the visual processing on the right hemisphere affects LC11 responses on the left hemisphere? To test this, we presented a moving grating window on the contralateral side and recorded object responses in LC11 (Figure 9). moving gratings on the contralateral side does not influence ipsilateral LC11 responses. Grating window placed on the ipsilateral side inhibited object responses. LC11 responded only when the object was not overlapping with the gratings. These results suggested that distinct parts of the ipsilateral visual field do not greatly influence one another. Some members of the LC11 class still responds to objects even when other members are inhibited by the presentation of grating window.

Discussion

Here we reported our ongoing investigations on the inhibitory current shaping size selectivity in LC11. Our results revealed that LC11 is likely to receive direct inhibition via GABA-A receptors in a non-cell type autonomous manner. Blocking the synaptic output of LC11 does not influence the size selectivity, suggesting that cell type autonomous

inhibition does not play a role. LC11 does not respond to a small moving object on a moving background. Object responses to small moving objects on a stationary background can be suppressed in a fast timescale by moving the background. Contralateral movement of large visual stimuli does not impair LC11s response to ipsilaterally moving objects suggesting that two populations of LC11s in each hemisphere does not influence one another.

LC11 likely receives excitatory input via nicotinic cholinergic receptor subunit-1 and inhibitory input via GABAA receptor *Rdl*. There are five GABAA receptor subunits listed on flybase (*Lcch3*, *CG8916, Grd, Rdl and CG12344*; flybase.org) and only *Rdl* has been studied extensively (Knipple and Soderlund, 2010). It is not clear if the GABAA receptor mediated inhibition is via homomeric or heteromeric *Rdl* receptors. *Rdl* can form a homooligomeric receptor (Buckingham et al., 1994). It is possible that LC11 receives inhibitory input via other GABAA receptors. LC11 dendrites does not overlap with Tm2, Tm3 and Tm9 presynaptic terminals. Layer 4 innervations of LC11 overlap slightly with Tm4. Our pre-synaptic candidate screen identified 3 independent Gal4 lines that show extensive overlap with LC11. Future efforts will be concentrated on elucidating if candidate cells are functionally connected to LC11.

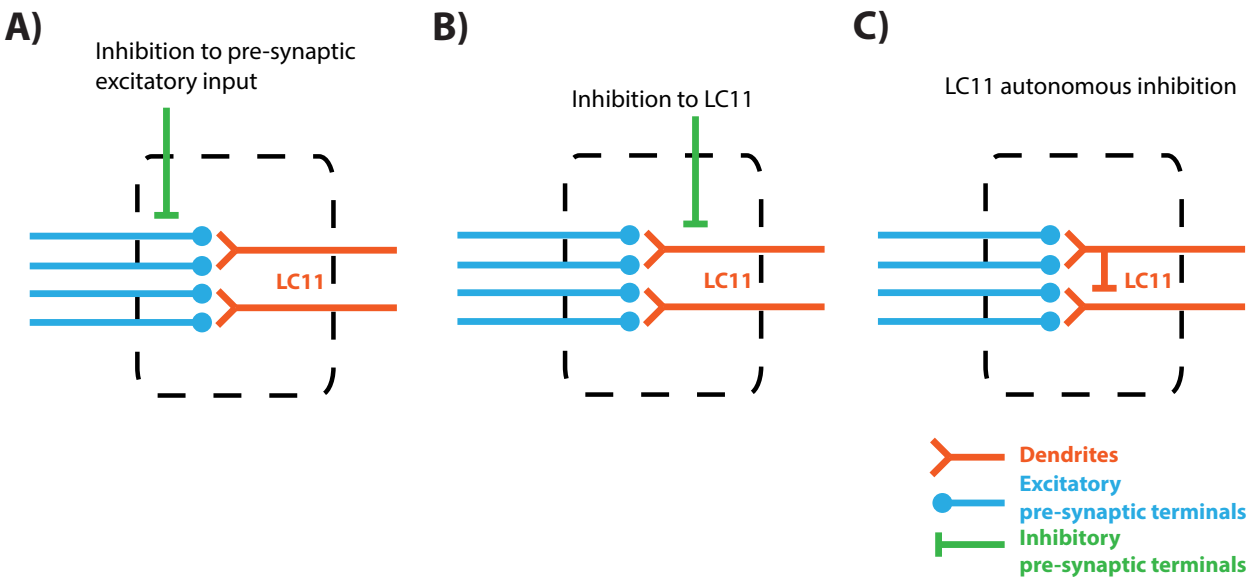

Figure 3.1: Proposed circuit mechanisms for object selectivity in LC11 A) Inhibitory currents that shape object selectivity act on pre-synaptic excitatory cell and reduces excitation that LC11 receives. **B)** Inhibitory currents act directly on LC11. Object selectivity is determined by excitation/inhibition ratio. **C)** Neighboring LC11s inhibit one another. Excited LC11s inhibit the neighboring LC11s. A large stimuli would elicit large excitation in LC11 cells leading to inhibition. Whereas small stimuli would elicit excitation in a small number of LC11s leading to minimal inhibition.

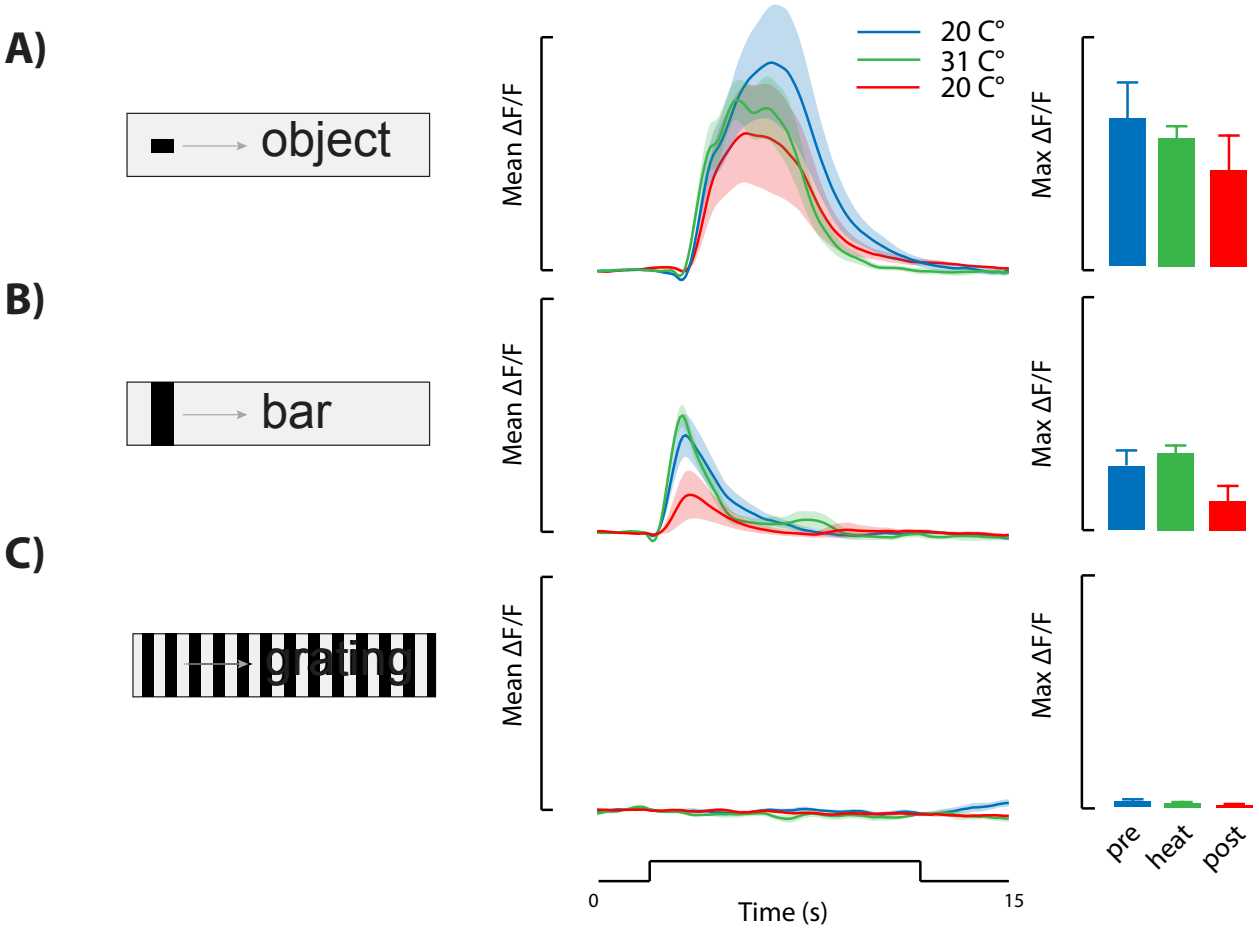

Figure 3.2: Blocking the synaptic output of LC11 does not influence object selectivity. LC11 expressing GCaMP and Shibire (ts1) tested with three stimuli**: A)** a small object, **B)** a bar and **C)** panoramic gratings, before (blue) and after (red) the temperature increased to 31 C° (green). Far right bar graphs indicate the mean maximum delta F/F for each condition. S.E.M., n=5.

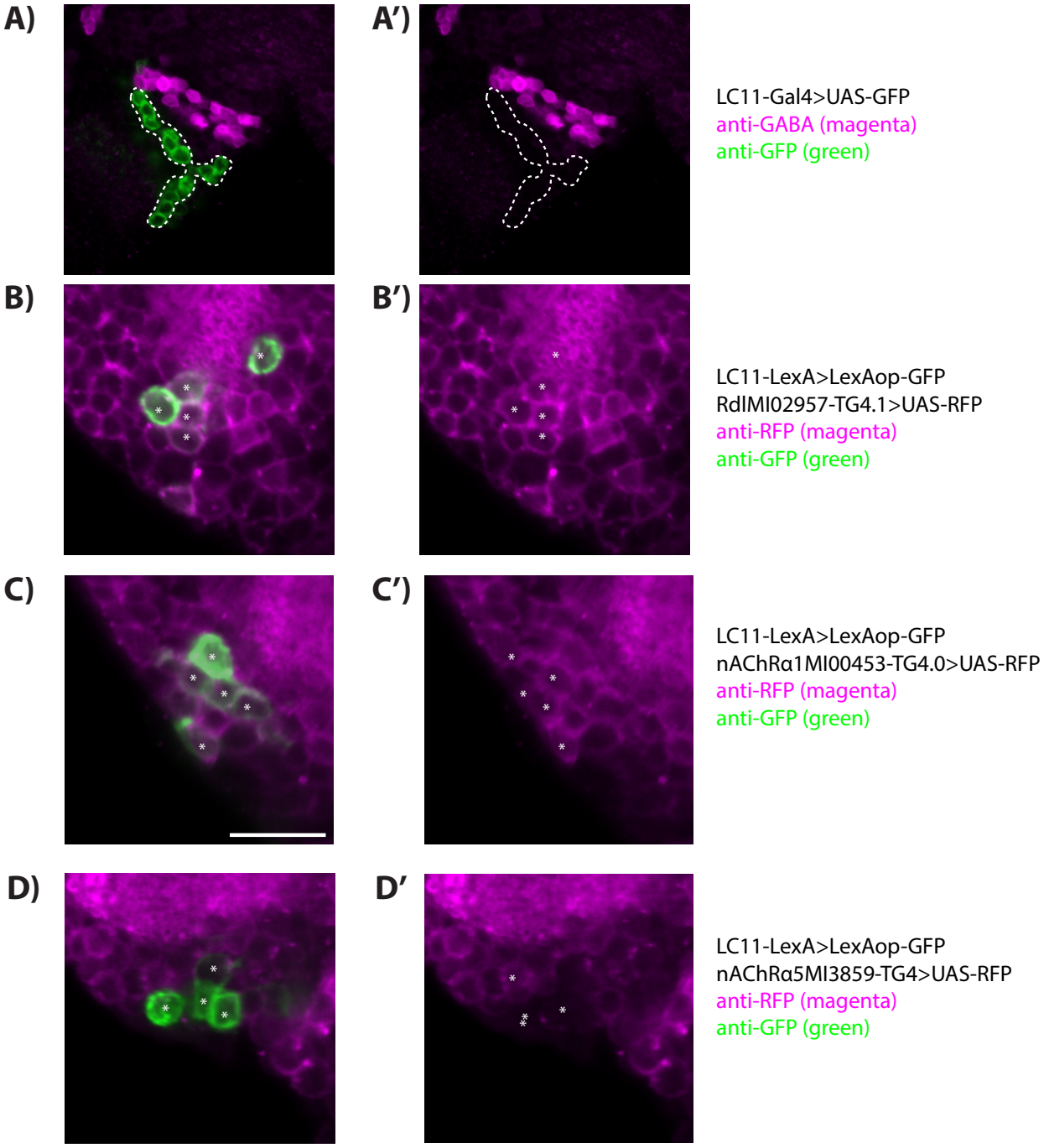

Figure 3.3: LC11 is not GABAergic and expresses GABAA and Cholinergic receptors. A and A') LC11 and GABAergic neurons labeled with anti-GFP (green) and anti-GABA (magenta), respectively. **B-D)** Cell bodies of candidate receptor lines (magenta) and LC11 (GFP). Candidate lines are crossed to following fly with the

genotype: UAS-RFP, LexAop-GFP; LC11-LexA. GFP positive LC11 cell bodies are labeled with an asterisk**. B'-D')** Same as B-D without the GFP positive cells.

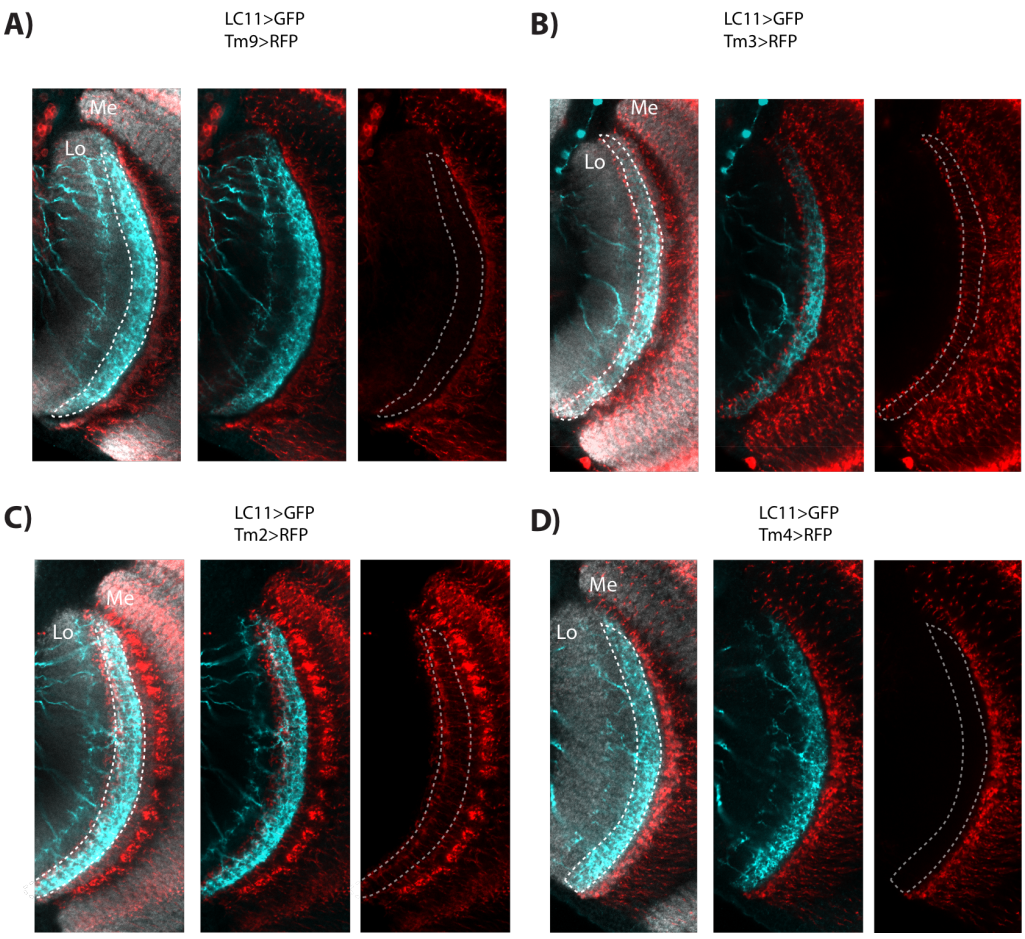

Figure 3.4: LC11 does not overlap with motion pathway. A-D) Motion pathway neurons Tm2, Tm3, Tm4 and Tm9 are expressing RFP (red), whereas LC11 is expressing GFP (cyan). First subpanels include nc82 staining to highlight neuropils. Me: Medulla, Lo: Lobula. Dashed path highlights LC11 dendrites.

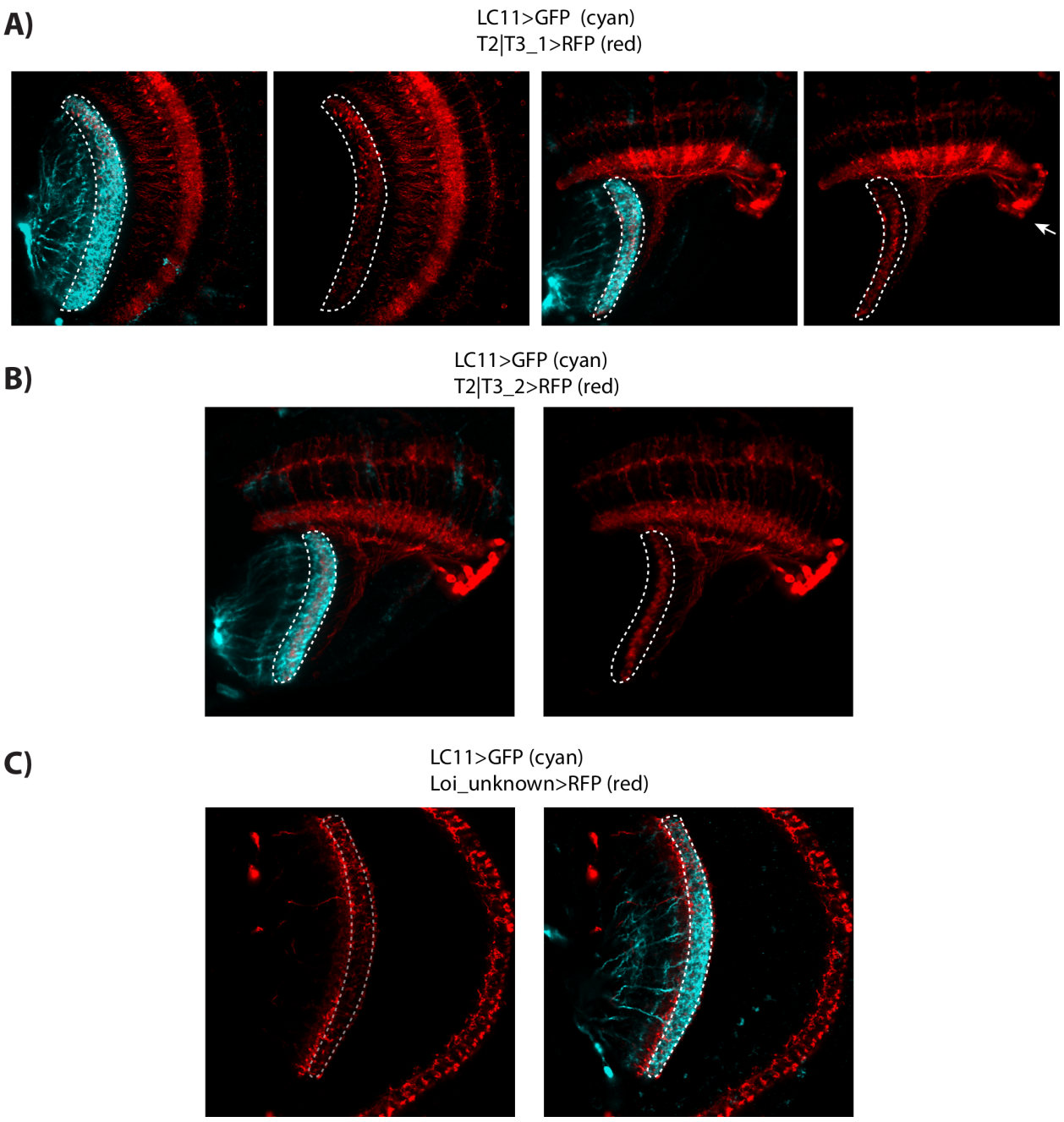

Figure 3.5: Putative pre-synaptic inputs to LC11. A-C) Candidate Gal4 lines expressing RFP (red) show anatomical overlap with LC11 dendrites (cyan). A-B indicates two independent Gal4 lines labeling similar populations of cells that project from medulla to lobula. Cell type identity is not clear and requires further anatomical characterization of the Gal4 line. Based on the cell body location (white arrowhead),

Gal4 lines likely to label T2 and/or T3 neurons. Third cell type is a previously unidentified Lobula Intrinsic Neuron (Loi).

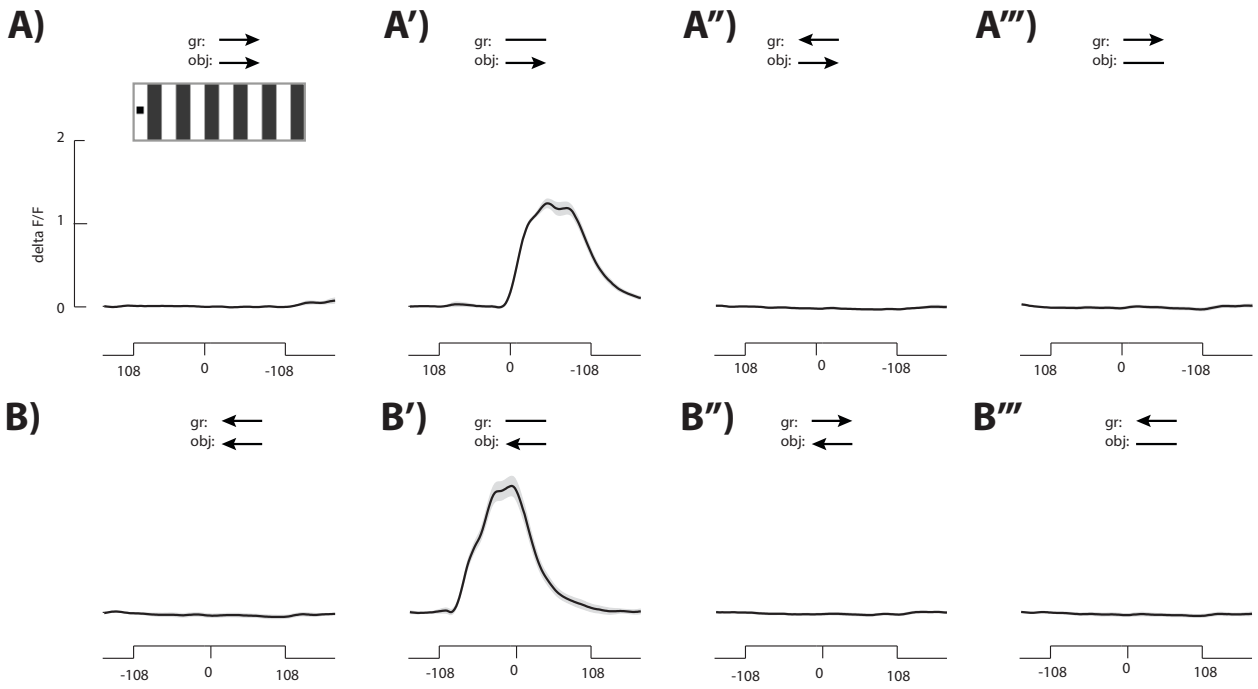

Figure 3.6: Object responses in LC11 is suppressed on a moving background.

LC11 expressing GCaMP6m tested for responses to object moving from **A)** contralateral to ipsilateral and **B)** ipsilateral to contralateral side. Representative visual stimulus is shown on the upper left corner. Objects moved on gratings moving front-to-back (A), back-to-front (A'') or on a stationary background (A'). gr: gratings, obj: object. S.E.M., n=8.

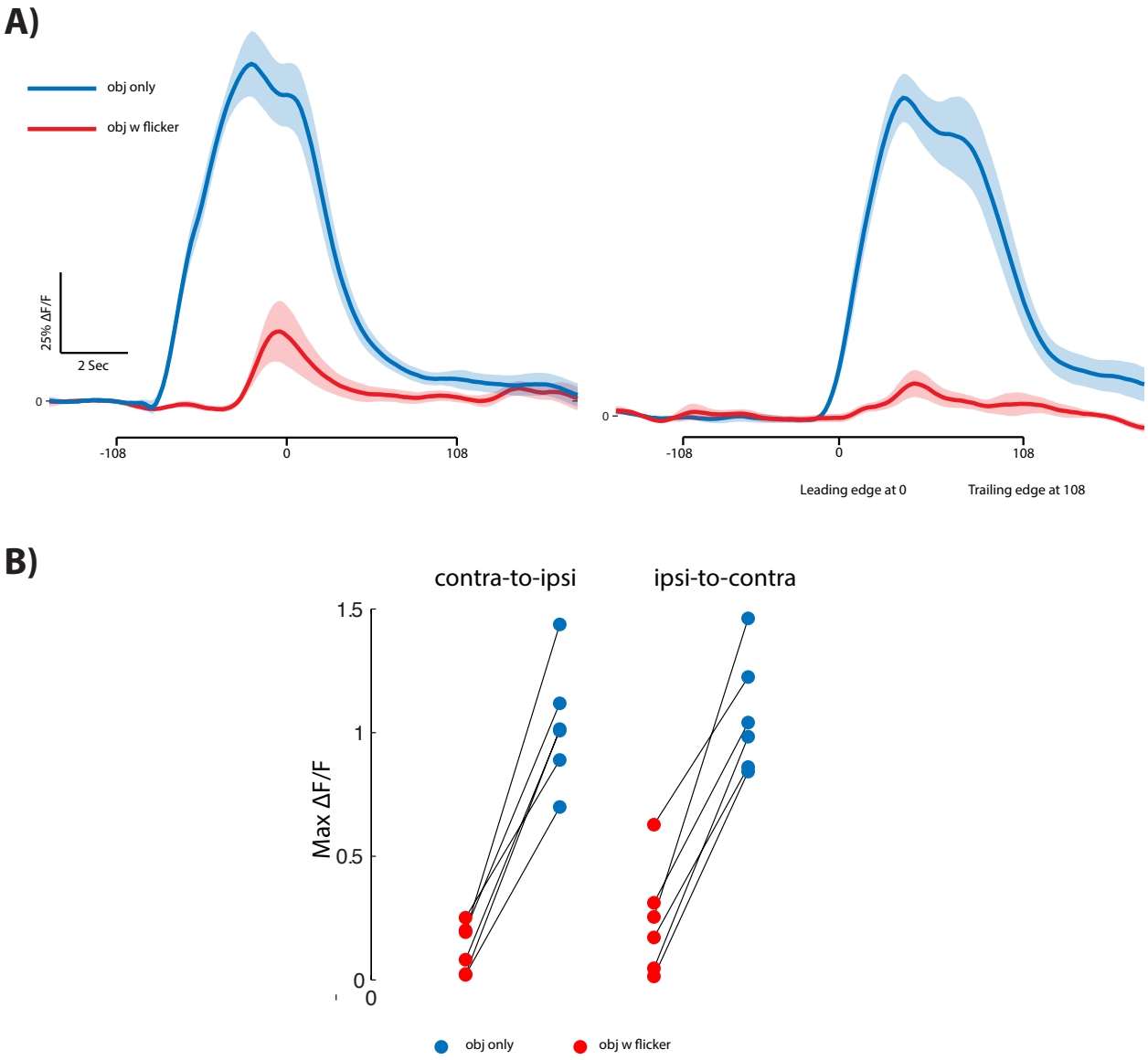

Figure 3.7: Coherent motion is not required for inhibitory suppression. A) LC11 neurons expressing GCaMP6m tested for object responses on a flickering or stationary background composed of bright and dark dots. Responses to the movement of an object from ipsilateral to contralateral or contralateral to ipsilateral shown on the left and right panels, respectively. **B)** Mean maximum delta F/F to the responses to object alone (red) and object on a flicker background (red). S.E.M., n=6;

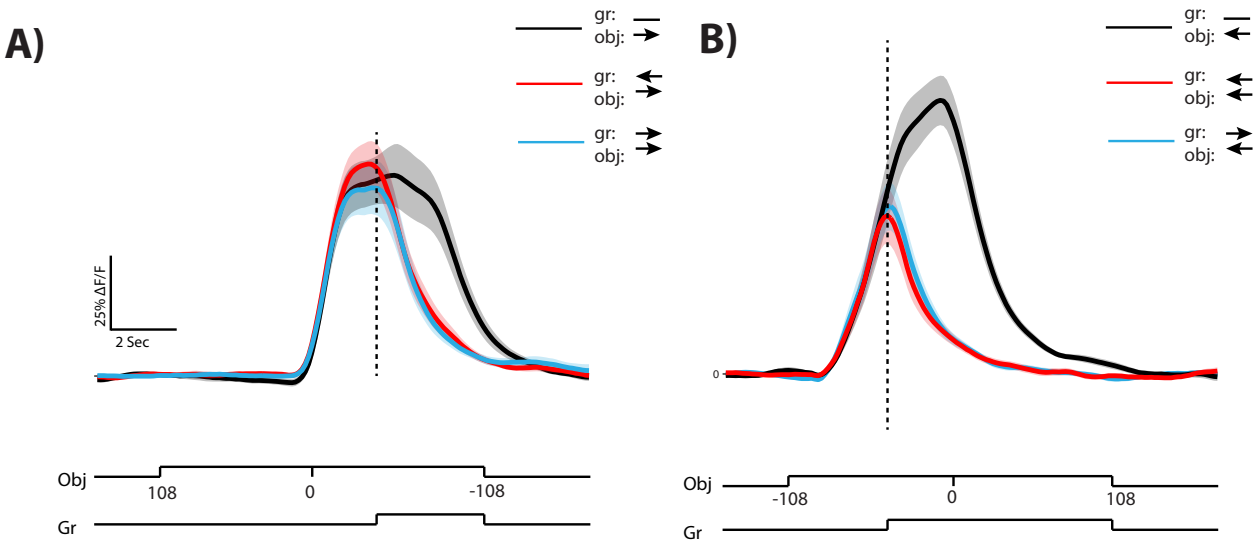

Figure 3.8: Inhibition suppresses object evoked calcium responses in LC11. A) GCaMP6m responses to an object moving contralateral to ipsilateral visual field in the absence (black) and presence of moving background gratings. Direction of gratings indicated on the top right side. Dashed line indicates the onset of the movement of background gratings. **B)** Object is moved from ipsilateral to contralateral side. S.E.M.

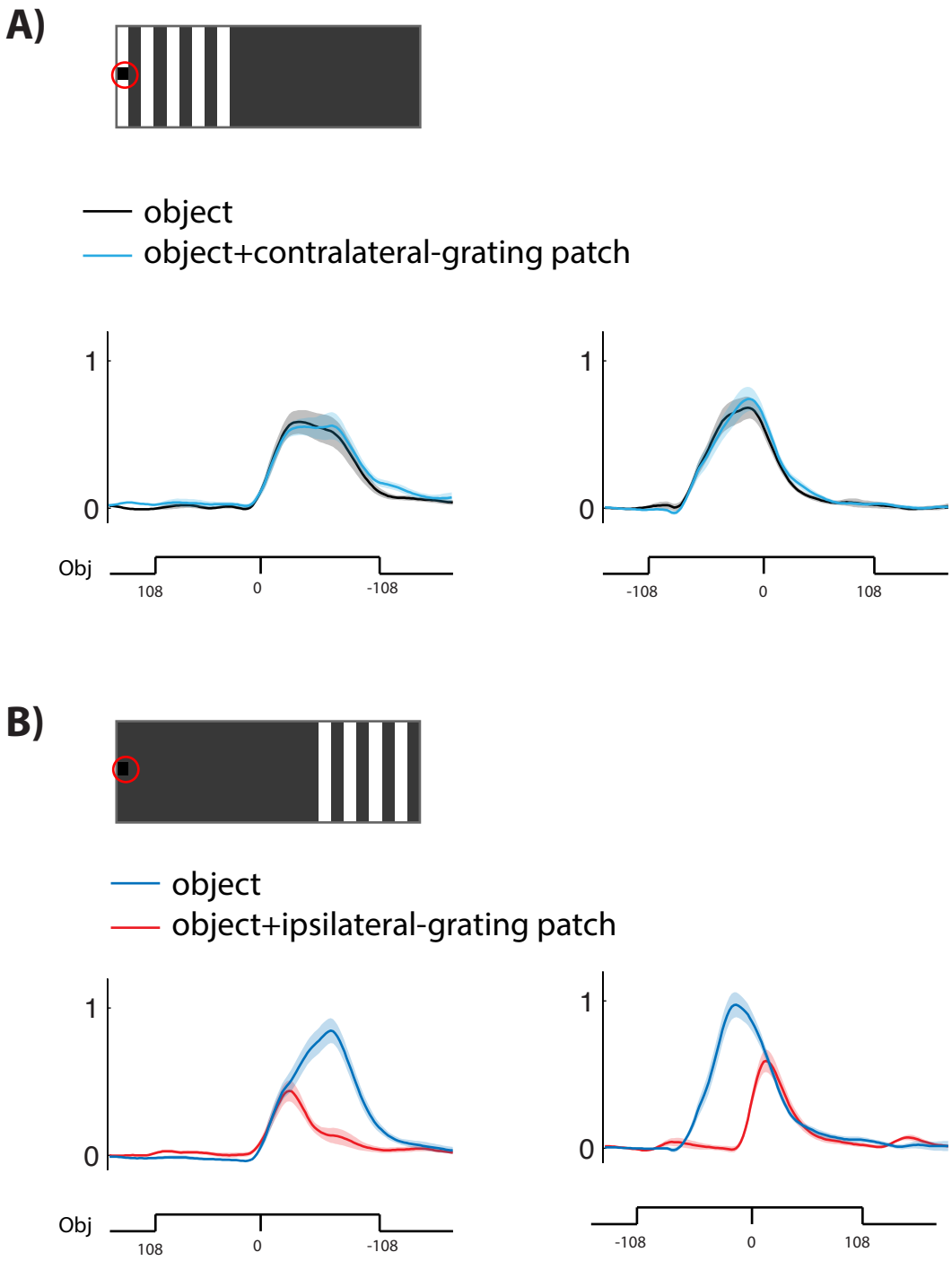

Figure 3.9: Movement of a grating patch on the contralateral side does not affect object responses in LC11. A) LC11 neurons expressing GCaMP6m tested for object movement with (blue) or without (black) a moving contralateral grating patch. A solid dark object is moved from contralateral to ipsilateral (left panel) and ipsilateral to

contralateral side. Red circle indicates object location **B)** Same as A but with grating patch moved to the ipsilateral side. S.E.M., n=9;

References:

Agrawal, S., Safarik, S., Dickinson, M., 2014. The relative roles of vision and chemosensation in mate recognition of Drosophila melanogaster. J. Exp. Biol. 217, 2796–805. doi:10.1242/jeb.105817

Asahina, K., Watanabe, K., Duistermars, B.J., Hoopfer, E., González, C.R., Eyjólfsdóttir, E.A., Perona, P., Anderson, D.J., 2014. Tachykinin-Expressing Neurons Control Male-Specific Aggressive Arousal in Drosophila. Cell 156, 221–235. doi:10.1016/j.cell.2013.11.045

Bahl, A., Ammer, G., Schilling, T., Borst, A., 2013. Object tracking in motion-blind flies. Nat Neurosci 16, 730–8. doi:10.1038/nn.3386

Buckingham, S.D., Hosie, A.M., Roush, R.L., Sattelle, D.B., 1994. Actions of agonists and convulsant antagonists on a Drosophila melanogaster GABA receptor (Rdl) homo-oligomer expressed in Xenopus oocytes. Neurosci. Lett. 181, 137–140. doi:10.1016/0304-3940(94)90578-9

Coen, P., Xie, M., Clemens, J., Murthy, M., 2016. Sensorimotor Transformations Underlying Variability in Song Intensity during Drosophila Courtship. Neuron 89, 629–644. doi:10.1016/j.neuron.2015.12.035

Fischbach, K.-F., Dittrich, a P., 1989. The optic lobe of Drosophila melanogaster. I: A. Golgi analysis of wild-type structure. Cell Tissue Res 258, 441–475. doi:doi: 10.1007/BF00218858

Fisher, Y.E., Leong, J.C.S., Sporar, K., Ketkar, M.D., Gohl, D.M., Clandinin, T.R., Silies,

M., 2015. A Class of Visual Neurons with Wide-Field Properties Is Required for Local Motion Detection. Curr. Biol. 25, 3178–3189. doi:10.1016/j.cub.2015.11.018

Jenett, A., Rubin, G.M., Ngo, T.T.B., Shepherd, D., Murphy, C., Dionne, H., Pfeiffer, B.D., Cavallaro, A., Hall, D., Jeter, J., Iyer, N., Fetter, D., Hausenfluck, J.H., Peng, H., Trautman, E.T., Svirskas, R.R., Myers, E.W., Iwinski, Z.R., Aso, Y., DePasquale, G.M., Enos, A., Hulamm, P., Lam, S.C.B., Li, H.H., Laverty, T.R., Long, F., Qu, L., Murphy, S.D., Rokicki, K., Safford, T., Shaw, K., Simpson, J.H., Sowell, A., Tae, S., Yu, Y., Zugates, C.T., 2012. A GAL4-Driver Line Resource for Drosophila Neurobiology. Cell Rep. 2, 991–1001. doi:10.1016/j.celrep.2012.09.011

Keleş, M.F., Frye, M.A., 2017. Object-Detecting Neurons in Drosophila. Curr. Biol. 27, 680–687. doi:10.1016/j.cub.2017.01.012

Knipple, D.C., Soderlund, D.M., 2010. The ligand-gated chloride channel gene family of Drosophila melanogaster. Pestic. Biochem. Physiol. 97, 140–148. doi:10.1016/j.pestbp.2009.09.002

Lettvin, J., Maturana, H., McCulloch, W., Pitts, W., 1959. What the Frog's Eye Tells the Frog's Brain. Proc. IRE 47, 1940–1951. doi:10.1109/JRPROC.1959.287207

Levick, W.R., 1967. Receptive fields and trigger features of ganglion cells in the visual streak of the rabbit's retina. J. Physiol. 188, 285–307. doi:10.1113/jphysiol.1967.sp008140

Maimon, G., Straw, A.D., Dickinson, M.H., 2008. A Simple Vision-Based Algorithm for Decision Making in Flying Drosophila. Curr. Biol. 18, 464–470.

doi:10.1016/j.cub.2008.02.054

Robie, A.A., Straw, A.D., Dickinson, M.H., 2010. Object preference by walking fruit flies, *Drosophila melanogaster*, is mediated by vision and graviperception. J. Exp. Biol. 213, 2494–2506. doi:10.1242/jeb.041749

Semmelhack, J.L., Donovan, J.C., Thiele, T.R., Kuehn, E., Laurell, E., Baier, H., Blondel, M., Prettenhofer, P., Weiss, R., Dubourg, V., 2014. A dedicated visual pathway for prey detection in larval zebrafish. Elife 3, E2391–E2398. doi:10.7554/eLife.04878

Shinomiya, K., Karuppudurai, T., Lin, T.Y., Lu, Z., Lee, C.H., Meinertzhagen, I. a., 2014. Candidate neural substrates for off-edge motion detection in drosophila. Curr. Biol. 24, 1062–1070. doi:10.1016/j.cub.2014.03.051

Strother, J.A., Wu, S.T., Wong, A.M., Nern, A., Rogers, E.M., Le, J.Q., Rubin, G.M., Reiser, M.B., 2017. The Emergence of Directional Selectivity in the Visual Motion Pathway of Drosophila. Neuron 94, 168–182.e10. doi:10.1016/j.neuron.2017.03.010

Takemura, S., Bharioke, A., Lu, Z., Nern, A., Vitaladevuni, S., Rivlin, P.K., Katz, W.T., Olbris, D.J., Plaza, S.M., Winston, P., Zhao, T., Horne, J.A., Fetter, R.D., Takemura, S., Blazek, K., Chang, L.-A., Ogundeyi, O., Saunders, M. a, Shapiro, V., Sigmund, C., Rubin, G.M., Scheffer, L.K., Meinertzhagen, I. a, Chklovskii, D.B., 2013. A visual motion detection circuit suggested by Drosophila connectomics. Nature 500, 175–81. doi:10.1038/nature12450

Takemura, S., Nern, A., Chklovskii, D.B., Scheffer, L.K., Rubin, G.M., Meinertzhagen, I.A., 2017. The comprehensive connectome of a neural substrate for “ON” motion detection in Drosophila. Elife 6, e24394. doi:10.7554/eLife.24394

Wu, M., Nern, A., Williamson, W.R., Morimoto, M.M., Reiser, M.B., Card, G.M., Rubin, G.M., 2016. Visual projection neurons in the Drosophila lobula link feature detection to distinct behavioral programs. Elife 5. doi:10.7554/eLife.21022

Zhang, Y., Kim, I.-J., Sanes, J.R., Meister, M., 2012. The most numerous ganglion cell type of the mouse retina is a selective feature detector. Proc. Natl. Acad. Sci. doi:10.1073/pnas.1211547109

Chapter 4

Behavioral Investigation of Figure Tracking in *Drosophila*

Abstract

As we move through the visual world, our brain is constantly detecting objects around us. The visual disparity cues that distinguish these objects include texture, brightness, color and shape. Yet, these different properties do not define how an object travels through space. The primate visual cortex disregards the diversity of disparity cues; motion sensitive neurons encode object direction regardless of the form that the object has (Albright, 1992; Grill-Spector et al., 1998; Sáry et al., 1993; Stoner and Albright, 1992). Flies in flight track the motion of an object even it contains paradoxical cues such as surface texture moving in the opposite direction of the window itself (Theobald et al., 2010, 2008). Yet, the neural mechanisms of how an object is detected by the movement of texture, brightness, color or shape is not well understood in any system. Here we build on a previous finding that object tracking in flies is achieved by the interaction of motion-dependent and motion independent visual streams (Aptekar et al., 2012). We show that flies respond to objects defined by motion contrast or luminance contrast in a quantitatively and qualitatively distinct way. Object tracking can be modulated by changing the relative motion or luminance strength of the visual stimuli. Neural circuits encoding directional motion prefer luminance contrast coupled with motion, whereas they do not respond strongly if the object boundaries are invisible when its stationary and only revealed when the object moves.

Introduction

Early studies on object tracking in flies posited the existence of two systems: one for motion velocity and one for static position of an object (Reichardt and Poggio, 1975).

This hypothesis was drawn from set of experiments measuring the behavioral responses to a moving or stationary figure defined by the most salient cue: luminance; i.e. a solid black object on a white surround (Figure 1) (Koffka, 1935; Livingstone and Hubel, 1987; Reichardt and Poggio, 1975).

Although this approach is powerful, it is limited due to the large parameter space it occupies. First, the moving object is always confounded by changing position and thus one cannot isolate the individual cues i.e. the bar could be moved at a fixed velocity, but then its position input is constantly varying. To overcome this limitation, Theobald et al. adapted a technique from primate visual psychophysics experiments using object stimuli that move but do not contain any coherent motion cues (e.g. a flickering object that moves across a computer display). It was shown that flies track these types of object better when they are in motion than when they are held stationary. Thus, flies seem to track not only the position of a stationary object, but also the changing position of a moving flickering object regardless of the direction of coherent motion or its presence at all (Theobald et al., 2010, 2008).

What is ‘coherent motion’? A solid object moving across a white surround generates continuous spatial variation in the first moment of luminance (the mean luminance), often called first-order motion (Cavanagh and Mather, 1989), which has been extensively studied in flies. A long running model for first-order motion vision, Hassenstein-Reichardt elementary motion detectors (HR-EMD) is composed of two spatially separated inputs (Hassenstein et al., 1956; Reichardt, 1987). The luminance signal detected by one input is delayed and then multiplied by the undelayed signal from its counterpart leading to enhancement of preferred direction movement. Only if the

luminance change moves from the delayed to the un-delayed direction does the detector produce an output. Although the physiological and behavioral evidence long supported this model (Behnia et al., 2014; Buchner, 1976; Maisak et al., 2013), recent connectomic, physiological and anatomical data indicate that HR model alone is insufficient to explain the data. A second model to detect motion was also proposed by Barlow and Levick (Barlow and Levick, 1965), that differs from HR-EMD. Instead of preferred direction enhancement, BL-EMD proposes suppression of responses to null motion. A variety of models proposed (Strother et al., 2017) including a hybrid HR-BL model (Haag et al., 2016) to explain motion detection in flies. Regardless, EMD relies on luminance correlations between neighboring inputs. Since the EMD is composed of two inputs, from neighboring photoreceptors for example, it can encode motion only over a very small region of space. An array of many such detectors is spatially pooled to compute motion across a large visual field.

Flies track moving objects that generate only ‘higher-order’ motion signals (Theobald et al., 2008) invisible to such models. But figures such as a dark bar on a white background often contain both first-order (e.g. velocity) and higher-order cues (including but not limited to position) simultaneously. To fully explore how flies, track the changing position of a visual object that does not generate coherent motion cues requires adapting the classical approach. A systems identification technique using a figure window that has a matching texture to the background, and can be controlled by white noise, while the internal texture of the window is controlled by a separate random white noise sequence was developed (Aptekar et al., 2012). This technique showed the presence of two parallel systems: one for the Elementary Motion (EM) of the texture

within an object – akin to the classical velocity system, and one system for Figure Motion (FM) of the figure window itself – akin to the position system but not confounded by luminance based positional cues (Aptekar et al., 2012). FM is a broad classification of a moving figure that include figure position, but also include any optical disparity such as shape, contrast, motion and color that would distinguish the edge of a figure from the visual background. The only constraint of FM cues is that they do not drive EMDs. The only constraint of EM cues is that they do.

EM and FM responses are measured at each point along the visual azimuth to reveal retinotopic characteristics of figure tracking and generate spatio-temporal action fields (STAFs) (Aptekar et al., 2012). Although the two systems described by this approach fully capture the behavioral dynamics of figure tracking, including figures that are un-detectable by the EMD, how these two systems are represented in the fly visual system remains unclear.

The fruit fly compound eye consists of ~750 repetitive individual facets. Retinal photoreceptor signals of luminance from each facet are relayed through two neuropiles – the lamina and medulla (see review for (Mauss et al., 2017)), before being processed by the third optic ganglion, the lobula plate, by two sets of directionally selective small field elementary motion detecting columnar neurons called T4 and T5 (Maisak et al., 2013). Incoming retinotopic T4/T5 motion signals are then integrated (summed) by the dendrites of wide-field lobula plate tangential cells (LPTCs) (Schnell et al., 2012, 2010). Flies show diminished wide-field optomotor behavior when T4/T5 cells are blocked, yet this manipulation does not interfere with a fly's ability to track a solid dark figure on a white background (Bahl et al., 2013).

The role of the lobula plate in processing first-order wide-field motion is undisputed. However, based on the T4/T5 inactivation result, it has been speculated that T4/T5 cells along with their synaptic partners, LPTCs, process only first-order motion, and are dispensable for figure tracking; that the higher-order properties of figures must be processed by different brain regions. But their experiments using a black bar on a white surround confound first-order EM and higher-order FM signals. Thus, their results fall short of capturing the rich behavioral repertoire of higher-order figure tracking that doesn't depend on luminance cues. Furthermore, it has been demonstrated that LPTCs show sensitivity to types of higher-order stimuli (Theobald et al., 2010, 2008), that EMDs cannot detect (Lee and Nordstrom, 2012). Thus, the circuitry for figure detection cannot be fully probed by using a simple 'classical' stimulus regime such as a dark bar on white ground. Here we tested whether flies show different behavioral responses to a first-order figure that confounds all of the cues (i.e. a dark bar on a white background) from a figure that does not (i.e. a bar that is randomly textured as same as the background, and thus is detectable only when it is moving). The same approach has been applied to the nervous system of primates to investigate 'form invariance' – whether the activity patterns of neurons in different regions of brain persist when objects defined by different forms are moved along the same trajectory (Appelbaum et al., 2006; Geesaman and Andersen, 1996; Van Essen and Gallant, 1994). Our results indicate unequivocally that even when these two types of figures moved with same trajectory they elicit distinct behavioral response confirming a complex interplay between EM dependent and FM dependent subsystems.

We show that textured and luminance defined figures are tracked in distinct ways, independent of their trajectory, speed, contrast and size. For a motion defined figure, flies exhibit a strong anti-directional turn when the figure first appears in the rear visual field. This is followed by a locked on syn-directional turn. For a luminance defined figure moving in the same trajectory, flies never exhibit a strong anti-directional turn and show strong syn-directional responses, even before the figure passes the visual midline. We propose that the behavioral differences seen arise from the differential circuit activation in T4/T5. A luminance defined figure elicits stronger calcium responses in T4/T5 than a motion defined figure hinting the possibility that EM activation is stronger. Overall, our results reveal simple illustration of how EM and FM interact with one another to generate complex bar tracking behavior.

Results

To investigate behavioral responses to first-order motion consisting of different figure forms, we used visual flight simulators and presented a revolving bar around the fly in open loop (Figure 2A) (Reichardt and Poggio, 1975; Reiser and Dickinson, 2008). Two distinct visual stimuli are used: one composed of a figure defined only by motion cues and the other composed of both motion and luminance cues. To eliminate the luminance cues we matched the texture of the figure to the background. Thus, the motion-defined figure is invisible when it stops (Figure 2B). The luminance defined figure, a solid dark bar on a uniform white background, is visible everywhere in the arena and therefore presents a strong positional cure when it stops (Figure 2B). The two figures are revolved around the arena at the same speed (90 deg/sec), along the same trajectory.

Interestingly, the behavioral responses to these two stimuli are fundamentally different from one another. For the luminance-defined figure, flies show strong syndirectional steering to the motion of the figure, which results in a robust phase-advanced steering response – i.e. the animal's steering response as the figure approaches visual midline appears to anticipate the figure's position. By contrast, for a motion-defined figure moving along the same trajectory, flies initially show a counter-directional turn toward the figure and "lock on" to the trajectory of the figure without any anticipation (Figure 3).

To test if the contrast has any effect on luminance-defined bar tracking behavior, we used bars with varying contrasts (Figure 4A). All the stimuli used have negative total contrast indicating that the luminance of the bar is smaller than the background. To our surprise, flies tracked all bars, even with -8% contrast value, equally well (Figure 4B). Furthermore, the tracking behavior did not change qualitatively, flies still exhibited a strong syndirectional steering to the motion of the figure. Flies showed phase-advanced steering responses to all contrasts (Figure 4C). The degree of the phase-advanced steering responses was weaker for the lowest contrast bar compared to the highest (Figure 4C). Regardless, our results indicate that as long as the bar has lower luminance values than the background (OFF bars) flies treat it the same way and show a strong syndirectional response.

To test if the contrast has any effect on motion-defined figure tracking, we varied the contrast of the visual stimuli while keeping the overall luminance same. The figure and the background have the same average luminance making the figure only visible when it moves (Figure 5A). Flies exhibited identical motion-defined figure tracking independent of the contrast for the three values we tested (Figure 5B, 100%, 75% and

43%). However, the tracking in the rear visual field is impaired when the contrast was at 14% revealing that the motion cue alone was not enough to elicit a response. Interestingly, front visual field tracking was intact and similar to the high contrast motion-defined figure tracking behavior (Figure 5B). Steering responses when the motion-defined figure is at the midline does not vary significantly from one another (Figure 5C). Indicating that contrast does not influence the locking on behavior seen in high contrast patterns. Thus, flies track motion-defined figures with an anti-directional turn followed by a syn-directional steering response independent of the overall contrast.

Next, we tested if the background contrast plays a role on motion-defined and luminance-defined figure tracking. In all of our experiments, the background is composed of two intensity values that allow us to create either a high contrast, large difference between the intensity values, or low contrast background, difference between the intensity values are small. To test the effect of background contrast on figure tracking, we fixed the average luminance of the figure and changed the background contrast. We first tested a figure that has the same average luminance as the background similar to the motion-defined figure defined in Figure 2B. However, this figure had a higher background contrast, leading to a difference in the standard deviation of the luminance. When tracking figures with different standard deviation of luminance, flies exhibited a behavior similar to motion-defined figure tracking. Initial anti-directional turn followed by a syn-directional steering response (Figure 6B). When the standard deviation of the background luminance is reduced, leading to a smaller background luminance and introducing a difference in the mean luminance between figure and background, flies switched their tracking behavior. At the highest contrast

between figure and ground, flies exhibited luminance-defined figure like tracking, indicating that the mean luminance between figure and ground is used as the cue to determine the tracking behavior (Figure 6B). The steering responses at the midline systematically shifted from locking on to the figure to the syndirectional responses as the mean luminance difference between the figure and the background is increased (Figure 6C). Furthermore, we tested if increasing the background luminance rather than decreasing have the same effect (Figure 7). The contrast between the figure and the background between these two experiments (Figure 6 and 7) were sign inverted. In Figure 6 the background luminance was decreased while keeping the same figure luminance, leading to a luminance-defined bright figure, whereas in Figure 7, the background luminance was increased leading to a luminance-defined dark figure. These results are difficult to interpret since the mean luminance of the background is not fixed as the contrast is varied. However, it suggests that the tracking behavior is highly influenced by the background contrast and can be modulated by it.

The subtle differences we observed when we compared a bright bar (Figure 6B, purple line) and a dark bar (Figure 7B, purple) responses prompted us to compare the responses to a luminance-defined bright figure to a motion-defined figure. As mentioned above, revolving a dark bar around the fly leads to a very subtle anti-directional turn that is much weaker than to motion-defined figure (Figure 3). Although the bright figure responses (Figure 8B) were very similar to the dark figure responses (Figure 3), flies did not exhibit the slight anti-directional turn for the bright figure. Flies either performed a slight syndirectional turn or maintained their steering at midline (Figure 8B). This indicates that the contrast polarity of a luminance-defined figure has an influence over

the tracking behavior, similar to another behavior that has been observed before (Reiser and Dickinson, 2008). Such differences could arise from the contribution of phototactic circuits to the behavior when a bright figure is presented.

Next, we asked if the initial perception of figures driven by distinct cues. What differs most in the behavioral response to the motion-defined and luminance-defined bar is the initial response as the figure moves into the visual periphery, with the former eliciting a turn towards the figure, and the latter eliciting no clear response at all. To quantify this difference, we picked eight trajectories that start at different locations but end in the same location (midpoint) along the visual azimuth. This experiment illustrated that flies show a counter directional steering to a textured figure moving back to front at all trajectories regardless of the length of the trajectory (Figure 9). Shortest trajectory which is about 225 milliseconds elicited a weaker syndirectional response to motion-defined figure compared to luminance-defined figure. Rest of the tested trajectories always elicited a counter directional steering effort even when the trajectory was as short as 30 degrees and 200 ms long (Figure 9). Furthermore, the responses to two figures are distinct with all tested different length trajectories. Interestingly, flies start the counter-directional steering earlier as the length of the trajectory is increased. This suggests that the first detection time of the motion defined figure initiates the steering effort and not the specific location of the figure on the retina. Thus, we concluded that the initial detection of these figures is qualitatively distinct.

To test if the size plays a role in motion-defined and luminance-defined figure tracking behavior, we used three different sizes (15,30 and 45 degrees, Figure 10). Overall tracking behavior was similar to what we observed before, strong anti-directional

responses to motion-defined figures and syn-directional phase advanced responses to luminance-defined figures. The difference between luminance-defined figure tracking and motion-defined figure tracking was qualitatively distinct independent of figure size (Figure 10B and C). At all sizes, flies showed a strong anti-directional turn towards the figure, when the figure was defined solely by its motion and strong syn-directional turn, when the figure was defined by its motion and luminance. It is important to note that in these experiments each figure passes the visual midline at different time points, making it hard to compare the figure tracking behavior within different sizes. Thus, we tested if the motion-defined figure tracking or luminance-defined figure tracking differs for different sized figures. We achieved this by setting the visual midline passing to the exact same time point for three sizes (15°, 30° and 45°, Figure 11). Interestingly, flies performed stronger anti-directional turns towards the 15° motion-defined figure than 45° motion-defined figure (Figure 11B), revealing that size might play a role in the initial responses to such figures. The locked-on steering responses once the object passed the visual midline were also dependent on size. Flies showed a stronger syn-directional turn when a 45° figure presented compared to a 15° figure. Some of these results could be explained by a previous finding that flies track edge of the figures independent of its size (Aptekar et al., 2015). Although the leading edge of figures enter the visual midline at the same time in these experiments, the trailing edge of larger figures pass the midline latest. Thus, the strong syn-directional responses seen could be the direct result of tracking of trailing edges. Regardless, our results reveal that the size does not affect the qualitative differences between motion-defined and luminance-defined figures

(Figure 10), but smaller sized motion-defined objects elicit stronger anti-directional responses and weaker syn-directional responses (Figure 11).

Next, we tested if the velocity of the figure has any effect on the qualitative differences between motion-defined and luminance-defined figure tracking. Six total velocities (15, 30, 60, 90, 120 and 240 deg/sec) used for both figures (Figure 12). Flies exhibited qualitative differences when tracking motion-defined and luminance-defined figures at all velocities (Figure 12B). Anti-directional turn that is seen in motion-defined figures were more pronounced at lower speeds, whereas flies showed no or little anti-directional turn towards the figure at higher speeds (Figure 12B). Thus, revealing that cells and circuits that are responsible for the anti-directional turn is more sensitive to slower speeds. Yet, the behavioral responses to motion-defined and luminance-defined figures were different at all speeds tested, indicating that velocity does not influence the qualitative differences seen in figure tracking (Figure 12B)

We tested a wide variety of conditions to further dissect the contribution of figure contrast and background luminance to figure tracking behavior. First, we kept the Weber contrast (difference between the mean luminance of the figure and the background) of the figure fixed while varying the standard deviation of the figure luminance. This allowed us to create figures that have the same total luminance but varied in contrast (Figure 13). In all cases the figures had smaller total luminance than the background, making them similar to luminance-defined figures. Figure tracking behavior shifted from luminance-defined figure like tracking to motion-defined figure tracking as the standard deviation of the figure luminance decreased (Figure 13). For example, behavioral responses to a high standard deviation luminance figure resembled

and largely overlapped with responses to motion-defined figure tracking (Figure 13, blue and red, lower row). However, the initial strong anti-directional turn was absent in these responses (Figure 13, blue, lower panel). When the standard deviation of the luminance is decreased (Figure 13, purple, stimulus 5), the tracking behavior matched luminance-defined figure tracking (Figure 13, purple, upper panel). This suggests, that the initial anti-directional turn is influenced by the standard deviation of luminance.

Previous work from our lab has shown that head movements in *Drosophila* play a role in tracking of small moving figures (Fox and Frye, 2014). We tested the hypothesis that the differences seen in motion-defined and luminance-defined figure tracking behaviors might be attributed to the head movements. We presented motion-defined and luminance-defined figures to both head-fixed and head-free flies (Figure 14A and B). Interestingly, restricting the head movements did not change the tracking behavior significantly (Figure 14B). Flies showed a strong anti-directional turn towards a motion-defined figure followed by locked-on tracking (Figure 14B, blue trace), where as they exhibited phase-advanced responses when a luminance-defined figure is presented. We next compared if the figure tracking behavior of luminance-defined or motion-defined figures are influenced by the head movements. When we compared head-free (Figure 14C, baby blue) and head-fixed (Figure 14C, orange) flies' responses to a luminance-defined (Figure 14C, left) and motion-defined figure (Figure 14C), we did not observe qualitatively different responses. Head-fixed flies oriented back to the visual midline right after the figure left the visual field, whereas this response was not as strong in head free flies (Figure 14C, green arrow).

Finally, we investigated if the behavioral differences seen are also represented in the neural circuitry. To show that these two stimuli indeed elicit unique responses in visual neurons, we expressed genetically encoded calcium indicator (GCaMP) in T4/T5 cells and imaged the cellular activity using a 2-photon microscope (Akerboom et al., 2012; Tian et al., 2009). T4/T5 cells showed stronger activation to luminance-defined figure compared to the motion-defined figure (Figure 15). These results could be explained by the fact that the spatial resolution of the fly eye is not enough to resolve individual pixels moving in the textured bar thus leading to a weaker activation in neurons responding to luminance changes. Yet, it is not enough to explain why the behavioral responses to these two stimuli are distinct.

Discussion

Here we presented evidence showing that flies show quantitatively and qualitatively distinct responses to motion-defined and luminance-defined figures. Flies exhibit strong anti-directional turns toward motion-defined figures when the figure is in the rear visual field. This is followed by a syndirectional turn that is locked on to the figure. In contrast, flies do not show this anti-directional turn when the figure is luminance-defined. When we probed the relationship between the figure tracking behavior and how a figure is defined based on its' luminance and its' relative contrast to the background, we found a simple principle to explain our results. The cue flies use to classify a figure is its mean luminance compared to the background. If the mean luminance of the figure is different than the background, flies classify it as a luminance-defined figure and perform luminance-defined figure tracking behavior (Figure 3). Flies exhibit distinct responses to figures that have higher mean luminance compared to the background than lower mean

luminance. These differences are limited to the rear visual field (Figure 3 and Figure 8) and might be influenced by the recruitment of circuits responsible for phototaxis.

We showed that if the mean luminance of the figure matched the mean luminance of the background, flies exhibit motion-defined figure tracking behavior (Figure 3). The total luminance and the variance in the background luminance had no effect on this behavior, supporting the notion that motion-defined and luminance-defined tracking are distinct modes of tracking.

Overall our results demonstrated that the figure tracking behavior is highly dynamic and depends on the difference between mean luminance of the figure and the background. We showed that the speed (Figure 12), trajectory (Figure 9) and the size (Figure 10 and 11) do not influence the differences between motion-defined and luminance-defined figure tracking. Neural circuits that respond motion in a directionally selective manner show stronger responses to luminance-defined figures, raising the possibility that some of the differences seen in behavior might be attributed to this (Figure 15). Changing the luminance contrast did not influence the figure tracking behavior for both motion-defined (Figure 5) and luminance-defined figure (Figure 4) tracking. In addition, we showed that restricting the head movement of the fly does not impair motion-defined or luminance-defined figure tracking (Figure 14).

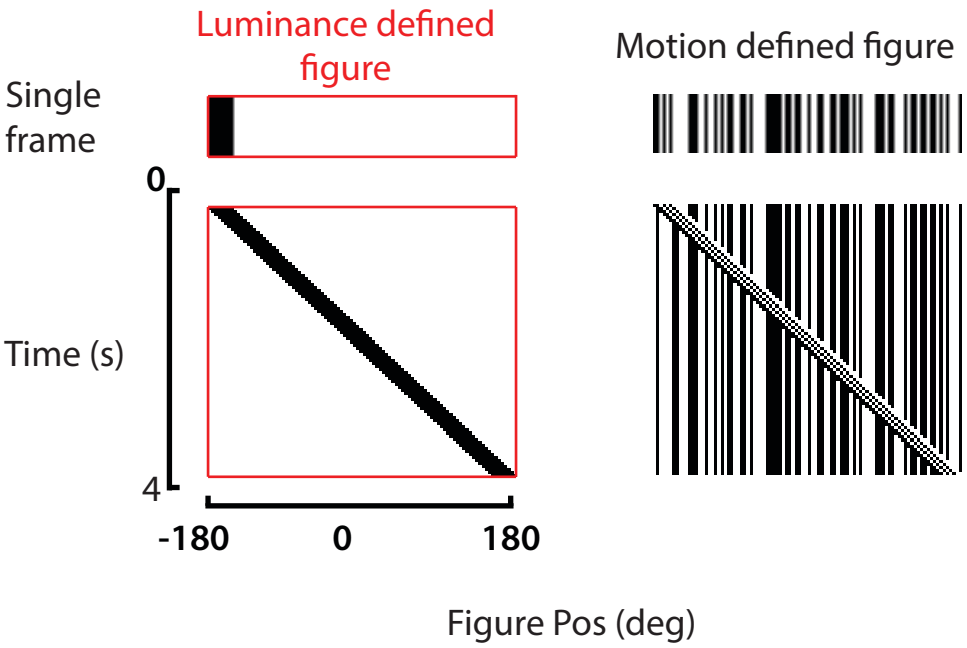

Figure 4.1: Classical studies used a figure defined by the most salient cue. A figure defined by the most salient cue (luminance) is shown in red outline. A figure defined by its motion is shown on the right. Space/time plots is shown for a full rotation around the 360° visual azimuth.

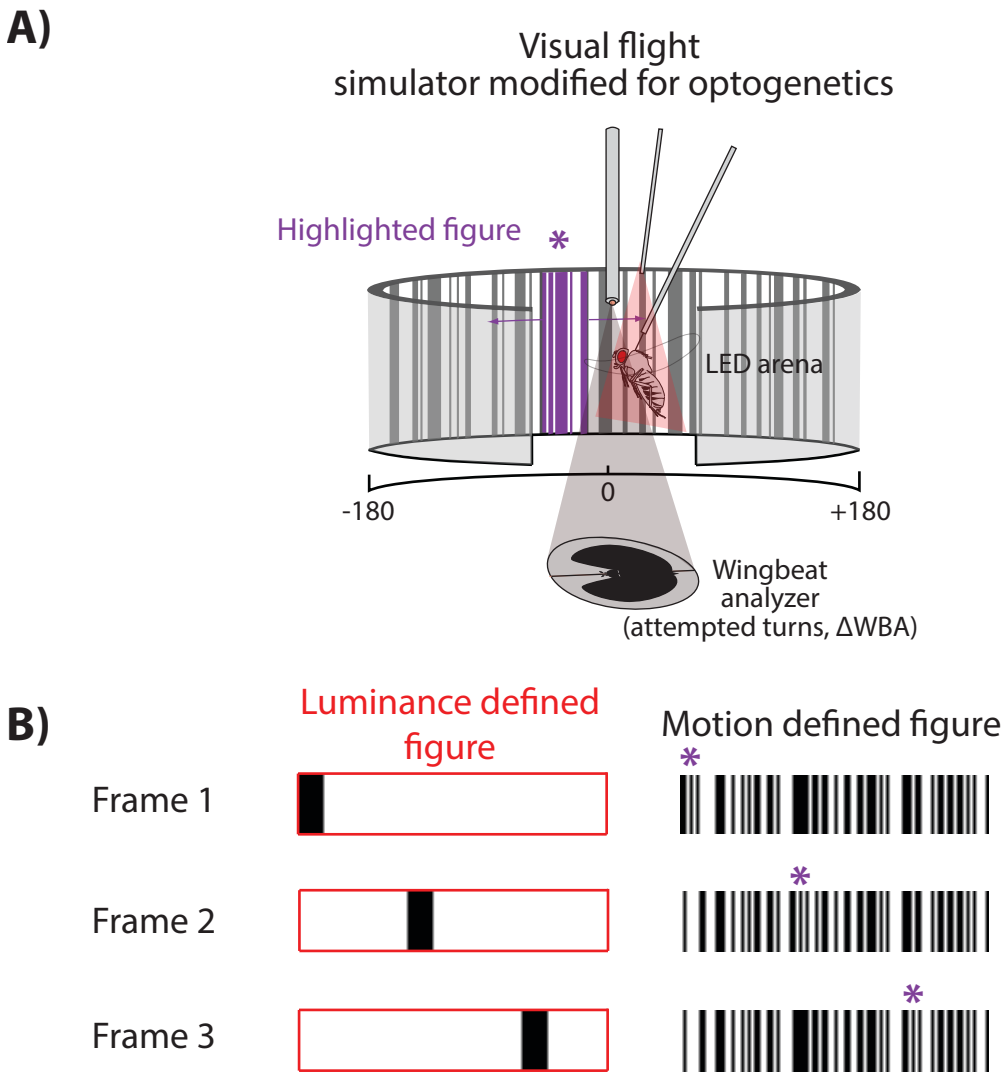

Figure 4.2: A) Virtual reality flight simulator modified for the use of optogenetics. Fly is illuminated with a 655-nm light to excite neurons expressing Chrimson. The same setup is also used for non-Chrimson experiments. A moving figure is depicted in purple. **B**) A luminance defined figure is always confounded by its positional cue (shown in red boxes). A motion defined figure is invisible when it stops.

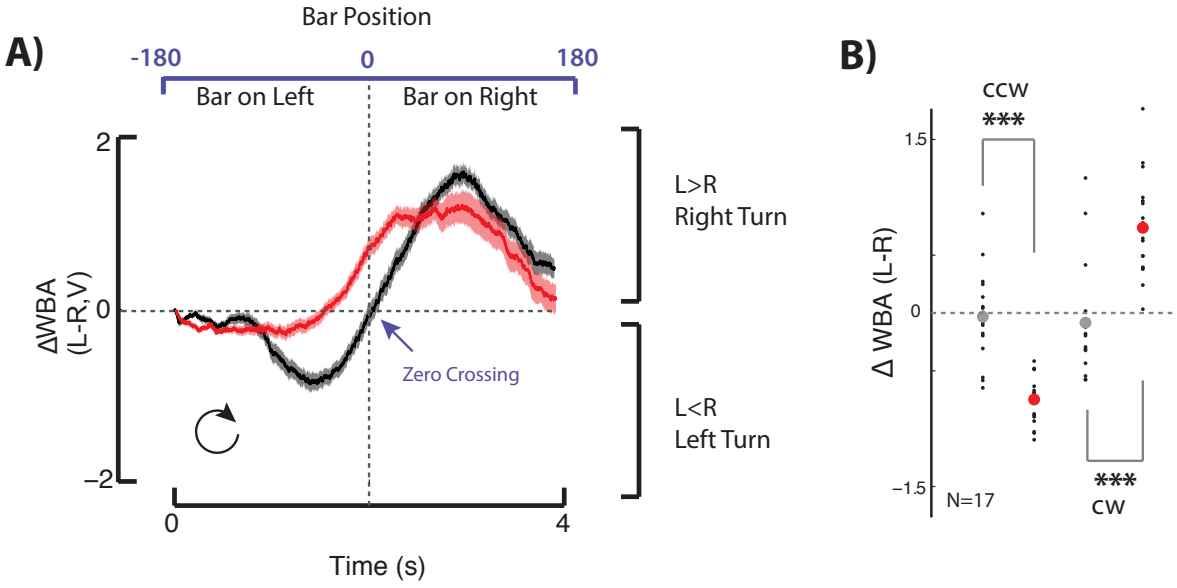

Figure 4.3: Figures carrying similar cues but different forms elicit distinct responses. A) Behavioral responses to clockwise rotation of a motion-defined (shown in black) and luminance-defined (shown in red) figures. Purple arrowhead indicates when the figure is directly in front of the fly. Motion-defined figure elicits strong initial counter directional steering and DWBA is zero when the figure is at zero crossing, indicating a lock on tracking mechanism. Flies start a syndirectional turn before the luminance defined bar passes midline so that DWBA is positive (right turn) as the figure crosses visual midline (Zero Crossing). Shaded regions indicate S.E.M. n=21**B)** Comparison of the steering direction at zero crossing between motion-defined (gray) and luminance-defined figure (red). two-sample t-test, *p<0.001*

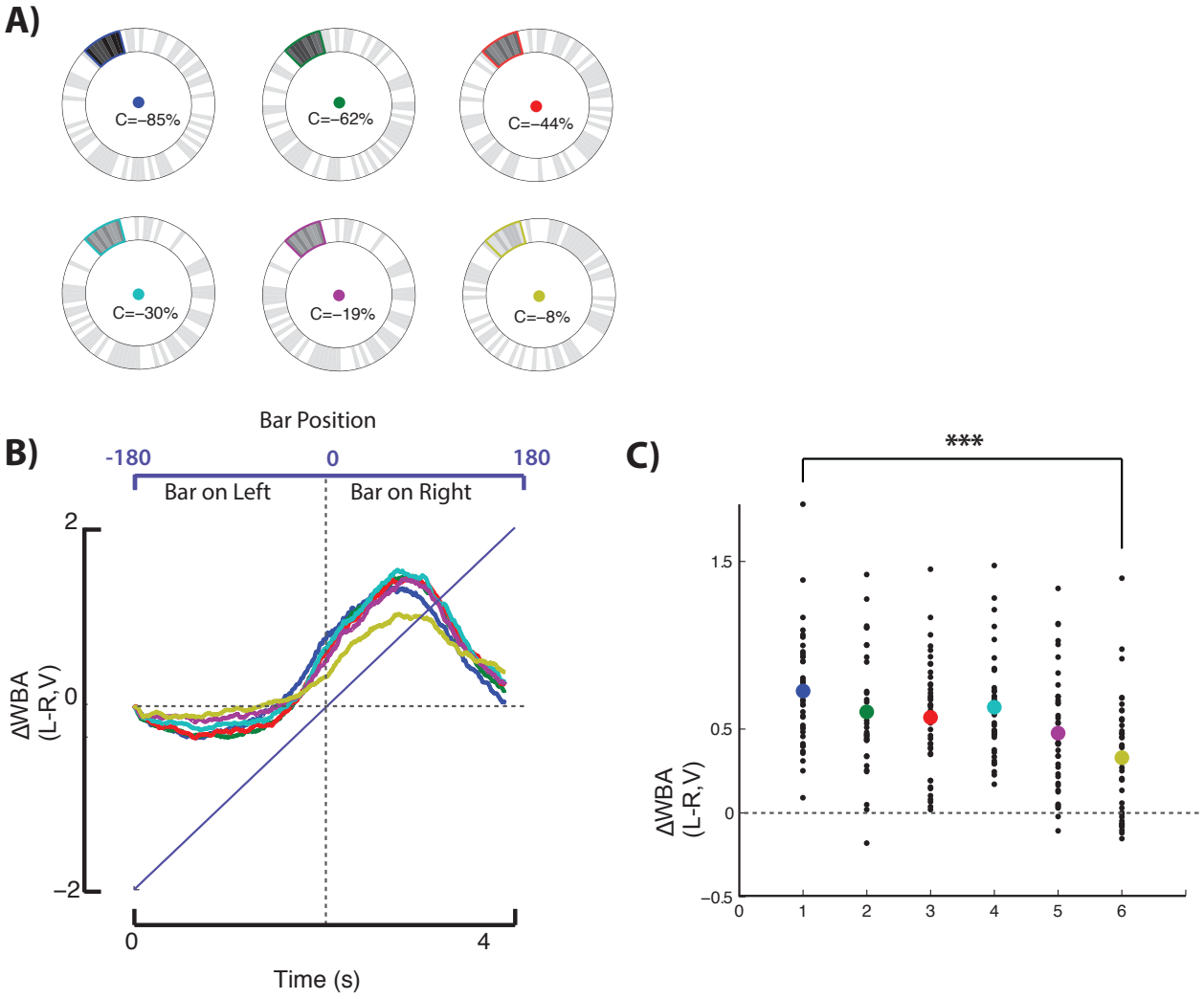

Figure 4.4: Contrast does not influence luminance-defined figure tracking. A) Luminance of a figure varied on a fixed luminance background. Colors indicate the tested visual stimuli in Fig 4B. **B)** Behavioral responses to clockwise rotation of a luminance defined figures at varying contrasts. Strong syndirectional steering responses persist at varying contrasts. n=42 **C)** Comparison of the steering direction at zero crossing between different contrast luminance-defined figures. Positive delta wing beat amplitude indicate a syndirectional turn before the figure crosses the visual midline. two-sample t-test, *p<0.001*

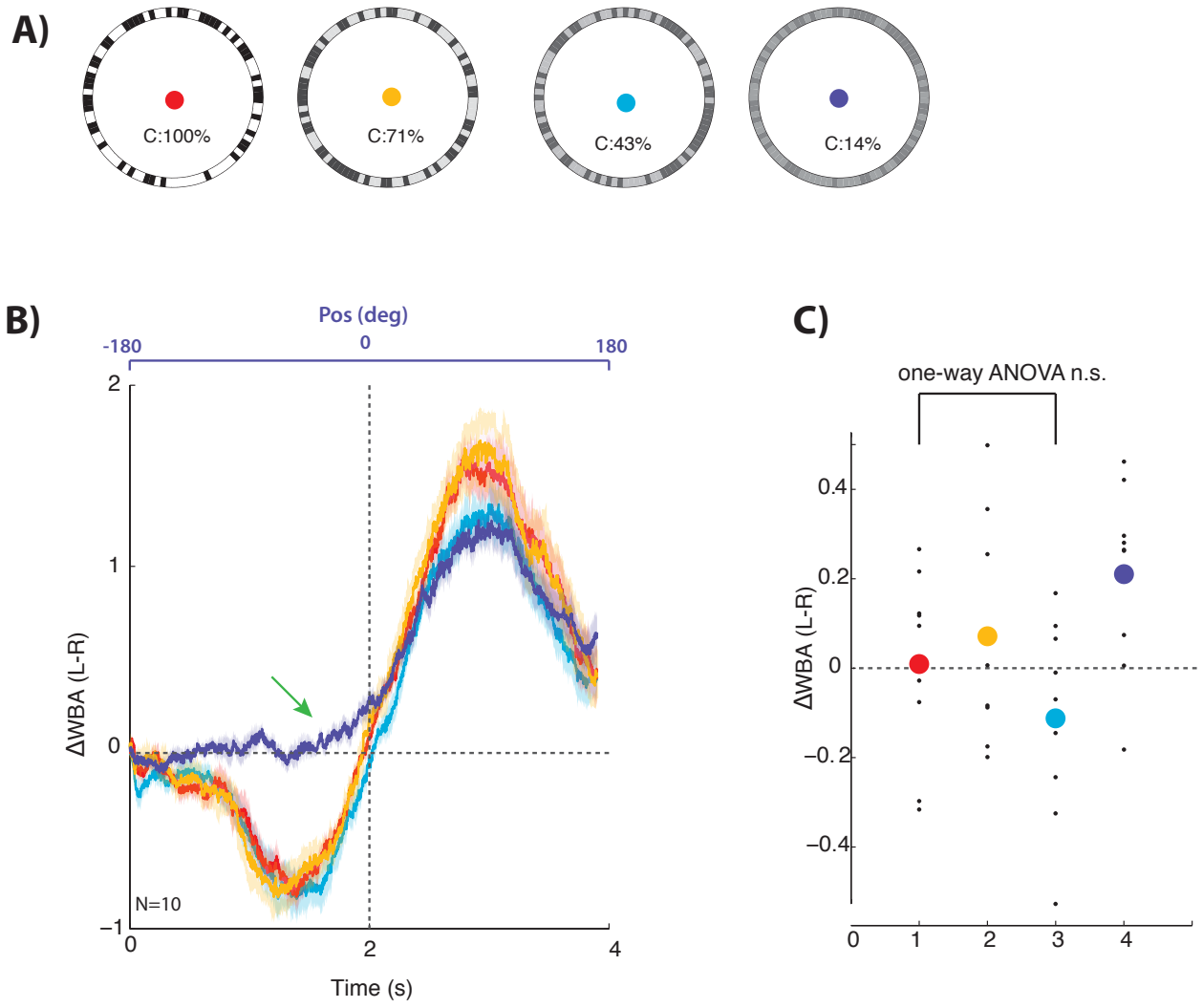

Figure 4.5: Low contrast impairs motion-defined figure tracking in the rear visual field. A) Overall contrast of a motion-defined figure is varied. Colors indicate the tested visual stimuli in Fig 5B. **B)** Behavioral responses to clockwise rotation of a motion-defined figure at varying contrasts. Tracking is impaired (purple line) when the contrast is at 14% (green arrow). S.E.M. n=10 **C)** Comparison of the steering direction at zero crossing between varying contrast motion-defined figures. Positive delta wing beat amplitude indicate a syndirectional turn before the figure crosses the visual midline, whereas zero indicates locking on to the figure. one way ANOVA n.s.

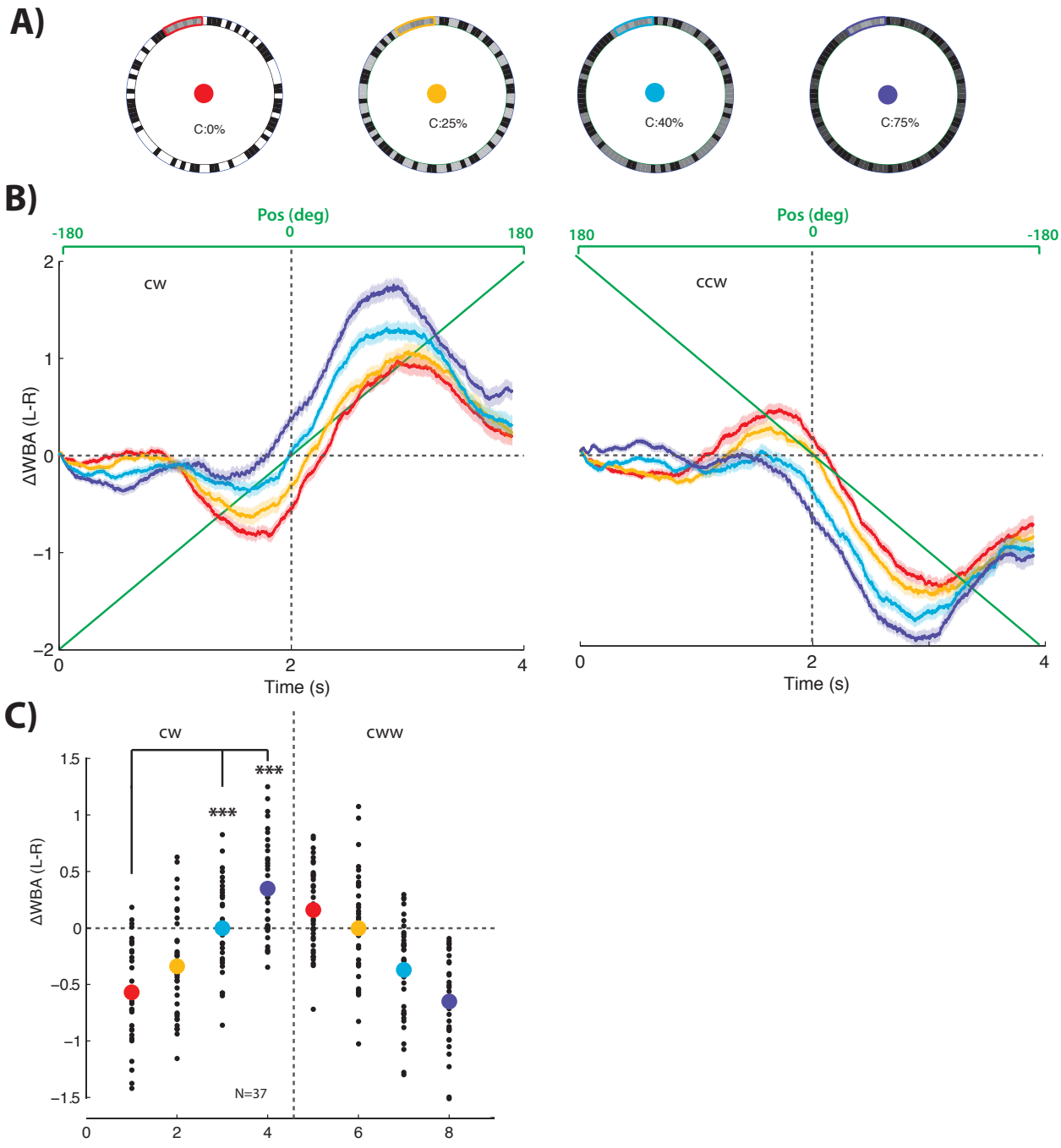

Figure 4.6: Flies switch tracking behavior with varying background luminance. A) Contrast of the background varied with a fixed figure luminance. Contrast between the figure and the ground is indicated. **B)** Behavioral responses to clockwise (CW) and counter-clockwise (CCW) rotation of a figures with same average luminance with varying background contrasts. Anti-directional turn disappears as the contrast between

the figure and background is increased. n=37 **C)** Comparison of the steering direction at zero crossing between figures with same average luminance but on different backgrounds that have varying contrasts. one way ANOVA, $p<0.001$

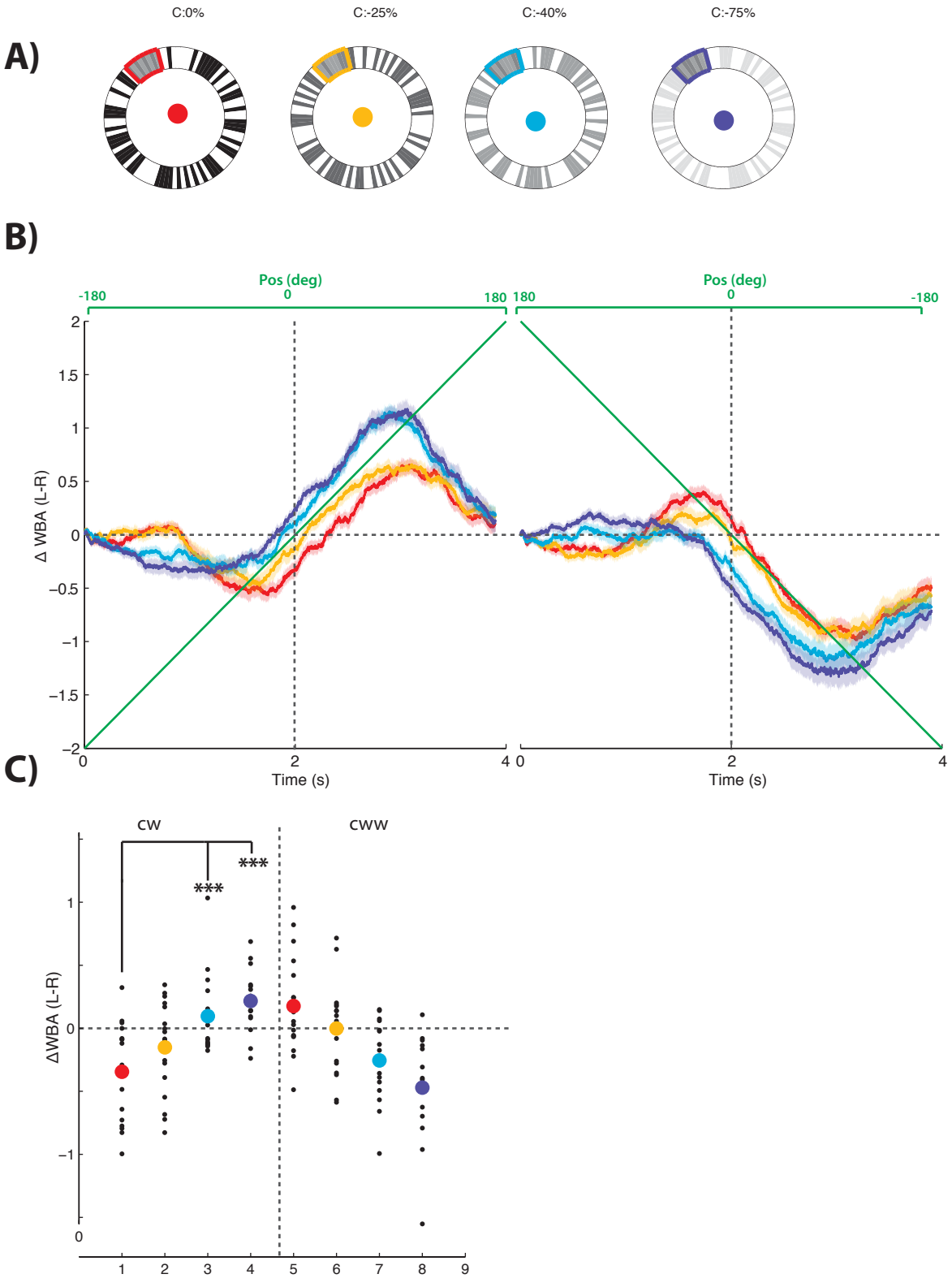

Figure 4.7: Flies switch tracking behavior with varying background luminance. A)

Contrast of the background varied with a fixed figure luminance. Contrast between the

figure and the ground is indicated. **B)** Behavioral responses to clockwise (CW) and counter-clockwise (CCW) rotation of a figures with same average luminance with varying background contrasts. Anti-directional turn disappears as the contrast between the figure and background is increased. n=19. **C)** Comparison of the steering direction at zero crossing between figures with same average luminance but on different backgrounds that have varying contrasts. one way ANOVA, $p<0.001$

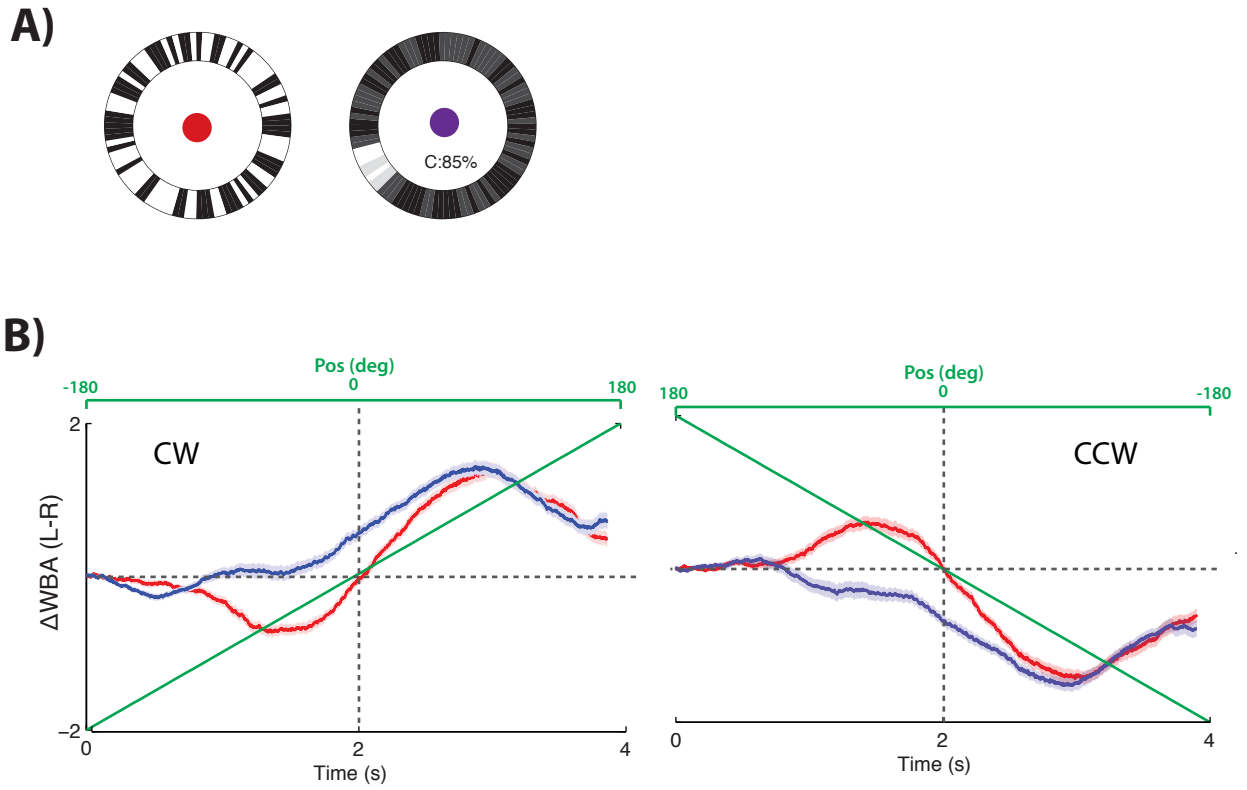

Figure 4.8: Luminance-defined figure tracking is sensitive to the contrast of the figure. A) Two visual stimuli used to test the differences between a luminance-defined figure brighter than the background and a motion defined figure. **B)** Behavioral responses to clockwise (CW) and counter-clockwise (CCW) rotation of a motion-defined and luminance-defined figures. Green line indicates the position of the figure. n=34.

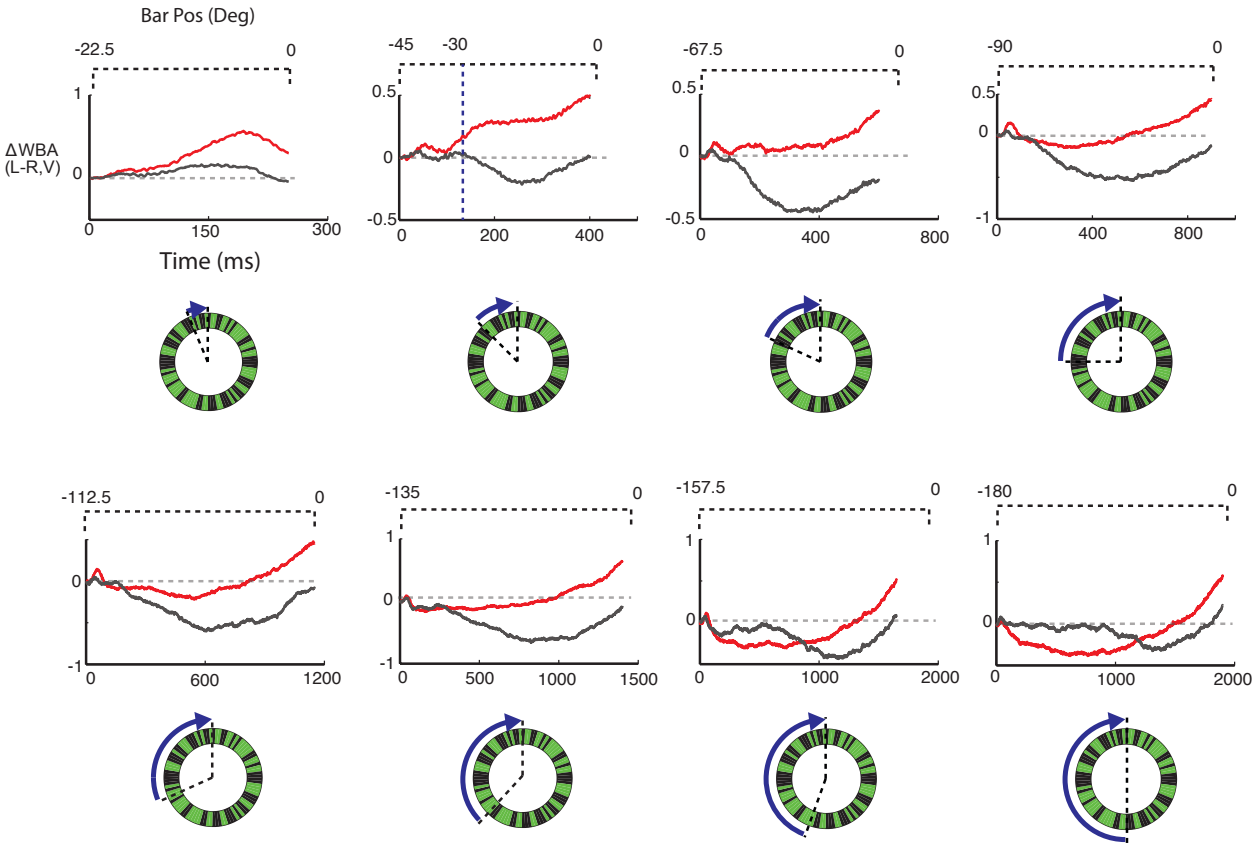

Figure 4.9: Initial perception of figures is driven by distinct cues. Steering responses to luminance-defined (red) and motion-defined (black) figures starting at eight different location along the visual azimuth. Cartoon illustrations of trajectories shown by blue arrows below the behavioral responses. Blue dashed line on the second panel indicates the start point of a counter directional turn observed at closest position on the arena to the midpoint. Counter directional turn for a motion defined figure doesn't depend on the length or the starting position of the trajectory. Flies show no counter-directional turn to luminance defined figures. n=37.

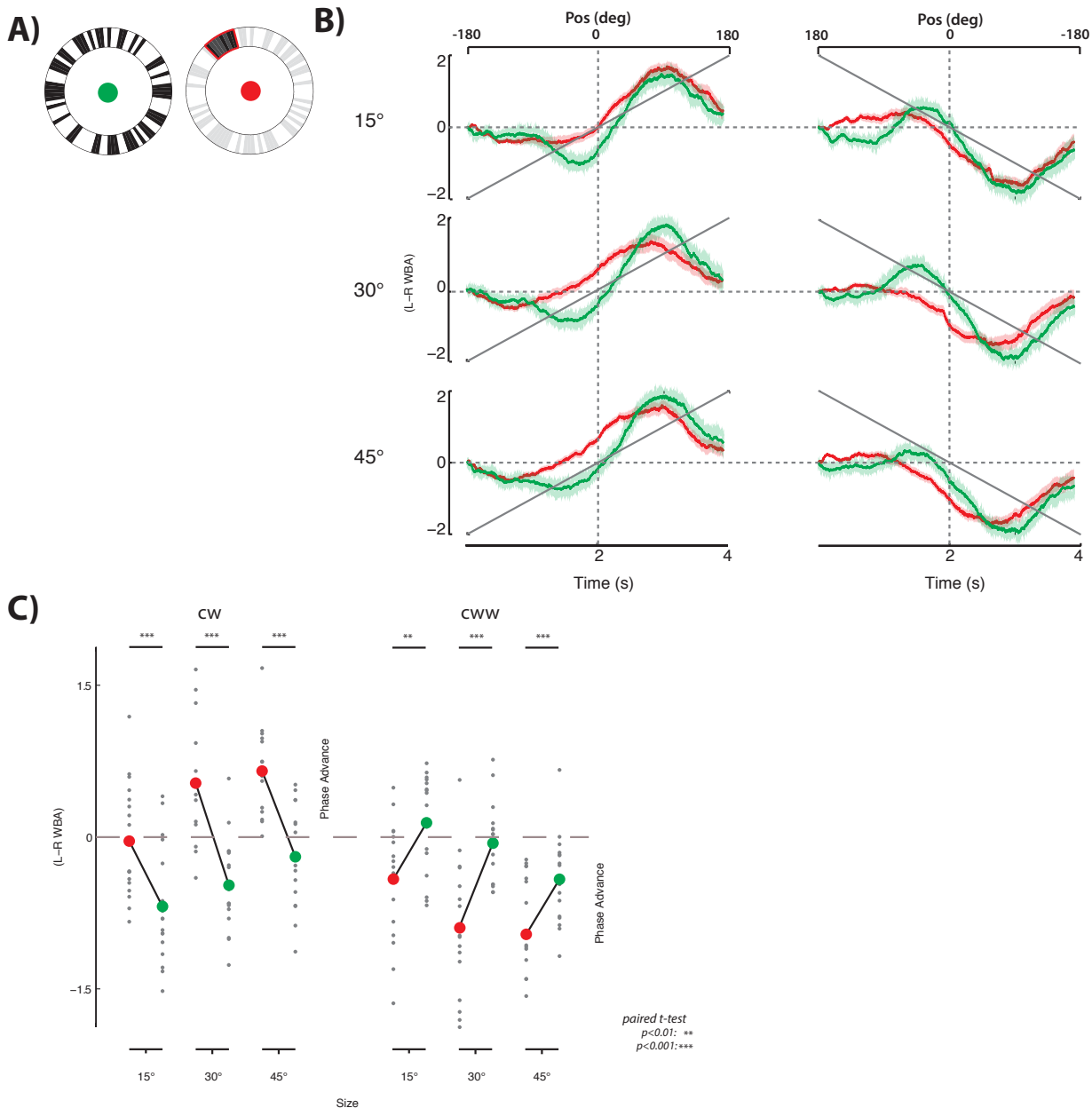

Figure 4.10: Size of a figure does not influence the qualitative differences between luminance and motion defined figure tracking A) Motion-defined (green) and luminance defined (red) figures used to test the effects of size **B)** Behavioral responses to clockwise (CW) and counter-clockwise (CCW) rotation of different size (15, 30 and 45 degrees) motion-defined (green) and luminance-defined (red) figures.

Shaded regions indicate S.E.M. n=17 **C)** Comparison of the steering direction at zero crossing between figures with different sizes. Significance is indicated on top.

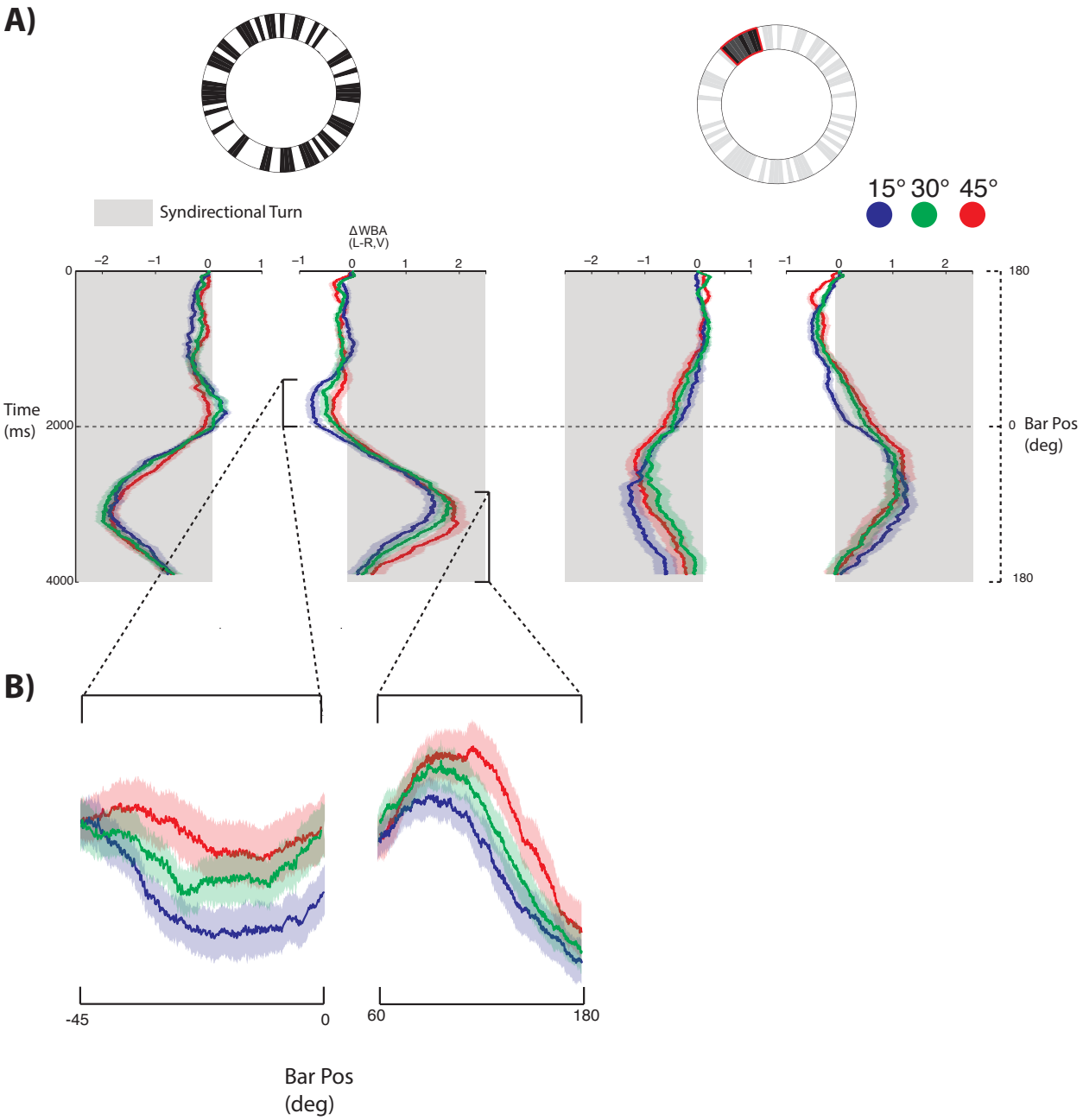

Figure 4.11: Size of a figure influences luminance and motion defined figure tracking. A) Behavioral responses to clockwise (CW) and counter-clockwise (CCW) rotation of motion-defined figure (left) and luminance-defined figure (right) with different size (15, 30 and 45 degrees labeled as blue, green and red, respectively). S.E.M., n=20.

B) Comparison of the steering responses to regressively (left) and progressively (right) moving different sized motion-defined figures.

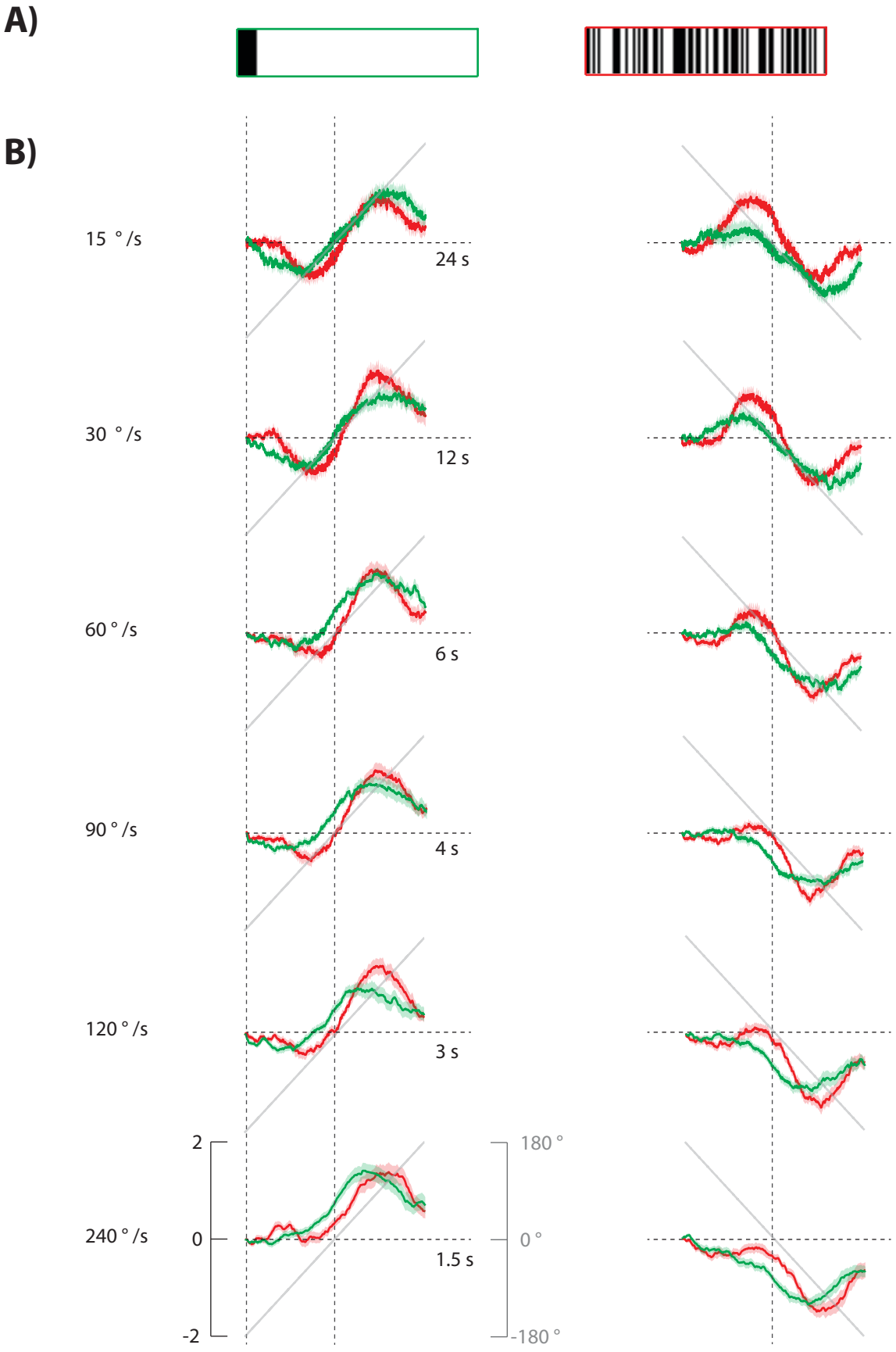
A)
B)
15 °/s
24 s
30 °/s
12 s
60 °/s
6 s
90 °/s
4 s
120 °/s
3 s
240 °/s
1.5 s
2
0
-2
180 °
0 °
-180 °

Figure 4.12: Figure velocity does not affect the qualitative differences between motion-defined and luminance-defined figure tracking A) A luminance-defined (outlined green) and motion-defined figure (outlined red) is used to test the effect of velocity on figure tracking. **B)** Behavioral responses to clockwise (CW) and counter-clockwise (CCW) rotation of motion-defined (red) and luminance-defined figure (green) at different velocities. S.E.M., n=26.

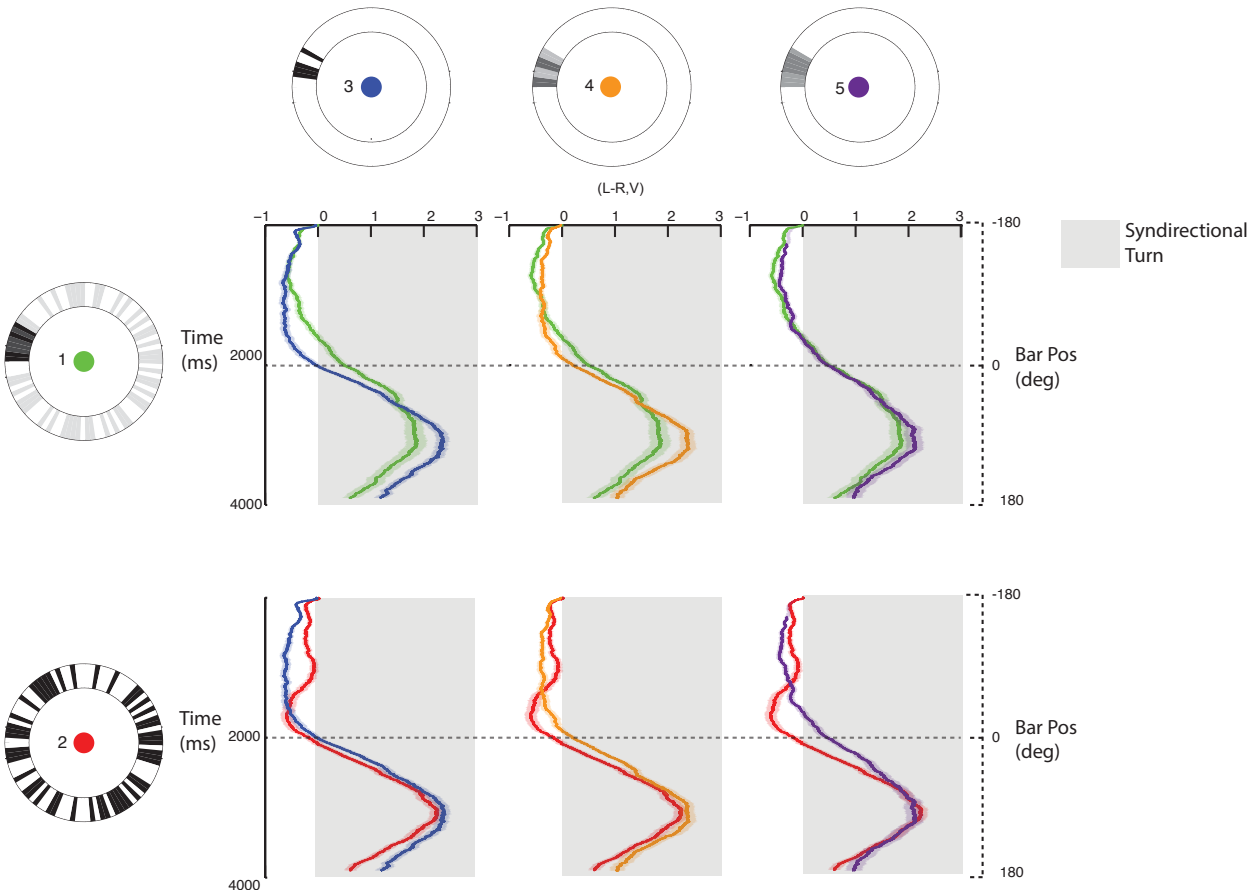

Figure 4.13: Figure tracking behavior shifts from luminance-defined figure tracking to motion-defined figure tracking as the standard deviation of the figure luminance decreased. Tracking of three different visual stimuli (labeled 3,4 and 5) composed of figures that have same mean luminance with varying standard deviation of luminance compared to the motion-defined (red, number 2) or luminance defined (green, number 1) figure tracking. Pairwise comparison of behavioral responses to clockwise rotation of a luminance-defined figure to three different visual stimuli (from left to right, stimulus 1-3, 1-4 and 1-5). Pairwise comparison of behavioral responses to clockwise rotation of a motion-defined figure to three different visual stimuli (from left to right, stimulus 2-3, 2-4 and 2-5). S.E.M. n=43

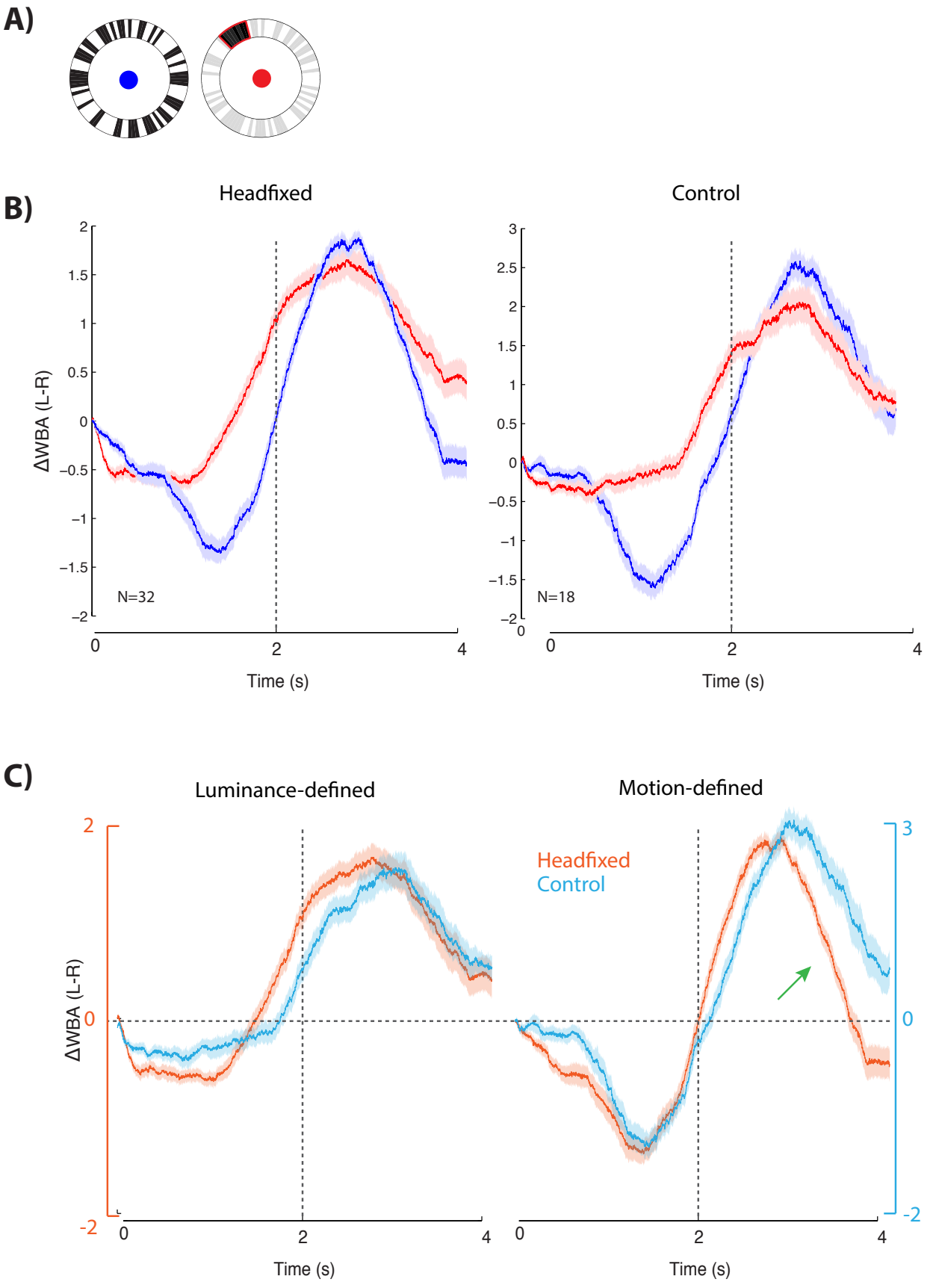
A)
B)
Headfixed
Control
ΔWBA (L-R)
N=32
N=18
Time (s)
C)
Luminance-defined
Motion-defined
Headfixed
Control
ΔWBA (L-R)
Time (s)

Figure 4.14: Head movements does not influence the differences between motion-defined and luminance-defined figure tracking. A) Visual stimuli used in the experiment; a motion-defined bar (labeled blue) and a luminance-defined bar (labeled red). **B)** Behavioral responses of head-fixed (left) and head-free (right) flies to both motion-defined and luminance-defined figures. **C)** Comparison of behavioral responses of head-fixed (orange) and head-free (baby blue) flies to luminance-defined (left) and motion-defined (right) figures. Green arrow indicates the responses that differ between head-free and head-fixed flies.

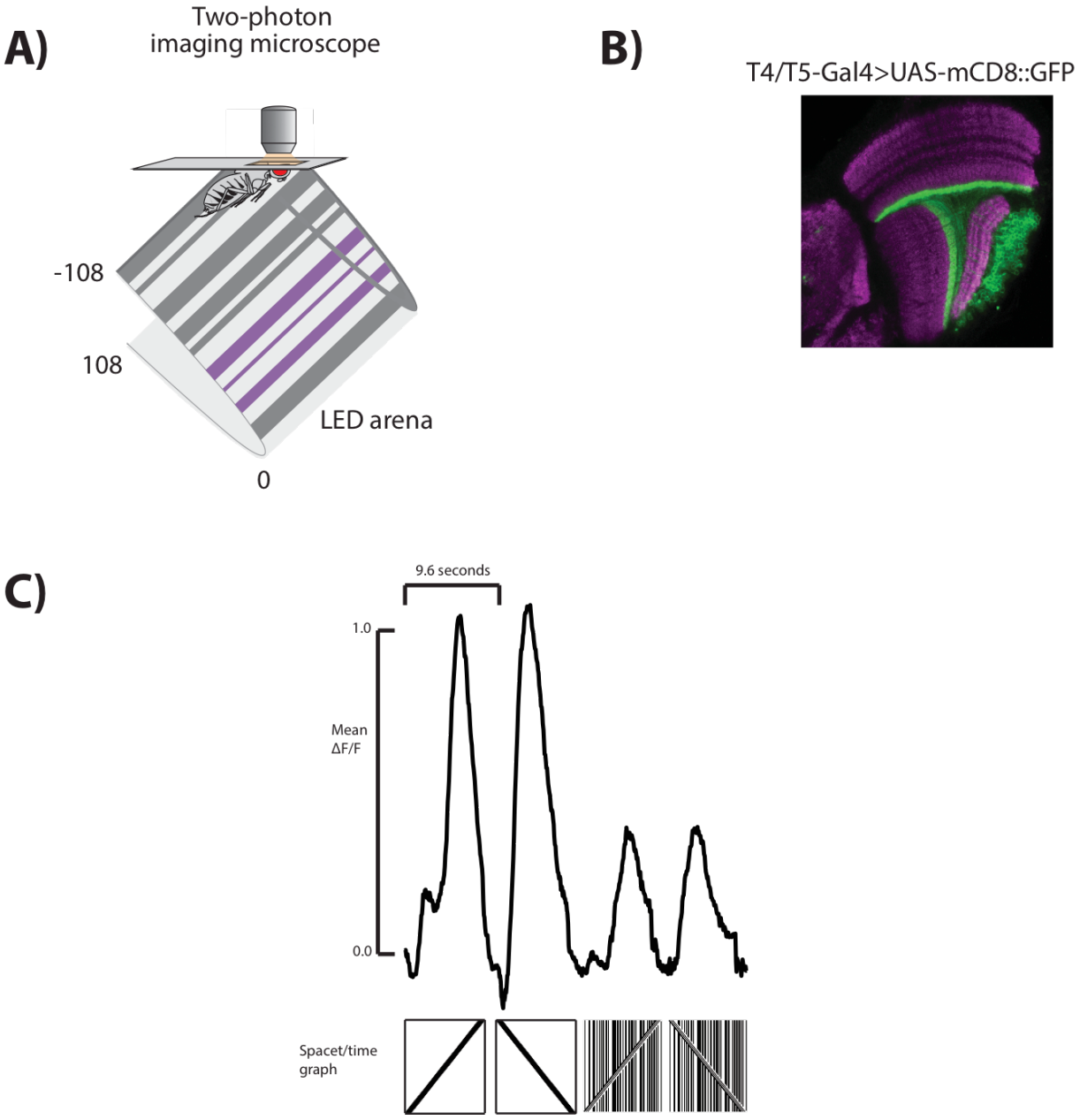

Figure 4.15: T4/T5 cells respond to luminance-defined figures in a stronger fashion than motion-defined figures. A) A fly is fixed to the stage of a two-photon excitation microscope. Head capsule is glued to the holder and the cuticle on the back of the head is dissected to expose the cells labeled by GCaMP expression. Visual stimuli delivered using an LED screen. **B)** Confocal image of GFP labeled T4/T5 cells is.

C) Mean delta F/F responses of aggregate ROIs across the dendrites of T4/T5 cells to the shown stimulus set (below).

References

Akerboom, J., Chen, T.-W., Wardill, T.J., Tian, L., Marvin, J.S., Mutlu, S., Calderon, N.C., Esposti, F., Borghuis, B.G., Sun, X.R., Gordus, A., Orger, M.B., Portugues, R., Engert, F., Macklin, J.J., Filosa, A., Aggarwal, A., Kerr, R.A., Takagi, R., Kracun, S., Shigetomi, E., Khakh, B.S., Baier, H., Lagnado, L., Wang, S.S.-H., Bargmann, C.I., Kimmel, B.E., Jayaraman, V., Svoboda, K., Kim, D.S., Schreiter, E.R., Looger, L.L., 2012. Optimization of a GCaMP Calcium Indicator for Neural Activity Imaging. J. Neurosci. doi:10.1523/JNEUROSCI.2601-12.2012

Albright, T.D., 1992. Form-cue invariant motion processing in primate visual cortex. Science 255, 1141–1143. doi:10.1126/science.1546317

Appelbaum, L.G., Wade, A.R., Vildavski, V.Y., Pettet, M.W., Norcia, A.M., 2006. Cue-invariant networks for figure and background processing in human visual cortex. J. Neurosci. 26, 11695–11708. doi:10.1523/JNEUROSCI.2741-06.2006

Aptekar, J.W., Keleş, M.F., Lu, P.M., Zolotova, N.M., Frye, M.A., 2015. Neurons forming optic glomeruli compute figure-ground discriminations in Drosophila. J. Neurosci. 35, 7587–99. doi:10.1523/JNEUROSCI.0652-15.2015

Aptekar, J.W., Shoemaker, P.A., Frye, M.A., 2012. Figure tracking by flies is supported by parallel visual streams. Curr. Biol. 22, 482–487. doi:10.1016/j.cub.2012.01.044

Bahl, A., Ammer, G., Schilling, T., Borst, A., 2013. Object tracking in motion-blind flies. Nat Neurosci 16, 730–8. doi:10.1038/nn.3386

Barlow, H.B., Levick, W.R., 1965. The mechanism of directionally selective units in

rabbit's retina. J. Physiol. 178, 477–504. doi:10.1113/jphysiol.1965.sp007638

Behnia, R., Clark, D. a., Carter, A.G., Clandinin, T.R., Desplan, C., 2014. Processing properties of ON and OFF pathways for Drosophila motion detection. Nature 512, 427–430. doi:10.1038/nature13427

Buchner, E., 1976. Elementary movement detectors in an insect visual system. Biol. Cybern. 24, 85–101. doi:10.1007/BF00360648

Cavanagh, P., Mather, G., 1989. Motion: the long and short of it. Spat. Vis. 4, 103–129. doi:10.1163/156856889X00077

Fox, J.L., Frye, M. a, 2014. Figure-ground discrimination behavior in Drosophila. II. Visual influences on head movement behavior. J. Exp. Biol. 217, 570–9. doi:10.1242/jeb.080192

Geesaman, B.J., Andersen, R.A., 1996. The analysis of complex motion patterns by form/cue invariant MSTd neurons. J. Neurosci. 16, 4716–4732.

Grill-Spector, K., Kushnir, T., Edelman, S., Itzchak, Y., Malach, R., 1998. Cue-invariant activation in object-related areas of the human occipital lobe. Neuron 21, 191–202. doi:10.1016/S0896-6273(00)80526-7

Haag, J., Arenz, A., Serbe, E., Gabbiani, F., Borst, A., 2016. Complementary mechanisms create direction selectivity in the fly. Elife 5, e17421. doi:10.7554/eLife.17421

Hassenstein, B., Reichard, W., Reichardt, W., 1956. Systemtheoretische Analyse der Zeit-, Reihenfolgen- und Vorzeichenauswertung bei der Bewegungsperzeption des

Rüsselkäfers Chlorophanus. Zeitschrift für Naturforsch. 11, 513–524.

Koffka, K., 1935. Principles of Gestalt Psychology, International library of psychology philosophy and scientific method. doi:10.1037/h0052629

Lee, Y.-J., Nordstrom, K., 2012. Higher-order motion sensitivity in fly visual circuits. Proc. Natl. Acad. Sci. doi:10.1073/pnas.1203081109

Livingstone, M.S., Hubel, D.H., 1987. Psychophysical evidence for separate channels for the perception of form, color, movement, and depth. J. Neurosci. 7, 3416–3468.

Maisak, M.S., Haag, J., Ammer, G., Serbe, E., Meier, M., Leonhardt, A., Schilling, T., Bahl, A., Rubin, G.M., Nern, A., Dickson, B.J., Reiff, D.F., Hopp, E., Borst, A., 2013. A directional tuning map of Drosophila elementary motion detectors. Nature 500, 212–6. doi:10.1038/nature12320

Mauss, A.S., Vlasits, A., Borst, A., Feller, M., 2017. Visual Circuits for Direction Selectivity. Annu. Rev. Neurosci. 40, 211–230. doi:10.1146/annurev-neuro-072116-031335

Reichardt, W., 1987. Evaluation of optical motion information by movement detectors. J. Comp. Physiol. A 161, 533–547. doi:10.1007/BF00603660

Reichardt, W., Poggio, T., 1975. A Theory of the Pattern Induced Flight Orientation of the Fly Musca Domestica II 80, 69–80.

Reiser, M.B., Dickinson, M.H., 2008. A modular display system for insect behavioral neuroscience. J. Neurosci. Methods 167, 127–139. doi:10.1016/j.jneumeth.2007.07.019

Sáry, G., Vogels, R., Orban, G.A., 1993. Cue-invariant shape selectivity of macaque inferior temporal neurons. Science 260, 995–997. doi:10.1126/science.8493538

Schnell, B., Joesch, M., Forstner, F., Raghu, S. V, Otsuna, H., Ito, K., Borst, A., Reiff, D.F., 2010. Processing of horizontal optic flow in three visual interneurons of the Drosophila brain. J. Neurophysiol. 103, 1646–1657. doi:10.1152/jn.00950.2009

Schnell, B., Raghu, S.V., Nern, A., Borst, A., Raghu, S.V., Schnell, B., Nern, A., 2012. Columnar cells necessary for motion responses of wide-field visual interneurons in Drosophila. J. Comp. Physiol. A Neuroethol. Sensory, Neural, Behav. Physiol. 198, 389–395. doi:10.1007/s00359-012-0716-3

Stoner, G.R., Albright, T.D., 1992. Motion coherency rules are form-cue invariant. Vision Res. 32, 465–475. doi:10.1016/0042-6989(92)90238-E

Strother, J.A., Wu, S.T., Wong, A.M., Nern, A., Rogers, E.M., Le, J.Q., Rubin, G.M., Reiser, M.B., 2017. The Emergence of Directional Selectivity in the Visual Motion Pathway of Drosophila. Neuron 94, 168–182.e10. doi:10.1016/j.neuron.2017.03.010

Theobald, J.C., Duistermars, B.J., Ringach, D.L., Frye, M.A., 2008. Flies see second-order motion. Curr. Biol. 18, R464-5. doi:10.1016/j.cub.2008.03.050

Theobald, J.C., Shoemaker, P.A., Ringach, D.L., Frye, M. a, 2010. Theta motion processing in fruit flies. Front. Behav. Neurosci. 4, 1–10. doi:10.3389/fnbeh.2010.00035

Tian, L., Hires, S.A., Mao, T., Huber, D., Chiappe, M.E., Chalasani, S.H., Petreanu, L.,

Akerboom, J., McKinney, S.A., Schreiter, E.R., Bargmann, C.I., Jayaraman, V., Svoboda, K., Looger, L.L., 2009. Imaging neural activity in worms, flies and mice with improved GCaMP calcium indicators. Nat. Methods 6, 875–881. doi:10.1038/nmeth.1398

Van Essen, D.C., Gallant, J.L., 1994. Neural mechanisms of form and motion processing in the primate visual system. Neuron. doi:10.1016/0896-6273(94)90455-3

Chapter 5

Visual input to the *Drosophila* central complex by developmentally and functionally distinct neuronal populations

Summary

The *Drosophila* central brain consists of stereotyped neural lineages, developmental-structural units of macrocircuitry formed by the sibling neurons of single progenitors called neuroblasts. We demonstrate that the lineage principle guides the connectivity and function of neurons providing input to the central complex, a collection of neuropil compartments important for visually-guided behaviors. One of these compartments is the ellipsoid body (EB), a structure formed largely by the axons of ring (R) neurons, all of which are generated by a single lineage, DALv2. Two further lineages, DALcl1 and DALcl2, produce neurons that connect the anterior optic tubercle, a central brain visual center, with R neurons. Finally, DALcl1/2 receives input from visual projection neurons of the optic lobe medulla, completing a three-legged circuit we call the anterior visual pathway (AVP). The AVP bears fundamental resemblance to the sky-compass pathway, a visual navigation circuit described in other insects. Neuroanatomical analysis and two-photon calcium imaging demonstrates that DALcl1 and DALcl2 form two parallel channels, establishing connections with R neurons located in the peripheral and central domains of the EB, respectively. Although neurons of both lineages preferentially respond to bright objects, DALcl1 neurons have small ipsilateral, retinotopically-ordered receptive fields, whereas DALcl2 neurons share a large excitatory receptive field in the contralateral hemifield. DALcl2 neurons become inhibited when the object enters the ipsilateral hemifield, and display an additional excitation after the object leaves the field of view. Thus, the spatial position of a bright feature, such as a celestial body, may be encoded within this pathway.

Introduction

The central complex (CX) is an evolutionarily conserved domain in the insect brain that has a highly ordered, modular neuronal architecture. In *Drosophila*, it comprises several compartments that are situated across the brain midline, including (from anterior to posterior), the ellipsoid body (EB), fan-shaped body (FB) with noduli (NO), and protocerebral bridge (PB) [1–3]. The ellipsoid body is flanked laterally by two compartments of the lateral complex, the bulb (BU) and lateral accessory lobe (LAL), which act as portals for input to and output from the central complex.

Numerous anatomical, functional, and genetic studies conducted in the past suggest that the central complex is involved, among other functions, in the control of motor output and spatial orientation. Stimulation of the CX alters a large number of behaviors that require fine motor control, including stridulation, walking, and escape [4,5]. Genetic lesions of the CX affect walking and flight [6,7]. Silencing specific classes of ring neurons innervating the ellipsoid body of the CX causes deficits in visual place learning and spatial orientation memory in *Drosophila* [8,9]. Along these lines, functional imaging studies in behaving flies suggest that populations of columnar neurons in the CX encode the fly's spatial orientation relative to its environment [10], suggesting that the CX could play a navigational role similar to that one of the hippocampus and entorhinal cortex in mammals [11].

Similar to the mushroom body, another highly structured neuropil domain of the insect brain known for its pivotal function in olfactory learning and memory, the central complex does not receive direct input from peripheral sense organs. Processed sensory information is relayed from the primary olfactory center (antennal lobe) to the mushroom

body and superior protocerebrum *via* antennal lobe projection neurons. These anatomically and functionally specialized neurons are derived from four developmentally defined classes, so called lineages [12,13]. A lineage comprises all neurons produced by a single neural progenitor (neuroblast). The fly brain is generated by approximately 100 pairs of such neuroblasts, each of which defined by a unique pattern of gene expression that dictates the morphology and function of the cells within the lineage [14]. Its lineage-based composition provides great conceptual and technical advantages to analyze the structure and development of the antennal lobe projection in great detail, making this input pathway one of the preeminent model systems to study the genetic mechanism controlling the assembly of a central brain circuit [15,16].

By comparison to the antennal lobe input pathway towards the mushroom body, very little is known about the circuitry providing input to the *Drosophila* central complex. It must receive input from the visual system; dendrites of ellipsoid body ring (R) neurons, located in the bulb, are sensitive to visual stimuli and form a retinotopically-ordered arrangement [17]. In other insects, neurons conducting visual information from the optic lobe to the CX have been characterized, using anatomical and electrophysiological methods, in considerable detail [18]. This circuit, called the sky-compass pathway, is thought to encode skylight cue information relevant for navigation, such as the spatial position of bright celestial bodies, the pattern of polarized skylight, or the sky's spectral gradient. It is a pathway consisting of multiple layers; neurons of the optic lobe medulla project to a known domain of visual input in the central brain called the anterior optic tubercle (AOTU). From there, information is relayed by another neuronal population to the bulb, the input domain of tangential neurons which arborize

in the central body lower division (homologous to *Drosophila* ring neurons and ellipsoid body) [19–24].

In this paper, we have investigated the visual input pathway to the central complex in *Drosophila*. Which, if any, lineages form the "building blocks" of this pathway? Does the lineage principle guide the structural connectivity and thus, the function of neuronal circuit elements within this pathway? Using clonal analysis, we and others previously identified the projection pattern for the majority of neuroblast lineages in the *Drosophila* brain [25–28]. This analysis revealed that ring (R) neurons of the ellipsoid body are derived from a single paired lineage (DALv2). Two additional lineages (DALcl1 and 2) were identified; similarly to neurons in the sky-compass pathway, they project from the anterior optic tubercle to the bulb, and we thus call them tuberculo-bulbar (TuBu) neurons. Identification of Gal4 drivers which reflect the projection pattern of neurons within these lineages allowed us to demonstrate a parallel pattern of topographically-ordered connectivity within this pathway. Double labeling and GFP reconstitution across synaptic partners (GRASP) demonstrates that TuBu neurons provide direct input to R neurons. Two-photon calcium imaging of TuBu neuron presynaptic terminals further corroborates this notion; TuBu neuron outputs from DALcl1, which predominantly innervate the superior domain of the bulb, exhibit similar response properties as R neuron dendrites from the same region, based on previous studies [17]. However, DALcl2 TuBu neuron outputs, which predominantly innervate the inferior domain of the bulb, do not respond in the same fashion, demonstrating that the lineage principle determines not only the structure, but also the function of neuronal populations.

Results

Discrete neural lineages form input pathways of the ellipsoid body

The pathway providing input from the optic lobe to the ellipsoid body, called the anterior visual pathway (AVP) in the following (Fig.1A), represents a circuit whose central part is formed by the neurons of three lineages. As known from previous works and summarized above, ring (R) neurons of lineage DALv2 project from the bulb to the ellipsoid body. Cell bodies of this lineage are located in the anterior brain cortex, surrounding the spur of the mushroom body. The bulb receives the short, proximal neurites of DALv2 neurons; DALv2 axons form a fiber tract, termed the anterior lateral ellipsoid body tract (LEa), which extends medially towards the EB (Fig.1B) [2,29].

We identified two hemilineages, DALcl1d and DALcl2d, which interconnect the bulb with the anterior optic tubercle (AOTU) *via* tuberculo-bulbar (TuBu) neurons (Fig.1C, D). The identified neurons resemble likely homologs, called tubercle-lateral accessory lobe type 1 neurons (TuLAL1 neurons), from the sky-compass pathway [18]. The AOTU consists of a large, spherical medial compartment (AOTUm) to which two smaller domains [intermediate AOTU (AOTUin) and lateral AOTU (AOTUl)] are attached [1] (Fig.1A). In many other insects, the AOTU is oriented such that the larger domain is located dorsally of the smaller domains, and are therefore called the upper unit (AOTU-UU) and lower unit, or lower unit complex (AOTU-LU, AOTU-LUC), respectively. DALcl1d TuBu neurons appear to have short, proximal processes in the lateral AOTU (AOTUl), and distal terminals in the superior and anterior BU (BUs; BUa; Fig.1C, E). DALcl2d TuBu neurons innervate complementary regions, connecting the intermediate

domain of the AOTU (AOTUin) with the inferior BU (BUi; Fig.1D, E). We did not identify neurons projecting directly from the large AOTUm compartment to the CX.

Visual interneurons of the medulla provide input to the AOTUl and AOTUin *via* a thick fiber bundle, the anterior optic tract (AOT). Gal4 driver lines reveal several discrete subpopulations of such medullo-tubercular (MeTu) neurons with proximal dendrites extending in medulla layer m6-8 (Fig.1F, G) and distal axonal branches confined to the lateral and intermediate AOTU. Putative homologies between neurons of the AVP and the sky-compass pathway from other insects are summarized in Table 1.

By expressing reporter proteins specifically targeted to presynaptic terminals (*UAS-syt.GFP*) and postsynaptic membranes (*UAS-DenMark*) we can show that the anterior visual pathway is directed from the medulla to the anterior optic tubercle and, from there, towards the ellipsoid body. Thus, projections of DALv2 R neurons are mostly axonal in the EB, and dendritic in the BU (Fig.1H). Likewise, projections of DALcl1/2 TuBu neurons have mostly presynaptic, axonal sites in the bulb, and postsynaptic, dendritic sites in the AOTU (Fig.1I). Proximal neurites of MeTu neurons in the medulla are exclusively dendritic; distal projections in the AOTU appear to possess intermingled presynaptic and postsynaptic sites (Fig.1J). Although the AVP is predominantly centripetal, the presence of dendritic and axonal signal in the centrifugal direction suggests potential feedback in this circuit.

Ring neuron subclasses of DALv2 establish a topographically ordered connectivity between the bulb and ellipsoid body

Global markers for neuropil [antibodies against DN-cadherin (DNcad) or Bruchpilot (Brp)] in conjunction with specific Gal4 driver lines reveal more detail about the intricate anatomy and connectivity within the anterior visual pathway. In the EB, five discrete domains can be distinguished based on different expression levels of DN-cadherin (Fig.2A-C). These comprise an inner posterior domain (EBip) and inner central domain (EBic) with low DNcad signal, an outer central domain (EBoc) with moderate DNcad signal, and an anterior domain (EBa) and outer posterior domain (EBop) with high signal. The bulb consists of three major domains defined by their position relative to the LEa fiber bundle formed by DALv2-derived ring (R) neuron axons. The superior and inferior domains of the bulb are located dorsally and ventrally of the LEa, respectively; the anterior bulb is attached to the lateral surface of the LEa at a position where it bends medially (Fig.2A, B). DNcad labeling reveals the individual, large input synapses, called microglomeruli, formed by R neuron dendrites (Fig.2B, arrowheads).

We screened the expression patterns of several Gal4 driver lines which label subpopulations of R neurons [30]. This analysis, in conjunction with single-cell labeling using the multicolor flip-out method (MCFO) [31], reveals that the ring domains of the ellipsoid body are connected in a topographically ordered pattern to the bulb, consistent with previous reports [32]. Previously unclassified R neurons innervating the anterior domain, which we call R5 (Fig.2D-F), and R2 neurons of the outer central domain (Fig.2G-I) have dendrites in the superior bulb; other R neurons innervating the outer central domain are connected to the anterior bulb (R4m; Fig.2J-L). R neurons innervating the inner central and inner posterior domain possess dendrites in the inferior bulb (R3; Fig.2M-O).

We did not identify any ring neurons which form axons in the outer posterior domain of the ellipsoid body. This domain, as well as the other domains of the EB, is innervated by two main classes of columnar neurons that interconnect the different compartments of the central complex, PB-EB-gall (“wedge”) neurons (Fig.2P, Q) and PB-EB-NO (“tile”) neurons (Fig.2R) [33]. Both represent sublineages of four large type II lineages (DM1/DPMm1, DM2/DPMpm1, DM3/DPMpm2, DM4/CM4) [26,34], whose cell bodies are located in the posterior brain. Wedge neurons have proximal branches in the protocerebral bridge; from here they extend forward, through the fan-shaped body, into the EB where they presumably receive R neuron input. Collateral branches of wedge neurons project further forward into the gall of the lateral accessory lobe (LAL) [1,33] (Fig.2P, Q); the LAL is a region thought to be relevant for locomotor output in insects [35]. Tile neurons have a more restricted projection to the outer posterior EB (Fig.2R), and therefore overlap extensively with wedge neurons but not R neurons.

Tuberculo-bulbar neurons of DALcl1 and DALcl2 form a topographically ordered projection between the anterior optic tubercle and bulb

In view of the ordered connectivity between bulb and ellipsoid body, it stands to reason that neurons of DALcl1 and DALcl2, which connect the anterior optic tubercle to the bulb, are also topographically organized. Based on DNcad expression, three subdomains (medial, intermediate, lateral) can be defined for the AOTU [1]. Closer inspection of DNcad-labeled brains revealed that the intermediate domain is further subdivided into two narrow, vertical slices, named (from lateral to medial), AOTUil and AOTUim (Fig.3A, B). The lateral domain, AOTUl, is divided into three finger-like

processes (AOTUla, AOTUlc, AOTUlp) that are most easily revealed in horizontal sections of the tubercle (Fig.3B).

We identified multiple Gal4 driver lines expressed in subpopulations of medullo-tubercular (MeTu) neurons and DALcl1 and 2-derived tuberculo-bulbar (TuBu) neurons whose projection is predominantly restricted to specific subdomains of the AOTU, additionally corroborated by MCFO-labeled single cell clones. The DALcl1-derived TuBu subpopulation with axons terminating primarily in the superior bulb ($TuBu_s$), has dendrites enriched in all three process of the lateral subdomain (AOTUla/c/p), and can be labeled by *R88A06-Gal4* (Fig.3D-F). TuBu neurons terminating in the anterior bulb ($TuBu_a$), also derived from DALcl1, actually exhibit dendrites filling the lateral slice of the intermediate AOTU subdomain (AOTUil) (Fig.3G-I). Dendrites of inferior bulb tuberculo-bulbar neurons ($TuBu_i$), derived from DALcl2, are concentrated in the medial intermediate subdomain (AOTUim) and express *R49E09-Gal4* (Fig.3J-L). The parallel pathways connecting the anterior optic tubercle with the bulb and ellipsoid body are schematically summarized in Fig.4.

MeTu neurons from the medulla (previously described [36] as medullar columnar 61 neurons; MC61) also terminate in specific subdomains of the lateral and intermediate AOTU defined by the dendrites of TuBu neurons. The AOTUm receives input from the lobula (lobula columnar 10; LC10) [37]. Numerous driver lines expressed in MeTu neurons have been identified; three representative examples are depicted in Fig.3M-T. Dendrites fill predominantly layer m7, with sparser branches reaching up into m6 (the layer contacted by photoreceptors R7) and deeper into m8. The somata of some MeTu neurons are distributed throughout the dorsal half of the medulla cortex, as shown here

for neurons innervating the AOTUil domain ($MeTu_{il}$; Fig.3Q, R) and the AOTUim domain ($MeTu_{im}$; Fig.3S, T). Cell bodies of other MeTu neurons, such as those innervating AOTUl ($MeTu_{l}$; Fig.3M, N), are spread out over the entire medulla. Single cell clones of $MeTu_{l}$ (*R73C04-Gal4*) reveal that the dendritic tree arborizes locally of the primary neurite and covers 10-15 contiguous medulla columns (Fig.3O-O''). Therefore, this class of neurons collectively innervates the entire medulla, rather than each individual neuron doing so, identifying MeTu neurons as special subclasses of multicolumnar medullary visual projection neurons. Their cell body location and projection pattern is reminiscent of *Drosophila* transmedullary neurons but, exhibit a single dendritic tree, and instead of targeting the lobula complex, directly project to the central brain [38].

Concomitant labeling of DALcl1 or DALcl2 TuBu neurons and DALv2 R neurons demonstrates that the endings of the former fully overlap with the proximal branches of the latter in the bulb (Fig.4B, C). Given the large size of the pre-and postsynaptic endings, forming microglomeruli of approximately 2μm diameter, it was evident that individual R neuron dendrites were directly contacted by TuBu neuron axons. To provide further evidence for a direct synaptic contact, we carried out a GRASP analysis, in which the post-synaptic cells are expressing CD2-RFP and split-GFP11, whereas the presynaptic cells express split-GFP1-10. As shown in Fig.4D and E, a strong GRASP signal is detected specifically in the bulb within the expected target region. DALcl1-derived $TuBu_{s}$ neurons innervate R2 neurons of EBoc with microglomerular dendrites in the superior bulb, whereas DALcl2-derived $TuBu_{i}$ neurons innervate R3 neurons of EBic in the inferior bulb, confirming the presence of parallel, superior and inferior bulb pathways.

Lineally-organized input channels to the ellipsoid body form parallel neural ensembles that are functionally-distinct

Previous studies utilizing pan-neuronal or ring neuron-specific (R2 and R4d) two-photon calcium imaging in the superior bulb demonstrated that a subpopulation of R neuron dendrites respond to visual features. Visually-responsive dendritic microglomeruli typically exhibit ipsilateral receptive fields, bright (ON)-selectivity, and vertical orientation tuning [17]. Our anatomical data demonstrate that TuBu neurons provide direct input to R neuron dendrites; we therefore tested the hypothesis that the microglomerular presynaptic terminals of TuBu neurons exhibit similar physiological properties as R neuron dendrites. We expressed the genetically-encoded calcium indicator GCAMP6m under the control of *R88A06-Gal4*, which predominantly labels $TuBu_s$, the superior bulb-innervating neurons of DALcl1 (Fig.3D-F and 4B). Quiescent flies were placed in front of a curved visual display of LEDs and presented with different visual stimuli (Fig.5A) while conducting two-photon calcium imaging from the microglomerular axonal outputs of these neurons (Fig.5B). Recordings were conducted in two planes to maximally detect microglomerular activity (see Supplemental Experimental Procedures). Responsive superior bulb microglomeruli from both planes exhibited qualitatively homogenous characteristics and were therefore analyzed collectively, in contrast to inferior bulb microglomeruli (see below).

Receptive field mapping with a small bright (ON) object revealed that $TuBu_s$ outputs in the superior bulb each exhibit small, retinotopically-organized receptive fields that are localized to, and provide wide coverage of, the ipsilateral visual hemifield

(Fig.5C,D). The average receptive field size was 29.2° and 44.2° (±3.5° and ±2.8° standard deviation, minor axis and major axis lengths respectively (Fig. 5E). The relative positioning of individual microglomeruli roughly corresponds to the positioning of the spatial receptive fields along the animal's visual elevation (Fig.5F and G, top panels) and azimuth (Fig.5F and G, bottom panels). In other words, microglomeruli with receptive fields located on the lower part of the visual field cluster in the ventrolateral part of the superior bulb, whereas microglomeruli located in the dorsomedial portion of the superior bulb have receptive fields located on the upper part of the visual field (Fig. 5F,G). Similarly, medially located microglomeruli tend to respond to visual stimulation on the medial portion of the ipsilateral visual field, whereas laterally located microglomeruli respond on the lateral portion of it (Fig.5F,G). Spatial receptive fields of individual presynaptic microglomeruli were similar in size within and between animals (Fig.5E).

As R neuron dendrites are tuned to vertically-oriented features, we next presented a horizontally moving bar spanning the full vertical extent of the display. Responses to a moving bright (ON) bar on a dark background much larger by comparison to OFF-bar response, indicating that $TuBu_s$ neurons, like their downstream ring neurons, are ON-selective (Fig 5H) [17]. As a population, $TuBu_s$ neurons respond maximally to a small ON object, slightly less to a bar and much less to a wide-field grating (Fig.5I). These results might suggest that $TuBu_s$ neurons respond to best to objects that fill the excitatory receptive field. Presentation of the ON object outside the excitatory receptive field did not generate measurable decreases in calcium accumulation (Fig.5J), suggesting that surround inhibition is weak if present at all.

Taken together, the response properties of $TuBu_s$ neuron presynaptic terminals resemble those of superior bulb-associated ring neuron dendrites from previous reports [17], corroborating their role as direct presynaptic inputs.

We hypothesized that due to their distinct developmental origin, DALcl2-derived $TuBu_i$ neurons, which innervate the inferior bulb, should exhibit functional dissimilarity to superior bulb innervating, DALcl1 $TuBu_s$ neurons (Fig.1C-E). Flies expressing GCAMP6m under the control of the predominantly $TuBu_i$ neuron driver, *R49E09-Gal4*, were presented with the same battery of visual stimuli as shown for $TuBu_s$ neuron microglomeruli. Unlike superior bulb $TuBu_s$ neurons, responses in the inferior bulb $TuBu_i$ neurons were heterogenous and variable (see Supplemental Experimental Procedures, Fig.S2); yet we identified one consistent response type for at least one microglomerulus in both imaging planes for every fly (Fig.6A,C). The receptive fields scanned in the first imaging plane typically showed excitation to objects in the contralateral visual hemifield and inhibition when the object entered the ipsilateral visual hemifield (Fig.6B, Fig.6D mint green). $TuBu_i$ microglomeruli showed peculiar secondary excitation as the object left the ipsilateral visual field at which time no visual stimulation was present (Fig.6B black arrows, Fig.6D mint green, black arrows). Qualitatively similar responses were observed from microglomeruli in the second imaging plane (Fig.6C), yet these responses were smaller in amplitude (Fig.6D orange). In addition, we observed microglomerular structures that did not respond to any of our stimuli (Fig.6C, microglomeruli that are not encircled orange).

$TuBu_i$ responses were asymmetric with respect to stimulus motion direction. When an object moved from the ipsilateral visual hemifield towards the contralateral

one, microglomeruli responded by slight excitation followed by inhibition (Fig.6D'). We observed a strong response as the object entered the contralateral visual field (Fig.6D'). Inferior bulb response characteristics were consistent across 104 microglomeruli in 15 flies (Fig.6E and E') and they were distinct from superior bulb responses. In contrast to the superior bulb, the physiological responses of ring neurons that extend dendrites into the inferior bulb (R3) have not been systematically characterized, preventing us from making direct input-output comparisons. Nevertheless, the optophysiological analysis of separate TuBu neuron populations derived from DALcl1 and DALcl2 confirm the notion that different lineages form functionally-distinct neuronal ensembles.

In addition to the distinct temporal dynamics of inferior and superior bulb TuBu neuron object responses, we noted that the inferior bulb microglomeruli have larger spatial receptive fields that cover the entire contralateral visual hemifield and are very similar across microglomeruli, showing strongest responses to visual stimuli presented on the upper portion of the display (Fig.6B) or after the stimulus left the screen. Whereas the spatial receptive fields and temporal response properties are distinct between superior bulb and inferior bulb, the preference for ON objects is similar (Fig.6F). Also, like superior bulb $TuBu_s$ neurons, the inferior bulb $TuBu_i$ neurons respond very weakly to wide-field gratings by comparison to small objects or bars (Fig.6G, see above). Our results indicate that both superior and inferior bulb-innervating TuBu neurons are sensitive to bright objects but sample unique hemifields; ipsilateral and contralateral fields, respectively, with distinct receptive field structure and temporal dynamics.

Discussion

The anterior visual pathway (AVP) described in this work serves to define the architecture of a circuit that projects from peripheral neuronal elements of the medulla to the EB neurons of the *Drosophila* CX sequentially *via* medullo-tubercular (MeTu) neurons, and parallel superior DALcl1 and inferior DALcl2 pathways ($TuBu_s$ and $TuBu_i$ neurons). The CX plays a pivotal role in innate and learned visually-guided behaviors. Recent studies by Seelig and Jayaraman [10,17] examined the physiological responses of neuronal subpopulations within the EB. They first observed that individual R neurons whose dendritic microglomeruli are localized in the superior bulb (R2 and R4d), respond to visual stimuli. Here, we identify the developmentally-related $TuBu_s$ neurons of DALcl1 as the direct pre-synaptic inputs to these superior bulb R neurons, and demonstrate that many of their visual tuning properties can already be observed in the upstream $TuBu_s$ population (Fig 5). In addition, we identify DALcl2-derived $TuBu_i$ neurons, which exhibits distinct receptive field properties from $TuBu_s$ neurons (Fig 6), and likely supply the inferior bulb R neurons (presumably R3 neurons of the EBic domain) that have not been systematically characterized previously. $TuBu_i$ neurons' unique receptive field and response properties suggest input from contralaterally located neurons. Indeed, neurons innervating the anterior optic tubercle on both sides, described in other insects, may account for the visual interhemispheric receptive field characteristics described here and in other neurons of the sky-compass pathway [39,41,50].

R neurons, whose axons cover the entire perimeter of the ellipsoid body, provide input to the large number of columnar neurons (so called "wedge neurons"; [33]), the neurites of which subdivide the torus-shaped volume of the ellipsoid body into narrow radial partitions. The calcium dynamics recorded from the population of wedge neurons

produces a localized “bump” of activity in the torus which, based on visual landmarks and proprioception, corresponds to an internal representation of the animal’s orientation in space [10]. Information likely reverberates between the EB and other CX neuropils, such as the protocerebral bridge, *via* different populations of columnar elements (wedge and tile neurons) which heavily interconnect them [33]. Similarly to the head direction system in mammalian brains, these dynamics produce stable neural activity consistent with an internal compass [10]. The EB displays a common organizational principle observed in complex nervous systems; in essence, it is a structure arranged into layers and columns by tangential (ring neurons) and columnar (wedge and tile neurons) elements, respectively. A receptive field-specific response in a single R neuron would presumably influence activity in an entire layer, and thus all columns. One of the most insightful lines of inquiry will be to investigate how this tangential input is translated into (or is even compatible with) the localized columnar activity (“bump”) within the wedge neurons of the EB. It is conceivable that R neurons, due to their peculiar bifurcated architecture, may influence EB wedges with a physiologically-relevant temporal offset, which could be utilized to modulate spatially-restricted activity patterns. Future work defining the circuit motifs present in this brain region may provide insight into the advantages of a layered and columnar organization for emergent neural properties, such as a cognitive-like internal representation and navigation.

The neurons and neuropil compartments of the *Drosophila* AVP have homologous counterparts in other insects, forming the so-called “sky-compass pathway”, most prominently investigated in the locust, (*Schistocerca gregaria*; [18,39,40]), monarch butterfly (*Danaus plexippus*; [42]), honeybee

(*Apis mellifera*; [22]) and bumblebee (*Bombus ignitus*; [21]). MeTu neurons providing input to the AVP form dendritic branches within the boundary region of distal and proximal medulla [21,22,43]. The target neuropil innervated by MeTu neurons is the lateral/intermediate part of the AOTU, called the “lower unit or lower unit complex” of the AOTU (AOTU-LU or LUC) in locust and other insects [1,39,44]. Two classes of neurons, TuLAL1a and TuLAL1b, likely counterparts of the TuBu neurons described in this paper, form two parallel pathways that convey the output from the AOTU-LUC to small neuropil foci within the LAL which are homologous to the bulb, formerly called the lateral triangle and median olive. From here, TL neurons, homologs of fly R neurons, carry the visual input to the lower unit of the central body, counterpart of the *Drosophila* ellipsoid body [18]. Based on the available anatomical and functional data, it is not yet possible to propose more specific homologies between neuron classes of the AVP in flies, and the corresponding sky compass pathway in other insects.

Most notably recognized as the polarization (POL) vision pathway, neurons of the sky-compass network are tuned to the e-vectors of polarized light which reflect the location of the sun, thus providing compass information used by these insects to navigate during long range migrations or local path integration in central place foraging [42,45]. Considering that *Drosophila* also exhibits physiological and behavioral correlates with POL sensitivity [46–48], we posit that the fly AVP is the neural circuit for POL information transmission to the CX. However, a recent report demonstrated that when flies are presented with a rotating field of polarized UV light in conjunction with pan-neuronal calcium imaging, robust calcium signals in any CX neuropils, including the bulb, were not observed [49]. In contrast, and in agreement with our findings, bright

objects elicited strong responses in the bulb and other regions of the CX. Indeed, neurons of the sky-compass pathway can encode both a specific e-vector and the azimuthal position of an unpolarized light source, the nature and degree of which depends on the insect and neuron type in question [24,40,42,50]. The extent of encoding strength to a given stimulus (polarized versus unpolarized light) likely reflects the ethology and ecological niche of the animal. For example, diurnal dung beetles utilize the position of a bright object (such as the sun or moon) to navigate regardless of ambient light intensity, whereas nocturnal beetles utilize polarized skylight specifically at low light intensities, rather than position of a celestial body such as the moon. This ethological distinction is reflected in the tuning properties of neurons within the sky-compass pathway, even between two closely-related insects [24].

In the Drosophila AVP, the spatial position of luminance cues emanating from a bright source, such as a celestial body or an escape route from within foliage, would be represented more strongly than the skylight pattern of polarized light [49]. This proposition is based on the following:

1) Anatomical and ethological evidence: In comparison to other insects examined, in which an aspect of their behavioral repertoire is thought to depend on POL vision, the ethological lifestyle of *Drosophila* suggests that it may be less likely to use the pattern of polarized skylight to navigate. This fact is reflected in their relatively rudimentary dorsal rim area (DRA), a region of the eye with specialized, POL-sensitive photoreceptors, and correspondingly inconspicuous dorsal rim area of the medulla (MEDRA), which receives input from DRA photoreceptors. In addition, likely homologues of MeTu neurons in other insects (transmedulla neurons) often exhibit long,

dorsally-projecting input neurites which ramify in the MEDRA, suggesting a high degree of POL input [21,22]. In contrast, we did not observe this characteristic feature in MeTu neurons in *Drosophila*; dendritic arborizations ramified locally of the primary neurite, which were distributed relatively evenly throughout the dorsal half of, or the whole eye.

2) Upstream TuBu as well as downstream R neurons and wedge neurons show strong excitation to bright objects [10,17], whereas dark object responses are weaker (Figs.5 and 6), suggesting specialization for detecting a bright object against a dark background. The ON-preference and weak tuning to object size by TuBu neurons (Figs.5 and 6) suggest that this pathway would poorly mediate stripe fixation behavior, which is activated more by dark bars or complex motion-defined edges [51]. However, the topographical organization of $TuBu_s$ neuron terminals (Fig.5) suggests that retinotopy is conserved and thus could serve spatial navigation, unlike other small-object visual projection neurons (VPNs) of the lobula and lobula plate where the retinotopy is apparently lost within the intermingled axon terminals of individual small-field columnar neurons [52,53].

3) The preference for bright objects of varying size suggests that the CX receives rather primitive spatial information by comparison to the complex filtering properties exhibited by other VPN pathways that act as precise spatial filters for directional patterns of optic flow, the spatial dynamics of looming objects, and the omni-directional motion of small OFF-contrasting objects [52–54].

4) Spatial interactions of excitation and inhibition: A single bright object presented ipsilaterally against a dark background would excite a spatially defined subset of

ipsilateral $TuBu_s$ neurons while simultaneously exciting multiple (possibly all) canonical contralateral $TuBu_i$ neurons. By contrast, two bright spots appearing in the left and right visual fields would simultaneously stimulate $TuBu_s$ neurons on both right and left side while leading to inhibition in all $TuBu_i$ neurons. Most intriguingly, $TuBu_i$ neurons show strong calcium currents as a bright object leaves the visual field suggesting that $TuBu_i$ neurons might be signaling to the R neurons some crucial information about 'losing' the visual bearing to a bright object. R neurons have shown to be indispensable for visual place learning [8] and it is possible that inferior bulb neurons have a crucial role in carrying some of the visual information that is used by R neurons to mediate this behavior.

Here we provide ample evidence that DALc1 and DALcl2-derived neurons have unique functional properties, come from distinct lineages, and supply visual information to the central complex. To our knowledge, this is the first extensive characterization of the visual input to the central complex in *Drosophila*, and a definitive example of how developmentally distinct lineages give rise to functionally distinct circuits.

Experimental Procedures

Drosophila stocks

Flies were reared at 25^{o}C using standard fly media unless otherwise noted. The *Drosophila* driver lines utilized in this study, as well as more specific genotype information, are listed in the Supplemental Experimental Procedures. The following general transgenic fly stocks were used: *UAS-DenMark::mCherry, UAS-Syt::GFP*, *su(Hw)attP8:HA_V5_FLAG_1* [31], *10xUAS-mCD8::GFP, 10XUAS-IVS-mCD8::RFP,*

13XLexAop2-mCD8::GFP, LexAop-CD2::RFP, UAS-CD4::spGFP1-10, LexAop-CD4::spGFP11, 20xUAS-GCAMP6m (Bloomington Stock Center, Bloomington, Indiana).

Clonal analysis

GFP-labeled adult neuroblast MARCM clones were induced at the late first instar/early second instar stage by heat-shocking in a water bath at 38 °C for 30-60 min. Larvae were approximately 12-44 hours old. Heat-shocked larvae were grown to adult for analysis.

Single cell analysis of neurons in the AVP pathway was conducted using the multicolor flip-out (MCFO) method described previously [31,33]. Briefly, depending on the cell density of a given Gal4 line, 1-3 day old flies were dissected to obtain single cell labeling.

Immunostaining, confocal microscopy, and image analysis

Immunohistochemistry was performed using standard procedures with some modifications [26], details for staining procedures and list of antibodies are in Supplemental Experimental Procedures. *Drosophila* adult brains labeled with antibody markers were viewed as whole-mounts in Vectashield mounting medium H-1000 (Vector Laboratories), by confocal microscopy [LSM 700 Imager M2 using Zen 2009 (Carl Zeiss Inc.); lenses: 40× oil (numerical aperture 1.3)]. Complete series of optical sections were taken from preparations between 1.2 and 2-μM intervals. Preparations were mounted anteriorly or dorsally. Dorsally-oriented preparations were acquired by sliding the brain dorsal-side up, inside the crevice between two closely apposed cover

slips. Captured images were processed by ImageJ or FIJI (National Institutes of Health, http://rsbweb.nih.gov/ij/ and http://fiji.sc/). In Fig.1B-G, background labeling was manually removed to improve clarity of specific neuronal morphologies. In Fig.1E, ventral hemilineages of DALcl1/2 were digitally removed, and z-projections of the labeled dorsal hemilineages were registered digitally with z-projections of a standard brain at the corresponding antero-posterior plane using the scaling and warping tool in the NIH ImageJ and Adobe Photoshop software programs. Easily recognizable landmarks, including the center of the peduncle and ellipsoid body, and the tips of the mushroom body lobes were used as fiduciary points. For multicolor flip-out experiments, additional non-overlapping neurons were manually removed, and anti-Brp labeled neuropil compartments were outlined with hatched lines from the same sample. Schematics were made in Adobe Illustrator and figures assembled in Adobe Photoshop.

Two-photon calcium imaging, visual stimuli, and two-photon imaging analysis

Calcium imaging was conducted as previously described [53]. Briefly, calcium-dependent fluorescent signals were detected using a two-photon excitation scanning microscope (3i, Boulder, CO) with Slidebook 6 software (3i, CO), at an image acquisition rate of 10 frames/sec. 3-7 day old female flies expressing *20xUAS-GCAMP6m* under the control of a specific Gal4 driver labeling tuberculo-bulbar neuron subpopulations were used; all recordings were conducted from the microglomerular presynaptic terminals of these neurons. Flies were immobilized in a custom holder and bathed in physiological saline; neurons of interest were made optically accessible by dissecting the posterior cuticle of the head capsule. Visual stimuli were presented to the

fly using a 96x32 pixel LED arena. Specific details of two-photon imaging setup, visual stimuli, and imaging analysis are provided in Supplemental Experimental Procedures.

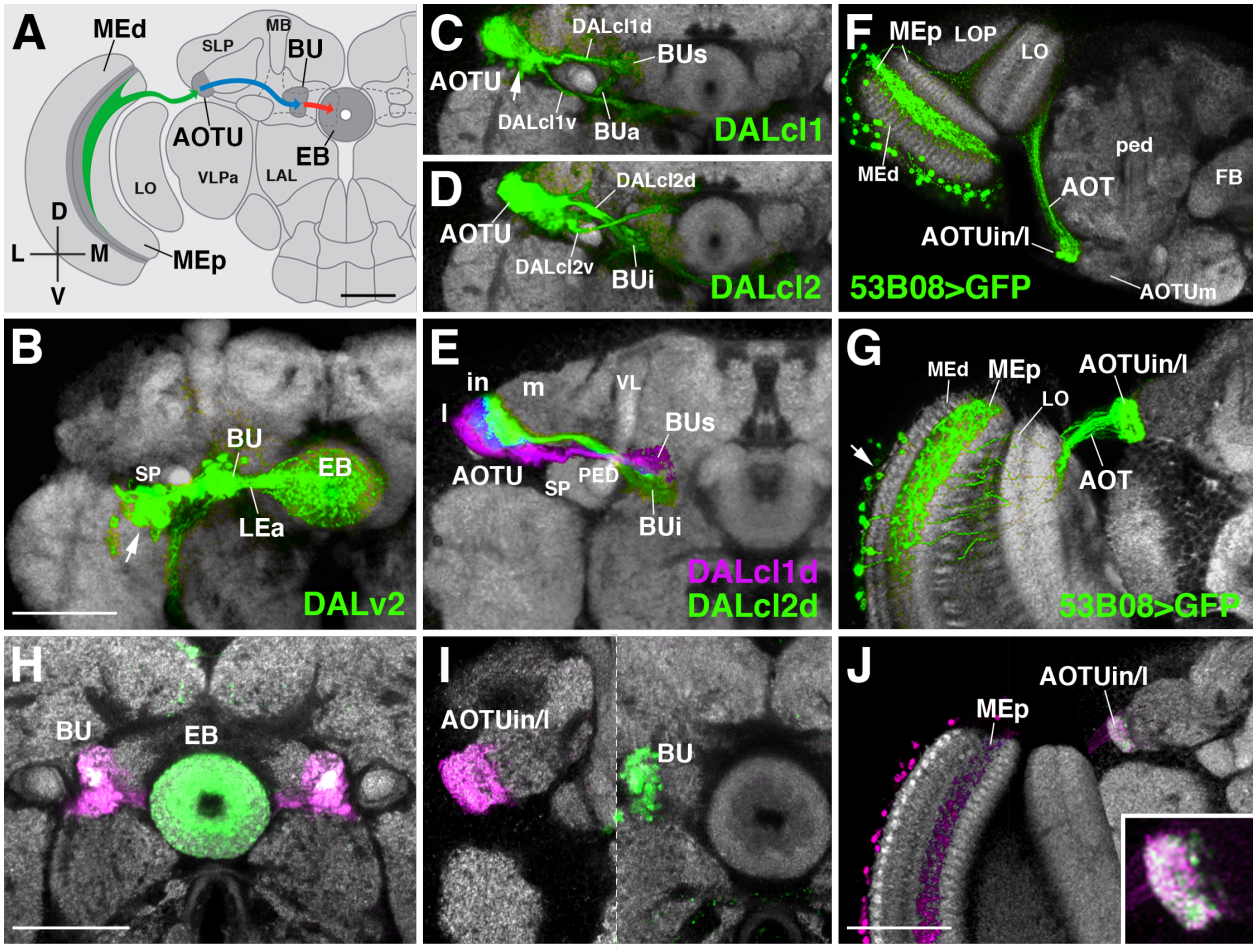

Figure 5.1

Discrete lineages constitute the central brain components of the anterior visual pathway.

(B-J) Confocal z-projections illustrating the anterior visual pathway (AVP) (frontal sections unless otherwise noted); adult brains labeled with anti-DN-cadherin (grey), cell body clusters depicted by arrows.

(A) Schematized overview of the three-legged AVP. First leg (green): from the optic lobe medulla to the anterior optic tubercle (AOTU). Second leg (blue): from the AOTU to bulb

(BU). Final leg (red): from the bulb (BU) to the ellipsoid body (EB) of the central complex.

(B-D) Mosaic analysis with a repressible cell marker (MARCM) clones of secondary lineages DALv2, DALcl1, and DALcl2 (green) (Nomenclature from [26,29]). (B) DALv2 forms all ring neurons of the EB (red leg in A), projecting from the BU to the EB *via* the anterior lateral ellipsoid body tract (LEa). (C and D) DALcl1 and DALcl2 form tuberculo-bulbar neurons (blue leg in A). Two tract components emanate from each neuroblast clone, a dorsal (DALcl1/2d) and a ventral (DALcl1/2v) component which we conclude are hemilineages. The dorsal, not ventral, hemilineages form the tuberculo-bulbar neurons.

(E) Isolation and registration of DALcl1/2 dorsal hemilineages (see experimental procedures) (DALcl1d; magenta, DALcl2d; green). Neurites of DALcl1d projects from the lateral domain of the AOTU (AOTUl) to the superior domain of the bulb (BUs), DALcl2d projects from the intermediate domain of the AOTU (AOTUin) to the inferior domain of the bulb (BUi). We did not identify neurons projecting from the large medial domain of the AOTU (AOTUm) to the bulb.

(F-G) Horizontal (F) and frontal (G) sections of *R53B05-Gal4* (green) labeling medullo-tubercular neurons, projecting from the medulla to the AOTUin/l *via* the anterior optic tract (AOT) (green leg in A).

(H-J) Expression of pre-synaptic marker *syt::GFP* (green) and dendritic marker DenMark (magenta) in distinct legs of the AVP. (H) *R20A02-Gal4* labels most ring neurons and shows enrichment of axonal output in the EB and dendrites in the BU. (I)

R48B06-Gal4 labels tuberculo-bulbar neurons and shows enrichment of output in the BU and dendrites in the AOTUin/l. (J) *R53B05-Gal4* demonstrates medullo-tubercular neurons are dendritic in the proximal medulla (MEp) but appears to have mixed dendritic and axonal specializations in the AOTUin/l (boxed inset).

Other abbreviations: LAL, lateral accessory lobe; LO, lobula; LOP, lobula plate; MB, mushroom body; MEd, distal medulla; PED, peduncle of the mushroom body; SP, spur of the mushroom body; SLP, superior lateral protocerebrum; VL, vertical lobe; VLPa, anterior ventrolateral protocerebrum

Scale Bars: 50μm (A, C, D, F); 50μm (B, E, G, J); 50μm (H, I)

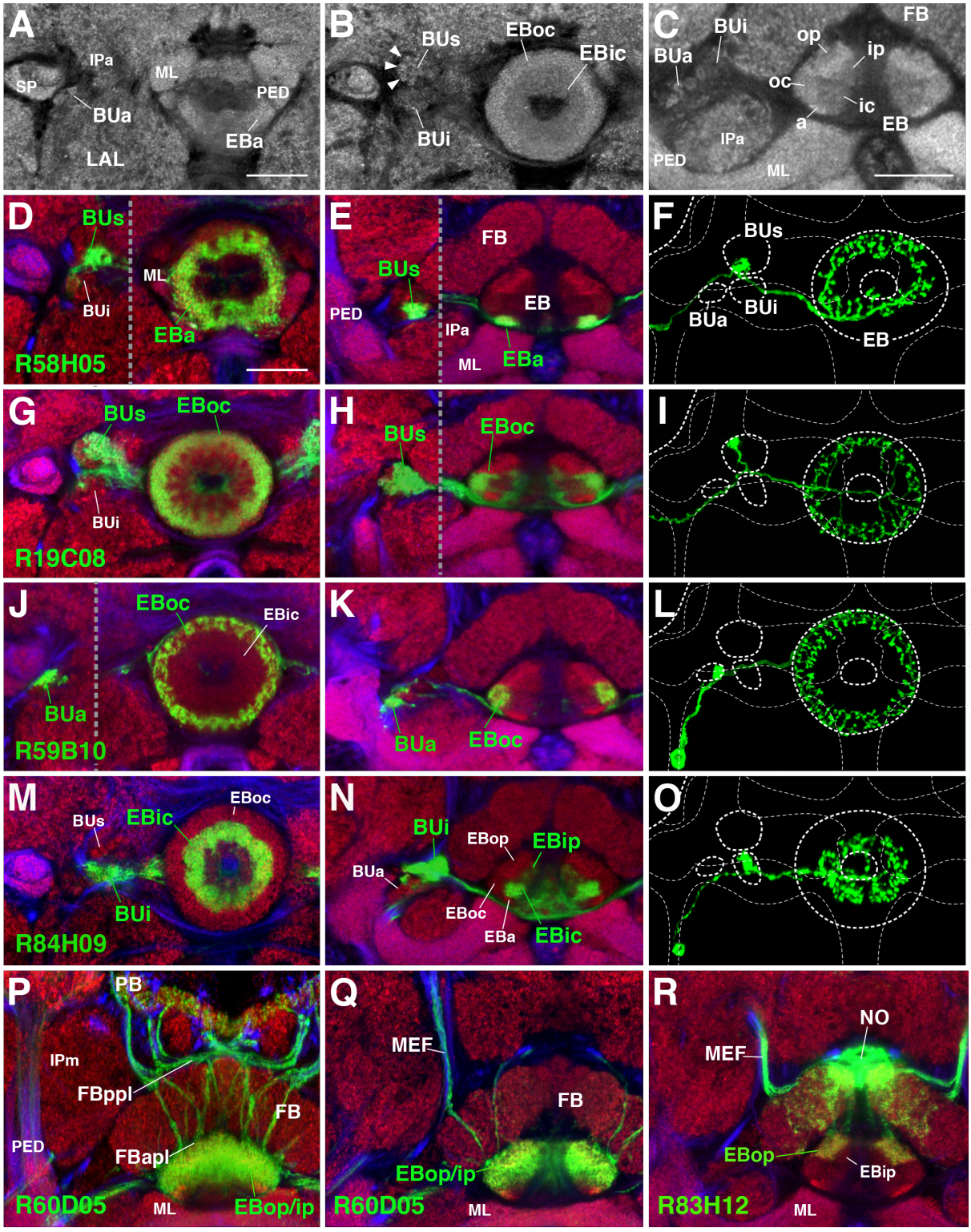
A
IPa
SP
ML
PED
BUa
EBa
LAL
B
BUs
EBoc
EBic
BUi
C
BUi
FB
op
ip
BUa
oc
ic
a
EB
IPa
PED
ML
D
BUs
ML
BUi
EBa
R58H05
E
FB
BUs
EB
PED
IPa
ML
EBa
F
BUs
BUi
BUa
EB
G
BUs
EBoc
BUi
R19C08
H
BUs
EBoc
I
J
EBoc
EBic
BUa
R59B10
K
BUa
EBoc
L
M
BUs
EBic
EBoc
BUi
R84H09
N
BUi
EBop
EBip
BUa
EBoc
EBa
EBic
O
P
PB
IPm
FBppl
FB
PED
FBapl
R60D05
ML
EBop/ip
Q
MEF
FB
EBop/ip
R60D05
ML
R
NO
MEF
EBop
EBip
R83H12
ML

Figure 5.2

DN-Cadherin domains and single cell labeling define the topology and architecture of ellipsoid body neurons.

(A-C) High magnification frontal (A and B) and horizontal (C) z-projections of the bulb and ellipsoid body neuropil labeled by anti-DN-cadherin (grey) reveals three distinct domains in the bulb and five distinct domains in the ellipsoid body. (A) Anterior frontal section reveals the anterior bulb (BUa) and the anterior domain of the EB (EBa). (B) Intermediate frontal section; reveals the superior (BUs) and inferior (BUi) domains of the bulb, and the outer central (EBoc) and inner central (EBic) domains of the EB. Arrowheads designate bulb microglomeruli. (C) Horizontal section through the EB canal reveals all five EB domains.

(D-O) Gal4 drivers which label distinct ring neuron subclasses defined by axon morphology, and topology within the BU and EB. Each row represents a distinct Gal4 driver; first and second columns are frontal and horizontal sections labeled with *10xUAS-mCD8::GFP*, respectively, grey hatched lines denote regions of interest that are not within the same plane. Neuropil labeled with anti-DN-cadherin (red) and axon tracts by anti-Neuroglian (blue). Third column is a single cell clone generated by MCFO using the same Gal4 (see Experimental Procedures); white hatched lines outline neuropil compartments from the same fly. (D-F) *R58H05-Gal4* (R5; BUs to EBa). (G-I) *R19C08-Gal4* (R2; BUs to EBoc). (J-L) *R59B10-Gal4* (R4m; BUa to EBoc). (M-P) *R84H09-Gal4* (R3; BUi to EBic/ip).

(P-R) Horizontal confocal z-projections of Gal4 drivers labeling columnar elements. (P-Q) *R60D05-Gal4* labels PB-EB-gall (“wedge”) neurons. (P) Z-projection depicting the complete projection pattern of the population in the CX. (Q) Section through the EB canal; “wedge” neurons most densely occupy posterior EB domains, but diffusely project into intermediate and anterior domains as well. (R) *R83H12-Gal4* labels PB-EB-NO (“tile”) neurons, which fill the outer posterior domain of the EB (EBop).

Other abbreviations: FB, fan shaped body; FBapl and FBppl, anterior and posterior plexus of the fan shaped body; IPa and IPm, anterior and medial inferior protocerebrum; LAL, lateral accessory lobe; MEF, medial equatorial fascicle; ML, medial lobe of the mushroom body; NO, noduli; PB; protocerebral bridge; PED, peduncle of the mushroom body; SMP, superior medial protocerebrum; SP, spur of the mushroom body; VL, vertical lobe

Scale Bars: 25μm (A, B); 25μm (C); 25μm (D-R)

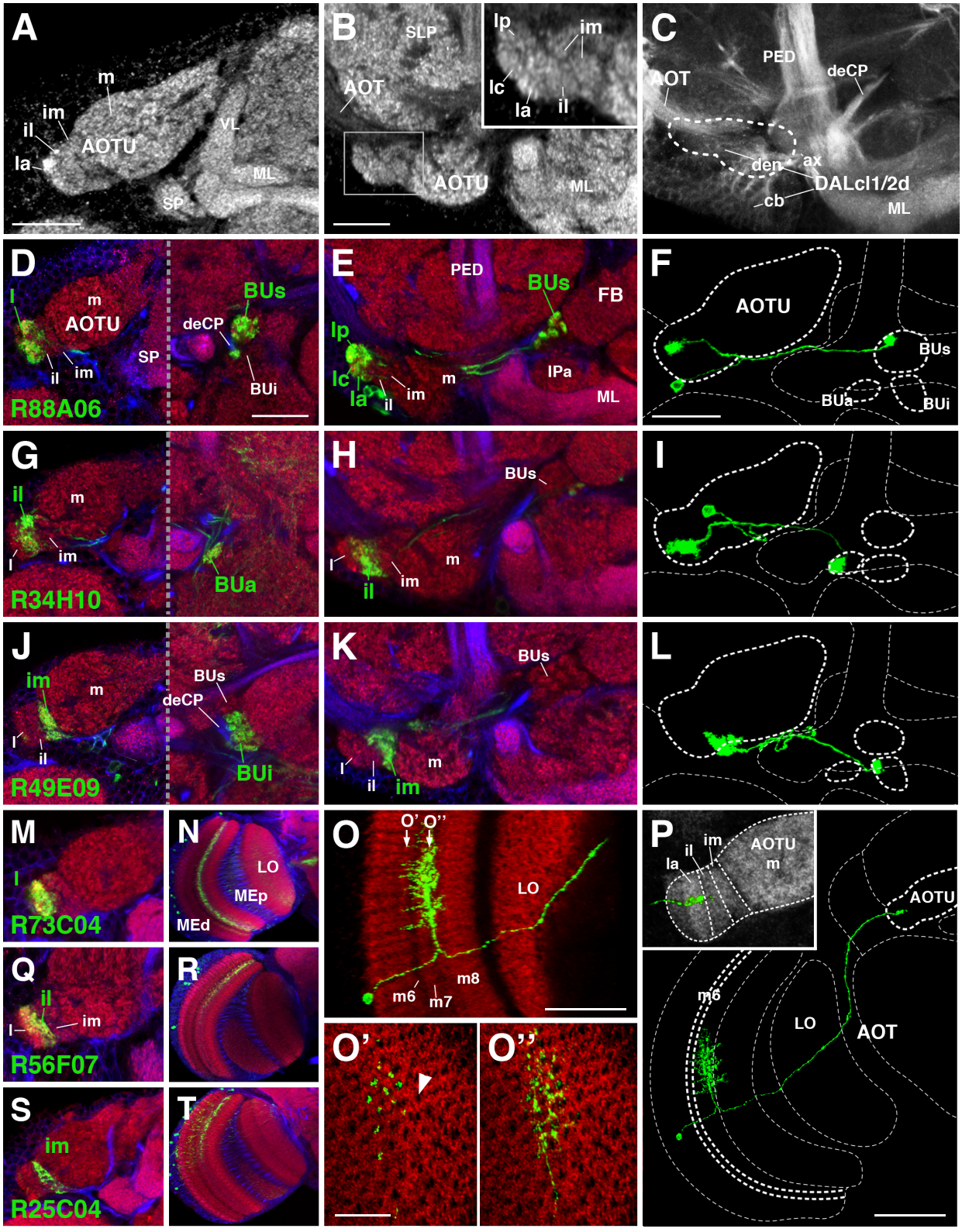
A
m
im
il
la
AOTU
VL
ML
SP
B
SLP
AOT
lp
im
lc
la
il
AOTU
ML
C
PED
deCP
AOT
den
ax
DALcl1/2d
cb
ML
D
l
m
AOTU
SP
il
im
BUs
deCP
BUi
R88A06
E
PED
BUs
FB
lp
lc
la
il
im
m
IPa
ML
F
AOTU
BUs
BUa
BUi
G
il
m
l
im
BUa
R34H10
H
BUs
l
m
il
im
I
J
im
m
BUs
deCP
l
il
BUi
R49E09
K
BUs
l
m
il
im
L
M
l
R73C04
N
LO
MEp
MEd
O
O' O''
LO
m8
m6
m7
P
il
im
AOTU
la
m
AOTU
m6
LO
AOT
Q
il
l
im
R56F07
R
S
im
R25C04
T
O'
O''

Figure 5.3

Topology and architecture of tuberculo-bulbar and medullo-tubercular neurons.

(A-C) High magnification frontal (A) and horizontal (B and C) z-projections of the anterior optic tubercle reveals six distinct domains in the AOTU (m, medial; im, intermediate medial; il, intermediate lateral; la/c/p, lateral anterior/central/posterior), highlighted by boxed inset in (B). Neuropil labeled by anti-DN-cadherin (grey; A and B), axon tracts labeled by anti-Neuroglian (grey; C) with AOTU location denoted by white hatched line with locations of DALcl1/2d cell bodies (cb), dendrites (den), and axons (ax).

(D-L) Gal4 drivers which label distinct tuberculo-bulbar neuron subclasses defined by topology within the AOTU and BU. Each row represents a distinct Gal4 driver; first and second columns are frontal and horizontal sections labeled with *10xUAS-mCD8::GFP*, respectively. Neuropil labeled with anti-DN-cadherin (red) and axon tracts by anti-Neuroglian (blue). Third column is a single cell clone generated by MCFO using the same Gal4; white hatched lines outline neuropil compartments from the same fly. (D-F) *R88A06-Gal4* (AOTUla/c/p to BUs). (G-I) *R34H10-Gal4* (AOTUil to BUa). (J-L) *R49E09-Gal4* (AOTUim to BUi).

(M-T) Gal4 drivers which label distinct medullo-tubercular neuron subclasses defined by topology within the medulla and AOTU. (M-P) *R73C04-Gal4* labels a class of medullo-tubercular neurons projecting from m7 layer of the medulla to AOTUl. (M) High magnification image of the AOTU, (N) is the medulla from the same fly. Neuropil labeled with anti-DN-cadherin (red) and axon tracts by anti-Neuroglian (blue). (O-P) Single cell

clone generated by MCFO with *R73C04-Gal4*, all panels are the same clone. Frontal section of the dendritic arborization (O) demonstrates that this cell type is not restricted to a single medulla layer. Successive tangential sections (O' and O'') reveal that the primary dendritic arborization (O'') extends multiple distal processes which occupy individual medulla columns. Neuropil labeled with anti-Brp (O-O''; red), white hatched lines outline neuropil compartments (P). (Q-R) *R56F07-Gal4* (dorsal half m7 layer to AOTUil). (J-L) *R25C04-Gal4* (dorsal half m7 layer to AOTUim).

Other abbreviations: AOT, anterior optic tract; deCP, central descending protocerebral fascicle; FB, fan shaped body; IPa, anterior inferior protocerebrum; IPm, medial inferior protocerebrum; LAL, lateral accessory lobe; LO, lobula; MEd, distal medulla; MEp, proximal medulla; ML, medial lobe of the mushroom body; PED, peduncle of the mushroom body; SLP, superior lateral protocerebrum; SP, spur of the mushroom body

Scale Bars: 25μm (A); 25μm (B-E, G, H, J, K, M, Q, S); 25μm (F, I, L); 50μm (N, R, T); 50μm (O); 20μm (O', O''); 50μm (P)

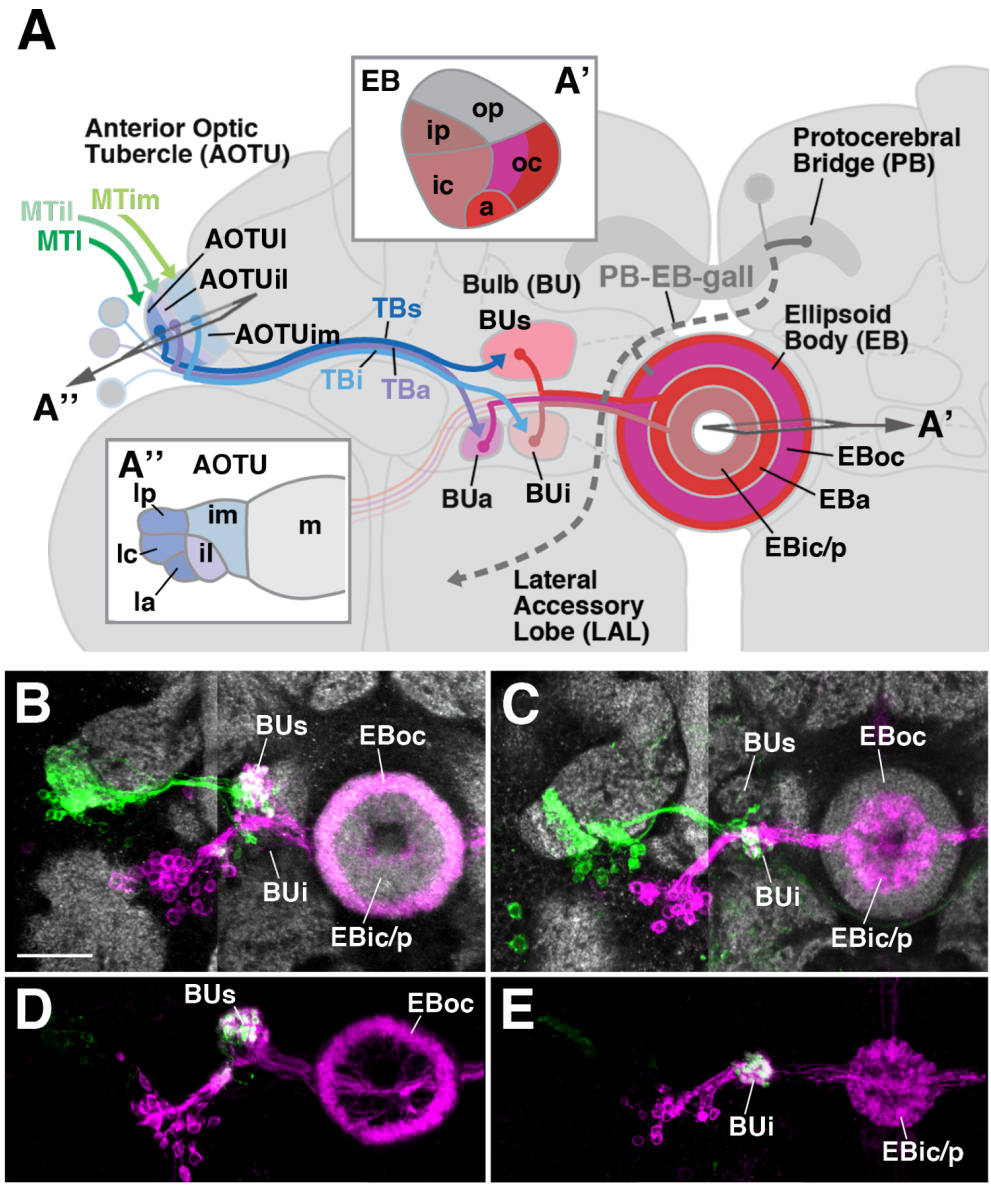

Figure 5.4

Framework of connectivity in the AVP - DALcl1 and DALcl2 provide direct, topographically-organized parallel input to ring neuron subclasses.

(A) Schematic overview of the anterior visual pathway. Insets depict horizontal sections of the EB (A') and AOTU (A'').

(B and C) Two-color labeling of superior bulb (B) and inferior bulb (C) components. Tuberculo-bulbar neurons labeled in green by Gal4, ring neurons labeled in magenta by LexA. (B) *R88A06-Gal4* labels DALcl1d tuberculo-bulbar neurons, *R19C08-LexA* labels EBoc R2 neurons; overlap observed in the superior bulb (BUs). (C) *R49E09-Gal4* labels DALcl2d tuberculo-bulbar neurons, *R54B05-LexA* labels EBic/ip R3 neurons; overlap observed in the inferior bulb (BUi).

(D and E) GRASP analysis of tuberculo-bulbar neuron – ring neuron synapses using the same driver combinations as B and C; post-synaptic cells are expressing CD2-RFP and split-GFP11, presynaptic cells expressing split-GFP1-10. Strong GRASP signal observed in the expected bulb subdomain.

Scale Bars: 25μm (B-E)

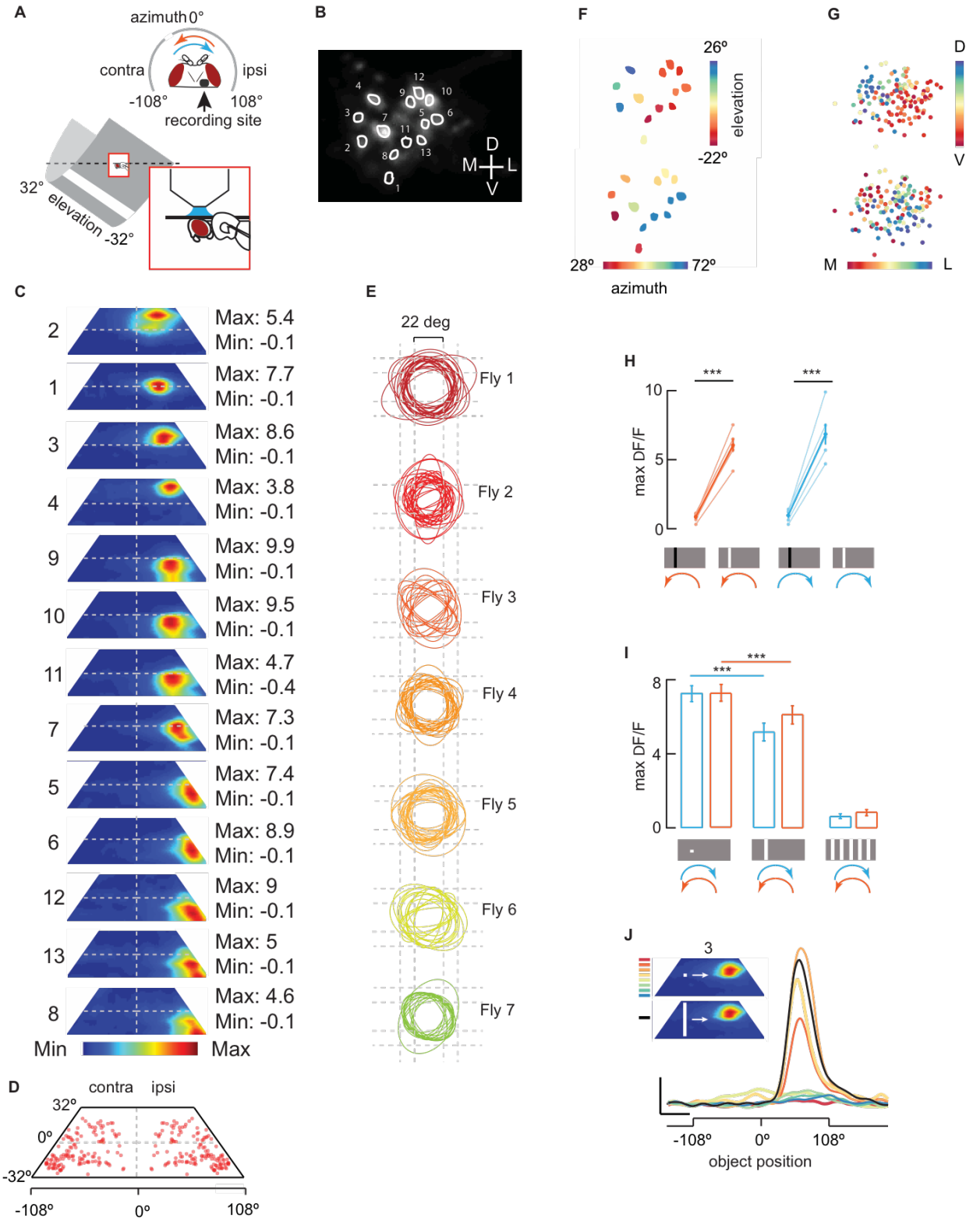
A
azimuth 0°
contra
ipsi
-108°
108°
recording site
32°
elevation
-32°
B
D
M
L
V
C
2
Max: 5.4
Min: -0.1
1
Max: 7.7
Min: -0.1
3
Max: 8.6
Min: -0.1
4
Max: 3.8
Min: -0.1
9
Max: 9.9
Min: -0.1
10
Max: 9.5
Min: -0.1
11
Max: 4.7
Min: -0.4
7
Max: 7.3
Min: -0.1
5
Max: 7.4
Min: -0.1
6
Max: 8.9
Min: -0.1
12
Max: 9
Min: -0.1
13
Max: 5
Min: -0.1
8
Max: 4.6
Min: -0.1
Min
Max
D
contra
ipsi
32°
0°
-32°
-108°
0°
108°
E
22 deg
Fly 1
Fly 2
Fly 3
Fly 4
Fly 5
Fly 6
Fly 7
F
26°
elevation
-22°
28°
72°
azimuth
G
D
V
M
L
H
***
***
10
5
0
max DF/F
I
***
***
8
4
0
max DF/F
J
3
-108°
0°
108°
object position

Figure 5.5

Physiological properties of tuberculo-bulbar neurons innervating the superior bulb

(A) Schematic of two-photon experimental setup. Quiescent female flies are spatially fixed in front of a curved array of LEDs. The upper corners of the LED display are obscured by the mounting stage and outside the field of view (dashed line), which is reflected in the parallelogram receptive field projections in C and D below.

(B) Two photon excitation image of a representative fly in which *R88A06-Gal4* is driving the expression of GCaMP6m in DALcl1-derived tubercular-bulbar neurons of the superior bulb ($TuBu_s$). All recordings are from the microglomerular presynaptic terminals of the right bulb. Responsive microglomeruli are randomly indicated numerically as individual regions of interest (ROIs; white).

(C) For individual microglomeruli enumerated from representative fly in panel B, receptive field maps were generated using a small object passed at 8 different elevation trajectories in both directions. Maps from 13 microglomeruli are sorted from highest to lowest elevation center of the receptive field 'hotspot' (C) to indicate the visual coverage by an ensemble of receptive fields. All receptive fields are mapped from ipsilateral microglomeruli. See also Figure S1.

(D) The location of receptive field centers from all receptive field measurements (136 ROIs) from all flies (n=7) are indicated with red dots, demonstrating the coverage across the visual field. To facilitate visual comparison, receptive field centers measured from

ipsilateral ROIs are reflected to the contralateral side under the presumptions of bilateral symmetry.

(E) Circumference tracings of receptive fields measured from 7 flies, 136 ROIs, demonstrate stereotypy of receptive field size across microglomeruli and across animals.

(F) The spatial arrangement of imaged microglomeruli ROIs recorded from a single fly (ROIs from panel B) are color coded according to receptive field location in elevation (top) and azimuth (bottom) to indicate retinotopic arrangement.

(G) Similar to panel F, the retinotopic distribution of microglomeruli recorded from all 7 flies and 136 microglomeruli ROIs. Each microglomerular ROI is indicated by a small uniform dot color coded as in panel F. D,V,M,L indicate dorsal, ventral, medial, lateral.

(H-I) Visual stimuli presented in both horizontal directions as shown in (A); ipsi-to-contra motion (orange) and contra-to-ipsi motion (blue). (H) Pairwise comparison between the mean of maximum $\Delta F/F$ responses from all ROIs and all preparations to both an OFF and ON bar n=7 ($p<0.001$, Wilcoxon signed rank test). (I) Mean of pooled peak amplitude responses relative to stimulus onset from six flies to an ON object (left), an ON bar (middle), and a wide-field grating (right). n=6. Error bars indicate S.E.M. $P<0.001$, Wilcoxon signed rank test.

(J) Superior bulb microglomeruli do not show surround inhibition. From a single representative ROI (microglomerulus 3 from panel B), calcium responses are shown for 8 different trajectories of an ON object (color indicates elevation of horizontal sweep) by comparison to an ON bar spanning the full elevation of the display (black trace). The bar

evokes nearly the same response as the object passing through the hotspot of the receptive field. Scale bar is 200% $\Delta F/F$ and 2 seconds, y and x axis respectively.

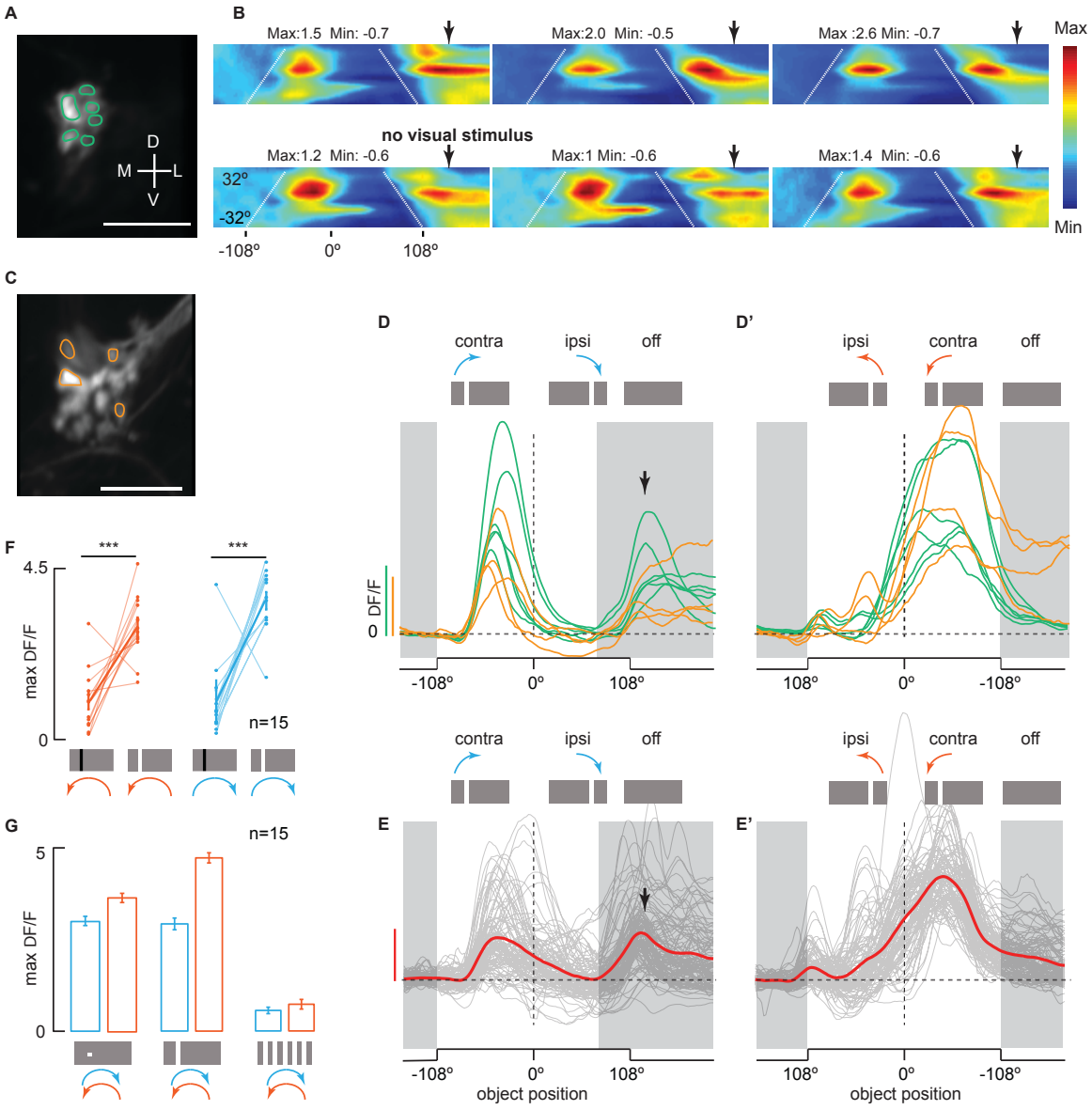

Figure 5.6

Physiological properties of tuberculo-bulbar neurons innervating the inferior bulb

(A-E') Canonical responses from a subset of inferior bulb microglomeruli.

(A) Two photon excitation image of a representative fly in which *R49E09-Gal4* is driving the expression of GCaMP6m in DALcl2 tubercular-bulbar neurons of the inferior bulb

($TuBu_i$). Imaging plane reflects the microglomeruli (ROIs; mint green) in the dorso-posterior most position in the inferior bulb.

(B) Receptive field maps of ROIs in (A) generated by contralateral to ipsilateral (contra-to-ipsi) motion of an ON object passed at 8 different elevation trajectories. Maps demonstrate stereotypy of a class of microglomeruli typically localized to this position in the inferior bulb. Receptive fields are large and centered in the contralateral visual hemifield. Calcium accumulation decreases for stimuli in the ipsilateral visual field as indicated by negative minimum delta F/F values. Note secondary excitation after the object has left the field of view (black arrows). White dashed lines indicate display boundaries.

(C) Second imaging plane from same preparation as (A) contains some microglomeruli which exhibit a canonical $TuBu_i$ response (light orange), but also many that do not (unlabeled microglomeruli).

(D-D') ON bar responses from inferior bulb microglomeruli which exhibit the canonical response described in (B) from the representative fly shown in (A-C). Responses from ROIs from the first plane (mint green) and second plane (light orange) are shown as traces from contra-to-ipsi presentation (D) and ipsilateral to contralateral (ipsi-to-contra) presentation (D') of the ON bar. Scale bars are 400% $\Delta F/F$ for mint green and 100% $\Delta F/F$ for light orange. Shaded grey envelopes indicate portions of the experiment when the stimulus is out of the visual field. Black arrow indicates secondary microglomeruli responses after the ON bar has left the visual field. See also Figure S2.

(E-E') Pooled population data from all ROIs and all flies, exhibiting on average distinct $TuBu_i$ response for contra-to-ipsi (E) and ipsi-to-contra (E') presentation of the ON bar. Raw traces shown in gray, mean of all traces in red. Scale bar is 200% $\Delta F/F$. Shaded grey envelopes and black arrow as described in D-D'. n=15, 104 ROIs.

(F-G) Visual stimuli presented in both horizontal directions; ipsi-to-contra motion (blue) and contra-to-ipsi motion (orange). (F) Pairwise comparison between the mean of maximum $\Delta F/F$ responses from all ROIs which exhibit a canonical $TuBu_i$ response from each preparation; indicating ON selectivity (n=15, $p<0.001$, Wilcoxon signed rank test) (G) Mean of pooled peak amplitude responses relative to stimulus onset from fifteen flies to an ON object (left), an ON bar (middle), and wide-field gratings (right). n=15, error bars indicate S.E.M.

Table 1

Comparative terminology for central complex pathways

Putative Homologies in other insects	Drosophila Neuron Classification	Abridged designation(s)	Subclasses	Lineage Designation
Transmedulla neurons, formerly line-tangential neurons	medullo-tubercular neurons	MeTu neurons	$MeTu_{l}$	Optic Lobe-Derived
			$MeTu_{ll}$	Optic Lobe-Derived
			$MeTu_{im}$	Optic Lobe-Derived
tubercle-lateral accessory lobe neuron type 1 (TuLAL1 neurons)	tuberculo-bulbar neurons	TuBu	$TuBu_{s}$	DALcl1
			$TuBu_{a}$	DALcl1
			$TuBu_{i}$	DALcl2
tangential neurons of the central body lower division (TL neurons)	ring neurons	R neurons	R1, R2, R3, R4m, R4d R5 (new designation -previously unclassified)	DALv2
Columnar neurons of the CBL type 1 (CL1 neurons)	protocerebral bridge-ellipsoid body-Gall neurons	PB-EB-gall (Wedge neurons)		DM1/DPMm1, DM2/DPMpm1, DM3/DPMpm2, DM4/CM4

Columnar neurons of the CBL type 2 (CL2 neurons)	protocerebral bridge-ellipsoid body-noduli neurons	PB-EB-NO (Tile neurons)		DM1/DPMm1, DM2/DPMpm1, DM3/DPMpm2, DM4/CM4

References

1. Ito, K., Shinomiya, K., Ito, M., Armstrong, J.D., Boyan, G., Hartenstein, V., Harzsch, S., Heisenberg, M., Homberg, U., Jenett, A., *et al.* (2014). A systematic nomenclature for the insect brain. Neuron *81*, 755–765.

2. Strausfeld, N.J. (1976). Atlas of an Insect Brain. Springer *52*, 1096–1109.

3. Hanesch, U., Fischbach, K.-F., and Heisenberg, M. (1989). Neuronal architecture of the central complex in Drosophila melanogaster. Cell Tissue Res. *257*, 343–366.

4. Huber, F. (1960). Untersuchungen über die Funktion des Zentralnervensystems und insbesondere des Gehirnes bei der Fortbewegung und der Lauterzeugung der Grillen. Zeitschrift für Vergleichende Physiol. *44*, 60–132.

5. Otto, D. (1971). Untersuchungen zur zentralnervösen Kontrolle der Lauterzeugung von Grillen. Zeitschrift für Vergleichende Physiol. *74*, 227–271.

6. Strauss, R., and Heisenberg, M. (1993). A higher control center of locomotor behavior in the Drosophila brain. J. Neurosci. *13*, 1852–61.

7. Ilius, M., Wolf, R., and Heisenberg, M. (2007). The central complex of Drosophila melanogaster is involved in flight control: studies on mutants and mosaics of the gene ellipsoid body open. J. Neurogenet. *21*, 321–38.

8. Ofstad, T.A., Zuker, C.S., and Reiser, M.B. (2011). Visual place learning in Drosophila melanogaster. Nature *474*, 204–207.

9. Neuser, K., Triphan, T., Mronz, M., Poeck, B., and Strauss, R. (2008). Analysis of a spatial orientation memory in Drosophila. Nature *453*, 1244–1247.

10. Seelig, J.D., and Jayaraman, V. (2015). Neural dynamics for landmark orientation and angular path integration. Nature *521*, 186–191.

11. Poucet, B., Chaillan, F., Truchet, B., Save, E., Sargolini, F., and Hok, V. (2015). Is there a pilot in the brain? Contribution of the self-positioning system to spatial navigation. Front. Behav. Neurosci. *9*, 292.

12. Lai, S.-L., Awasaki, T., Ito, K., and Lee, T. (2008). Clonal analysis of Drosophila antennal lobe neurons: diverse neuronal architectures in the lateral neuroblast lineage. Development *135*, 2883–93.

13. Das, A., Gupta, T., Davla, S., Prieto-Godino, L.L., Diegelmann, S., Reddy, O.V., Raghavan, K.V., Reichert, H., Lovick, J., and Hartenstein, V. (2013). Neuroblast lineage-specific origin of the neurons of the Drosophila larval olfactory system. Dev. Biol. *373*, 322–37.

14. Hartenstein, V., Spindler, S., Pereanu, W., and Fung, S. (2008). The Development of the Drosophila Larval Brain. In Brain Development in Drosophila melanogaster (New York, NY: Springer New York), pp. 1–31.

15. Jefferis, G.S.X.E., Marin, E.C., Stocker, R.F., and Luo, L. (2001). Target neuron prespecification in the olfactory map of Drosophila. Nature *414*, 204–208.

16. Marin, E.C., Jefferis, G.S.X.E., Komiyama, T., Zhu, H., and Luo, L. (2002). Representation of the glomerular olfactory map in the Drosophila brain. Cell *109*, 243–55.

17. Seelig, J.D., and Jayaraman, V. (2013). Feature detection and orientation tuning in the Drosophila central complex. Nature *503*, 262–266.

18. el Jundi, B., Pfeiffer, K., Heinze, S., and Homberg, U. (2014). Integration of polarization and chromatic cues in the insect sky compass. J. Comp. Physiol. A *200*, 575–589.

19. Träger, U., Wagner, R., Bausenwein, B., and Homberg, U. (2008). A novel type of microglomerular synaptic complex in the polarization vision pathway of the locust brain. J. Comp. Neurol. *506*, 288–300.

20. Heinze, S., Florman, J., Asokaraj, S., el Jundi, B., and Reppert, S.M. (2013). Anatomical basis of sun compass navigation II: The neuronal composition of the central complex of the monarch butterfly. J. Comp. Neurol. *521*, 267–298.

21. Pfeiffer, K., and Kinoshita, M. (2012). Segregation of visual inputs from different regions of the compound eye in two parallel pathways through the anterior optic tubercle of the bumblebee (Bombus ignitus). J. Comp. Neurol. *520*, 212–229.

22. Zeller, M., Held, M., Bender, J., Berz, A., Heinloth, T., Hellfritz, T., and Pfeiffer, K. (2015). Transmedulla neurons in the sky compass network of the honeybee (Apis mellifera) are a possible site of circadian input. PLoS One *10*, e0143244.

23. Held, M., Berz, A., Hensgen, R., Muenz, T.S., Scholl, C., Rössler, W., Homberg, U., and Pfeiffer, K. (2016). Microglomerular synaptic complexes in the sky-compass network of the honeybee connect parallel pathways from the anterior optic tubercle to the central complex. Front. Behav. Neurosci. *10*, 186.

24. el Jundi, B., Warrant, E.J., Byrne, M.J., Khaldy, L., Baird, E., Smolka, J., and Dacke, M. (2015). Neural coding underlying the cue preference for celestial orientation. Proc. Natl. Acad. Sci. U. S. A. *112*, 11395–400.

25. Lovick, J.K., Ngo, K.T., Omoto, J.J., Wong, D.C., Nguyen, J.D., and Hartenstein, V. (2013). Postembryonic lineages of the Drosophila brain: I. Development of the lineage-associated fiber tracts. Dev. Biol. *384*, 228–257.

26. Wong, D.C., Lovick, J.K., Ngo, K.T., Borisuthirattana, W., Omoto, J.J., and Hartenstein, V. (2013). Postembryonic lineages of the Drosophila brain: II. Identification of lineage projection patterns based on MARCM clones. Dev. Biol. *384*, 258–89.

27. Ito, M., Masuda, N., Shinomiya, K., Endo, K., and Ito, K. (2013). Systematic Analysis of Neural Projections Reveals Clonal Composition of the Drosophila Brain. Curr. Biol. *23*, 644–655.

28. Yu, H.H., Awasaki, T., Schroeder, M.D., Long, F., Yang, J.S., He, Y., Ding, P., Kao, J.C., Wu, G.Y.Y., Peng, H., *et al.* (2013). Clonal development and organization of the adult Drosophila central brain. Curr. Biol. *23*, 633–643.

29. Pereanu, W., Kumar, A., Jennett, A., Reichert, H., and Hartenstein, V. (2010). Development-based compartmentalization of the Drosophila central brain. J. Comp. Neurol. *518*, 2996–3023.

30. Jenett, A., Rubin, G.M., Ngo, T.T.B., Shepherd, D., Murphy, C., Dionne, H., Pfeiffer, B.D., Cavallaro, A., Hall, D., Jeter, J., *et al.* (2012). A GAL4-Driver Line Resource for Drosophila Neurobiology. Cell Rep. *2*, 991–1001.

31. Nern, A., Pfeiffer, B.D., and Rubin, G.M. (2015). Optimized tools for multicolor stochastic labeling reveal diverse stereotyped cell arrangements in the fly visual system. Proc. Natl. Acad. Sci. *112*, 201506763.

32. Renn, S.C., Armstrong, J.D., Yang, M., Wang, Z., An, X., Kaiser, K., and Taghert, P.H. (1999). Genetic analysis of the Drosophila ellipsoid body neuropil: organization and development of the central complex. J. Neurobiol. *41*, 189–207.

33. Wolff, T., Iyer, N.A., and Rubin, G.M. (2015). Neuroarchitecture and neuroanatomy of the *Drosophila* central complex: A GAL4-based dissection of protocerebral bridge neurons and circuits. J. Comp. Neurol. *523*, 997–1037.

34. Yang, J.S., Awasaki, T., Yu, H.-H., He, Y., Ding, P., Kao, J.-C., and Lee, T. (2013). Diverse neuronal lineages make stereotyped contributions to the *Drosophila* locomotor control center, the central complex. J. Comp. Neurol. *521*, 2645–2662.

35. Namiki, S., and Kanzaki, R. (2016). Comparative neuroanatomy of the lateral accessory lobe in the insect brain. Front. Physiol. *7*, 244.

36. Otsuna, H., Shinomiya, K., and Ito, K. (2014). Parallel neural pathways in higher visual centers of the Drosophila brain that mediate wavelength-specific behavior. Front. Neural Circuits *8*, 8.

37. Panser, K., Tirian, L., Schulze, F., Villalba, S., Jefferis, G.S.X.E., Bühler, K., and Straw, A.D. (2016). Automatic Segmentation of Drosophila Neural Compartments Using GAL4 Expression Data Reveals Novel Visual Pathways. Curr. Biol. *26*, 1943–1954.

38. Fischbach, K.-F., and Dittrich, a P. (1989). The optic lobe of Drosophila melanogaster. I: A. Golgi analysis of wild-type structure. Cell Tissue Res *258*, 441–475.

39. Homberg, U., Hofer, S., Pfeiffer, K., and Gebhardt, S. (2003). Organization and neural connections of the anterior optic tubercle in the brain of the locust,Schistocerca gregaria. J. Comp. Neurol. *462*, 415–430.

40. Pfeiffer, K., Kinoshita, M., and Homberg, U. (2005). Polarization-sensitive and light-sensitive neurons in two parallel pathways passing through the anterior optic tubercle in the locust brain. J. Neurophysiol. *94*, 3903–3915.

41. Heinze, S., Gotthardt, S., Homberg, U., and Biologie, F. (2009). Transformation of Polarized Light Information in the Central Complex of the Locust. J. Neurosci. *29*, 11783–11793.

42. Heinze, S., and Reppert, S.M. (2011). Sun compass integration of skylight cues in migratory monarch butterflies. Neuron *69*, 345–358. Available at: http://www.ncbi.nlm.nih.gov/pubmed/21262471 [Accessed January 17, 2017].

43. el Jundi, B., Pfeiffer, K., and Homberg, U. (2011). A distinct layer of the medulla integrates Sky compass signals in the brain of an insect. PLoS One *6*, e27855.

44. Heinze, S., and Reppert, S.M. (2012). Anatomical basis of sun compass navigation I: The general layout of the monarch butterfly brain. J. Comp. Neurol. *520*, 1599–1628.

45. Homberg, U., Heinze, S., Pfeiffer, K., Kinoshita, M., and el Jundi, B. (2011). Central neural coding of sky polarization in insects. Philos. Trans. R. Soc. Lond. B. Biol. Sci. *366*, 680–7.

46. Weir, P.T., and Dickinson, M.H. (2012). Flying drosophila orient to sky polarization. Curr. Biol. *22*, 21–27.

47. Wernet, M.F., Velez, M.M., Clark, D.A., Baumann-Klausener, F., Brown, J.R., Klovstad, M., Labhart, T., and Clandinin, T.R. (2012). Genetic dissection reveals two separate retinal substrates for polarization vision in drosophila. Curr. Biol. *22*, 12–20.

48. Weir, P.T., Henze, M.J., Bleul, C., Baumann-Klausener, F., Labhart, T., and Dickinson, M.H. (2016). Anatomical Reconstruction and Functional Imaging Reveal an Ordered Array of Skylight Polarization Detectors in Drosophila. J. Neurosci. *36*, 5397–5404.

49. Weir, P.T., and Dickinson, M.H. (2015). Functional divisions for visual processing in the central brain of flying Drosophila. Proc. Natl. Acad. Sci. U. S. A. *112*, E5523-32.

50. Pfeiffer, K., and Homberg, U. (2007). Coding of Azimuthal Directions via Time-Compensated Combination of Celestial Compass Cues. Curr. Biol. *17*, 960–965.

51. Maimon, G., Straw, A.D., and Dickinson, M.H. (2008). A Simple Vision-Based Algorithm for Decision Making in Flying Drosophila. Curr. Biol. *18*, 464–470.

52. Wu, M., Nern, A., Williamson, W.R., Morimoto, M.M., Reiser, M.B., Card, G.M., and Rubin, G.M. (2016). Visual projection neurons in the Drosophila lobula link feature detection to distinct behavioral programs. Elife *5*.

53. Keleş, M.F., and Frye, M.A. (2017). Object-Detecting Neurons in Drosophila. Curr. Biol. in press.

54. Maisak, M.S., Haag, J., Ammer, G., Serbe, E., Meier, M., Leonhardt, A., Schilling, T., Bahl, A., Rubin, G.M., Nern, A., *et al.* (2013). A directional tuning map of Drosophila elementary motion detectors. Nature *500*, 212–6.